LIBRARY
CALIFORNIA AIR RESOURCES BOARD
P.O. BOX 2815
SACRAMENTO, CA 95812

MODEL FORMULATION AND USER'S GUIDE FOR

THE CALPUFF DISPERSION MODEL

May, 1990

by

Joseph S. Scire
David G. Strimaitis
Robert J. Yamartino

Report No. A025-2

Prepared for

California Air Resources Board
1131 S Street
Sacramento, California 95814

TD
890
S3
1990

Table of Contents

Table of Contents - Continued

Table of Contents - Concluded

1. INTRODUCTION

1.1 Background

The California Air Resources Board (ARB) has sponsored a study by Sigma Research Corporation to design and develop a generalized non-steady-state air quality modeling system. Systems Application, Inc. (SAI) served as a subcontractor to Sigma Research with the responsibility for developing the wind field modeling component of the modeling system.

The ARB design specifications for the model include: (1) point and area source capabilities, (2) a modeling domain from tens of meters to hundreds of kilometers from the source, (3) predictions for averaging times ranging from one-hour to one year, (4) applicability to inert pollutants and those subject to linear removal and chemical conversion mechanisms, and, (5) applicability for rough or complex terrain situations.

In order to meet these objectives, a modeling system was designed (Scire et al., 1987) consisting of three components: (1) a meteorological modeling package with both diagnostic and prognostic wind field generators, (2) a Gaussian puff dispersion model with chemical removal, wet and dry deposition, building downwash, complex terrain algorithms, and other effects, and (3) postprocessing programs for the output fields of meteorological data, concentrations and deposition fluxes produced by the models. The meteorological model and puff dispersion model were named CALMET and CALPUFF, respectively.

In July, 1987, the ARB initiated a second project with Sigma Research to upgrade and modernize the Urban Airshed Model (UAM) to include state-of-the-science improvements in many of the key technical algorithms including the numerical advection and diffusion schemes, dry deposition, chemical mechanisms, and chemical integration solver. It was decided to integrate the new photochemical model, called CALGRID, into the CALMET/CALPUFF modeling framework to create a complete modeling system for both reactive and non-reactive pollutants. CALPUFF is best at estimating primary pollutant concentrations and source culpability analysis in the absence of non-linear

effects, whereas CALGRID is most reasonable for secondary pollutant species, such as ozone, involving highly non-linear chemical effects. The CALPUFF and CALGRID models were designed to be compatible with a common meteorological model, CALMET, and share a postprocessor for the time-averaging and display of the modeling results.

1.2 Overview of the Modeling System

The overall modeling system configuration is presented in Figure 1.2-1. The major components of the modeling system are summarized below.

METSCAN is a meteorological preprocessor which performs quality assurance checks on the surface meteorological data used as input to the CALMET model.

READ56 and READ62 are meteorological preprocessors which extract and process upper air wind and temperature data from standard data formats used by the National Climatic Data Center (NCDC). READ56 and READ62 process TD-5600 and TD-6201 formatted data, respectively.

SMERGE is a meteorological preprocessor which processes hourly surface observations from a number of stations and reformats the data into a single file with the data sorted by time rather than by station.

PXTRACT is a meteorological preprocessor which extracts from a larger data base the precipitation data for the spatial region and time period of interest.

PMERGE is a meteorological preprocessor responsible for reformatting and optionally packing the precipitation data.

CSUMM (a version of the Colorado State University Mesoscale Model) is a primitive equation wind field model which simulates mesoscale airflow resulting from differential surface heating and terrain effects. The diagnostic wind field model within CALMET contains options which allow wind fields produced by CSUMM to be combined with observational data as part of the CALMET objective analysis procedure.

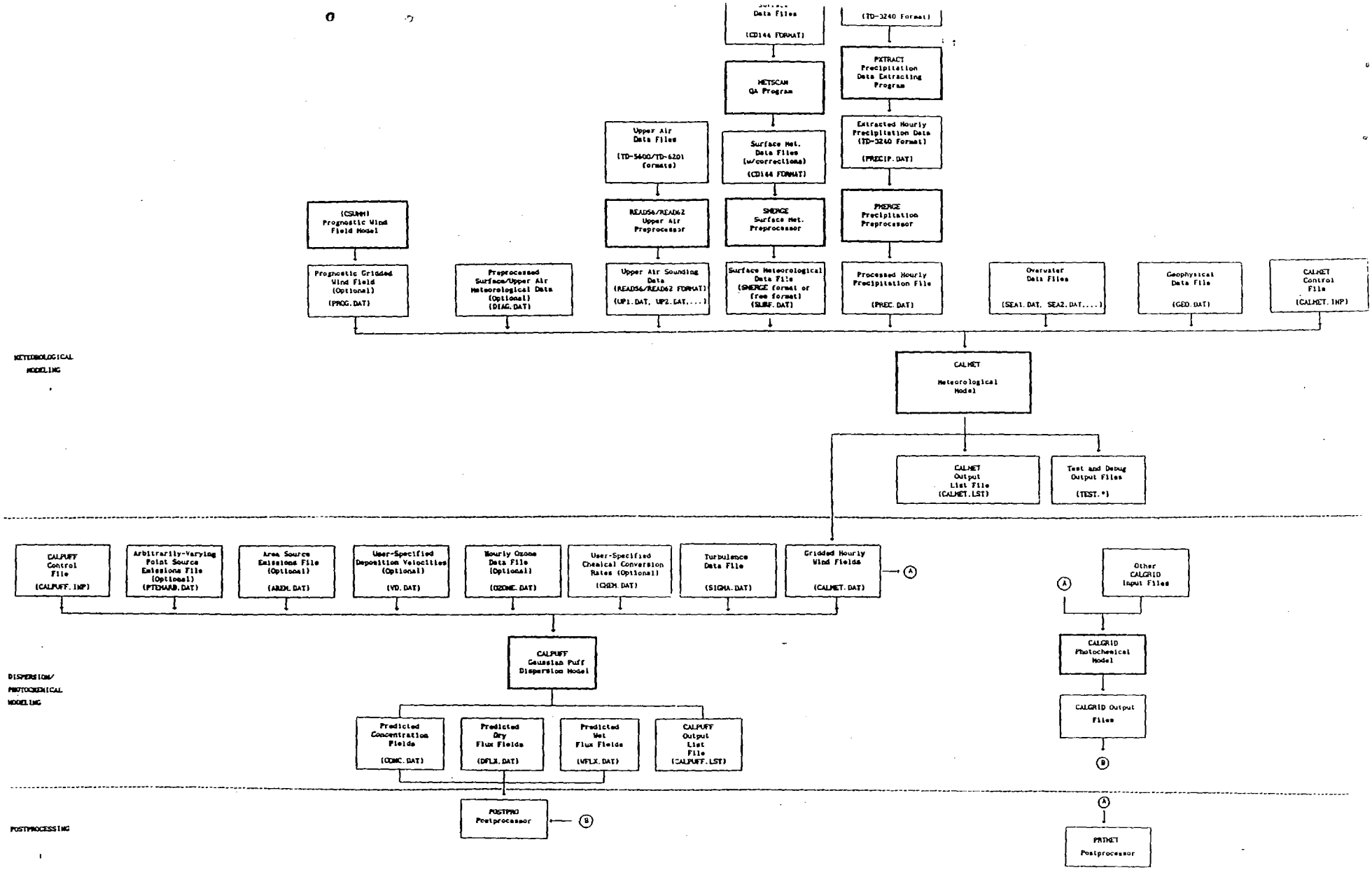

Figure 1.2-1. CALPUFF Modeling System Flow Diagram

CALMET is a meteorological model which includes a diagnostic wind field generator containing objective analysis and parameterized treatments of slope flows, kinematic terrain effects, terrain blocking effects, and a divergence minimization procedure, and a micrometeorological model for overland and overwater boundary layers.

OPTHILL is an optimized curve fitting routine which helps the user determine the most appropriate terrain length scales to use in the CALPUFF complex terrain module from a set of data points.

CALPUFF is a non-steady-state Gaussian puff model containing modules for complex terrain effects, overwater transport, coastal interaction effects, building downwash, wet and dry removal, and simple chemical transformation.

CALGRID is an Eulerian photochemical transport and dispersion model which includes modules for horizontal and vertical advection/diffusion, dry deposition, and a detailed photochemical mechanism.

PRTMET is a postprocessing program which displays user-selected portions of the meteorological data base produced by the CALMET meteorological model.

POSTPRO is a postprocessing program with options for the computation of time-averaged concentrations and deposition fluxes predicted by the CALPUFF and CALMET models.

This report describes the CALPUFF model and its related processing programs. Section 2 contains a description of the technical formulation of CALPUFF. The structure of the CALPUFF code is discussed in Section 3. The inputs and outputs of the CALPUFF model, the preprocessing program OPTHILL, and the POSTPRO postprocessor are described in Section 4. Appendix A contains a tree diagram showing the sequence of subroutines and function calls in CALPUFF. A brief description of each CALPUFF routine is provided in Appendix B. A set of test case input and output files is presented in Appendixes C and D, respectively.

A series of companion reports describe other components of the modeling system. The technical formulation and user's instructions for the CALMET meteorological model and its associated data processing programs are described in a report by Scire et al. (1990). The prognostic wind field model, CSUMM, is described by Kessler (1989). A stand-alone version of the CALMET diagnostic wind field model is discussed by Douglas and Kessler (1988). Finally, the CALGRID model is documented in two reports by Yamartino et al. (1989) and Scire et al. (1989).

1.3 Major Model Features and Options

CALPUFF is a multi-layer, multi-species non-steady-state puff dispersion model which can simulate the effects of time- and space-varying meteorological conditions on pollutant transport, transformation, and removal. CALPUFF is designed to use the three dimensional meteorological fields developed by the CALMET model. CALMET includes a diagnostic wind field generator, and overland and overwater boundary layer modules. CALMET has the ability to combine the wind fields generated by the CSUMM prognostic primitive equation model with observational data through an objective analysis procedure.

CALPUFF contains algorithms for near-source effects such as building downwash, transitional plume rise, subgrid scale terrain interactions as well as longer range effects such as pollutant removal (wet scavenging and dry deposition), chemical transformation, overwater transport and coastal interaction effects. It can accommodate arbitrarily-varying point source and gridded area source emissions. Most of the algorithms contain options to treat the physical processes at different levels of detail depending on the model application.

The major features and options of the CALPUFF model are summarized in Table 1.3-1. Some of the technical algorithms are briefly described below.

Dry Deposition: A full resistance-based model is provided in CALPUFF for the computation of dry deposition rates of gases and particulate matter as a function of geophysical parameters, meteorological conditions, and pollutant species. Options are provided to allow user-specified,

Table 1.3-1.

Major Features of the CALPUFF Model

- Non-steady-state emissions and meteorological conditions
- Efficient sampling functions
  - Integrated puff formulation
  - Elongated puff (slug) formulation
- Dispersion coefficient (σ_y, σ_z) options
  - Direct measurements of σ_v and σ_w
  - Estimated values of σ_v and σ_w based on similarity theory
  - PGT dispersion coefficients (rural areas)
  - MP dispersion coefficients (urban areas)
- Plume Rise
  - Partial penetration
  - Buoyant and momentum rise
  - Stack tip effects
  - Vertical wind shear
  - Building downwash effects
- Building downwash
  - Huber-Snyder method
  - Schulman-Scire method
- Subgrid scale complex terrain
  - Dividing streamline, H_d:
    - Above H_d, puff flows over the hill and experiences altered diffusion rates
    - Below H_d, puff deflects around the hill, splits, and wraps around the hill

(Continued)

Table 1.3-1.

Major Features of the CALPUFF Model

(Concluded)

- Dry Deposition
  - Gases and particulate matter
  - Three options:
    - Full treatment of space and time variations of deposition with a resistance model
    - User-specified diurnal cycles for each pollutant
    - No dry deposition

- Overwater and coastal interaction effects
  - Overwater boundary layer parameters
  - Abrupt change in meteorological conditions, plume dispersion at coastal boundary
  - Plume fumigation

- Chemical transformation options
  - Pseudo-first-order chemical mechanism for SO_2, $SO_4^{=}$, NO_x, HNO_3, and NO_3^{-} (MESOPUFF II method)
  - User-specified diurnal cycles of transformation rates
  - No chemical conversion

- Wet Removal
  - Scavenging coefficient approach
  - Removal rate a function of precipitation intensity and precipitation type

diurnally varying deposition velocities to be used for one or more pollutants instead of the resistance model (e.g., for sensitivity testing) or to by-pass the dry deposition model completely.

Wet Deposition: An empirical scavenging coefficient approach is used in CALPUFF to compute the depletion and wet deposition fluxes due to precipitation scavenging. The scavenging coefficients are specified as a function of the pollutant and precipitation type (i.e., frozen vs. liquid precipitation).

Chemical Transformation: CALPUFF includes options for parameterizing chemical transformation effects using the five species scheme (SO_2, $SO_4^=$, NO_x, HNO_3, and NO_3^-) employed in the MESOPUFF II model or a set of user-specified, diurnally-varying transformation rates.

Subgrid Scale Complex Terrain: The complex terrain module in CALPUFF is based on the approach used in the Complex Terrain Dispersion Model (CTDM). Plume impingement on subgrid scale hills is evaluated using a dividing streamline (H_d) to determine which pollutant material is deflected around the sides of a hill (below H_d) and which material is advected over the hill (above H_d). Individual puffs are split into up to three sections for these calculations.

Puff Sampling Functions: A set of accurate and computationally efficient puff sampling routines are included in CALPUFF which solve many of the computational difficulties with applying a puff model to near-field releases. For near-field applications during rapidly-varying meteorological conditions, an elongated puff (slug) sampling function is used. An integrated puff approached is used during less demanding conditions. Both techniques reproduce continuous plume results exactly under the appropriate steady state conditions.

Building Downwash: The Huber-Snyder and Schulman-Scire downwash models are both incorporated into CALPUFF. An option is provided to use either model for all stacks, or make the choice on a stack-by-stack and wind sector-by-wind sector basis. Both algorithms have been implemented

in a such a way as to allow the use of wind direction specific building dimensions.

Overwater and Coastal Interaction Effects: Because the CALMET meteorological model contains both overwater and overland boundary layer algorithms, the effects of water bodies on plume transport, dispersion, and deposition can be simulated with CALPUFF. The puff formulation of CALPUFF is designed to handle spatial changes in meteorological and dispersion conditions, including the abrupt changes which occur at the coastline of a major body of water.

Dispersion Coefficients: Several options are provided in CALPUFF for the computation of dispersion coefficients, including the use of turbulence measurements (σ_v and σ_w), the use of similarity theory to estimate σ_v and σ_w from modeled surface heat and momentum fluxes, or the use of Pasquill-Gifford-Turner (PGT) or McElroy-Pooler dispersion coefficients.

1.4 Summary of Data and Computer Requirements

Data Requirements

The input data sets used by CALPUFF are summarized in Table 1.4-1 (also see the modeling system flow diagram, Figure 1.2-1). CALPUFF reads user inputs from a "control file" call CALPUFF.INP. This file contains the user's selections for the various model options, technical input variables, output options, and other user-controllable options.

A meteorological data file (CALMET.DAT) contains hourly gridded fields of micrometeorological parameters and three-dimensional wind and temperature fields. The meteorological data file also contains geophysical data such as terrain heights and land use which are required by both the meteorological model (e.g., for terrain adjustment of the wind fields) and by the CALPUFF model. The contents of the CALMET.DAT input file and the other input data bases are summarized in Table 1.4-2.

Three files are provided for the input of emissions data. The control file, CALPUFF.INP includes point and area source data for sources with

Table 1.4-1

Summary of CALPUFF Input Files

File Name	Contents	Unit* Number	Type
CALPUFF.INP	Control file inputs	IO5	Formatted
CALMET.DAT	Geophysical and hourly meteorological data	IO7	Unformatted
PTEMARB.DAT	Source and emissions data for point sources with arbitrarily-varying emission parameters (Optional)	IO16	Unformatted
AREM.DAT	Emissions data for area sources with time-varying emission parameters (Optional)	IO18	Unformatted
VD.DAT	User-specified deposition velocities (Optional)	IO20	Formatted
OZONE.DAT	Hourly ozone measurements at one or more ozone stations (Optional)	IO22	Formatted
CHEM.DAT	User-specified chemical transformation rates (Optional)	IO24	Formatted
SIGMA.DAT	Hourly turbulence measurements (σ_v,σ_w) (Optional)	IO26	Formatted

* Variable shown is the parameter controlling the Fortran unit number associated with the file. Usually, the value assigned to the parameter is consistent with the name (i.e., IO7 = 7). However, the value can be easily changed in the parameter file to accommodate reserved unit numbers on a particular system

Table 1.4-2

Summary Input Data Used by CALPUFF

Geophysical Data (CALMET.DAT)

Gridded fields of:

- surface roughness lengths (z_o)
- land use categories
- terrain elevations
- leaf area indices

Meteorological Data (CALMET.DAT)

Gridded fields of:

- u, v, w wind components (3-D)
- air temperature (3-D)
- surface friction velocity (u_*)
- mixing height (z_i)
- Monin-Obukhov length (L)
- PGT stability class
- Precipitation rate

Hourly values of the following parameters at surface met. stations:

- air density (ρ_a)
- air temperature
- short-wave solar radiation
- relative humidity
- precipitation type

Emissions Data

Point source emissions:

- source and emissions data for point sources with constant emission parameters (CALPUFF.INP)
- source and emissions data for point sources with arbitrarily-varying emission parameters (PTEMARB.DAT)

Area source emissions

- emissions and initial size, height, and location for area sources with constant emission parameters (CALPUFF.INP)
- gridded emissions data for area sources with time-varying emission parameters (AREM.DAT)

Deposition Velocity Data

- deposition velocity for each user-specified species for each hour of a diurnal cycle (VD.DAT)

(Continued)

Table 1.4-2

Summary Input Data Used by CALPUFF

(Concluded)

Ozone Monitoring Data

- hourly ozone measurements at one or more monitoring stations (OZONE.DAT)

Chemical Transformation Data

- species-dependent chemical transformation rates for each hour of a diurnal cycle (CHEM.DAT)

Turbulence Observational Data

- hourly measurements of turbulence (σ_v, σ_w) at an onsite meteorological tower (SIGMA.DAT)

constant emission parameters. Arbitrarily-varying point source data is read from a file call PTEMARB.DAT. Gridded, time-varying area source emissions are obtained from the area source file AREM.DAT.

Hourly observations of ozone data are used in the calculation of SO_2 and NO_x transformation rates if the MESOPUFF II chemical transformation scheme is selected. The hourly ozone data for one or more ozone stations are read from a data file called OZONE.DAT.

Two additional input files, VD.DAT and CHEM.DAT, contain diurnal cycles of user-specified deposition velocities and chemical transformation rates, respectively. These files are necessary only if the user wishes to substitute the values normally computed internally by the deposition and chemical models with sets of time-varying but spatially-uniform externally specified values.

Another optional input file, SIGMA.DAT, contains hourly observations of σ_v and σ_w. These parameters can be used to compute the plume dispersion coefficients σ_y and σ_z.

The structure, format and contents of each CALPUFF input data set are described in Section 4.2. The CALPUFF output files are summarized in Table 1.4-3. The list file contains a copy of the inputs used in the run, optional output fields of gridded and discrete receptor concentrations, wet deposition fluxes, and dry deposition fluxes and other run data. The CONC.DAT, WFLX.DAT, and DFLX.DAT files contain the output concentrations, wet and dry fluxes, respectively, in an unformatted form suitable for further processing by the postprocessing program, POSTPRO.

Computer Requirements

The memory management scheme used in CALPUFF is designed to allow the maximum array dimensions in the model to be easily adjusted to match the requirements of a particular application. An external parameter file contains the maximum array size for all of the major arrays. A re-sizing of the program can be accomplished by modifying the appropriate variable or variables in the parameter file and re-compiling the program. All appropriate arrays in

Table 1.4-3

Summary of CALPUFF Output Files

File Name	Contents	Unit* Number	Type
CALPUFF.LST	List file produced by CALPUFF	IO6	Formatted
CONC.DAT	One-hour averaged concentrations (g/m^3) at the gridded and discrete receptors for species selected by the user in the control file	IO8	Unformatted
DFLX.DAT	One-hour averaged dry deposition fluxes ($g/m^2/s$) at the gridded and discrete receptors for species selected by the user in the control file	IO9	Unformatted
WFLX.DAT	One-hour averaged wet deposition fluxes ($g/m^2/s$) at the gridded and discrete receptors for species selected by the user in the control file	IO10	Unformatted

* Variable shown is the parameter controlling the Fortran unit number associated with the file. Usually, the value assigned to the parameter is consistent with the name (i.e., IO8 = 8). However, the value can be easily changed in the parameter file to accommodate reserved unit numbers on a particular system

the model will be automatically re-sized by the updated parameter values. For example, the maximum number of horizontal grid cells allowed in the model, MXNX and MXNY, are two of the variables which can be adjusted within the parameter file. No change to the parameter file is necessary if the model application uses fewer than the specified maximum values in the parameter file.

The memory required by CALPUFF will be a strong function of the specified maximum array dimensions in the parameter file. However, as an example, CALPUFF required approximately 300 K bytes of memory for a test run with a 10 x 10 horizontal grid, with 5 vertical layers, and a maximum number of puffs of 100.

The run time of CALPUFF will vary considerably depending on the model application. Variations of factors of 10-20 a likely depending of the size of the domain, the number of sources, selection of technical options, and meteorological variables such as the mean wind speed. Because each puff is treated independently, any factor which influence the number and residence time of puffs on the computational grid will affect the run time of the model.

The test run for the grid described above, which included 100 gridded receptors and two point sources, required 42 seconds for a two hour simulation on a 12-MHz 286 PC with a math coprocessor.

2. TECHNICAL DISCUSSION

2.1 Solution of the Puff Equations

Puff models represent a continuous plume as a number of discrete packets of pollutant material. Most puff models (e.g., Ludwig et al., 1977; van Egmond and Kesseboom, 1983; Peterson, 1986) evaluate the contribution of a puff to the concentration at a receptor by a "snapshot" approach. Each puff is "frozen" at particular time intervals (sampling steps). The concentration due to the "frozen" puff at that time is computed (or sampled). The puff is then allowed to move, evolving in size, strength, etc., until the next sampling step. The total concentration at a receptor is the sum of the contributions of all nearby puffs averaged for all sampling steps within the basic time step. Depending on the model and the application, the sampling step and the time step may both be one hour, indicating only one "snapshot" of the puff is taken each hour.

A traditional drawback of the puff approach has been the need for the release of many puffs to adequately represent a continuous plume close to a source. Ludwig et al. (1977) have shown that if the distance between puffs exceeds a maximum of about 2 σ_y, inaccurate results may be obtained (see Figure 2.1-1). Better results are obtained if the puff separation is reduced to no more than one σ_y. If the puffs do not overlap sufficiently, the concentrations at receptors located in the gap between puffs at the time of the "snapshot" are underestimated, while those at the puff centers are overestimated.

Ludwig et al. (1977) recommend spacing puffs uniformly in space rather than in time with a puff merging/purging scheme to reduce the total number of puffs. Zannetti (1981) suggests tracking fewer puffs than necessary for adequate sampling, but then saturating the area near a receptor with artificially generated puffs to provide the required puff overlap (see Figure 2.1-2). Although both schemes act to reduce the number of puffs carried by the model, the snapshot sampling method still requires that an uneconomically large number of puffs be generated near the source. For example, at a receptor 100 meters from a source, and assuming PGT dispersion rates, puffs at a density corresponding to a release rate of over 1300 puffs/hour are required to meet the 2 σ_y criterion for F stability, 3 m/s wind conditions. During

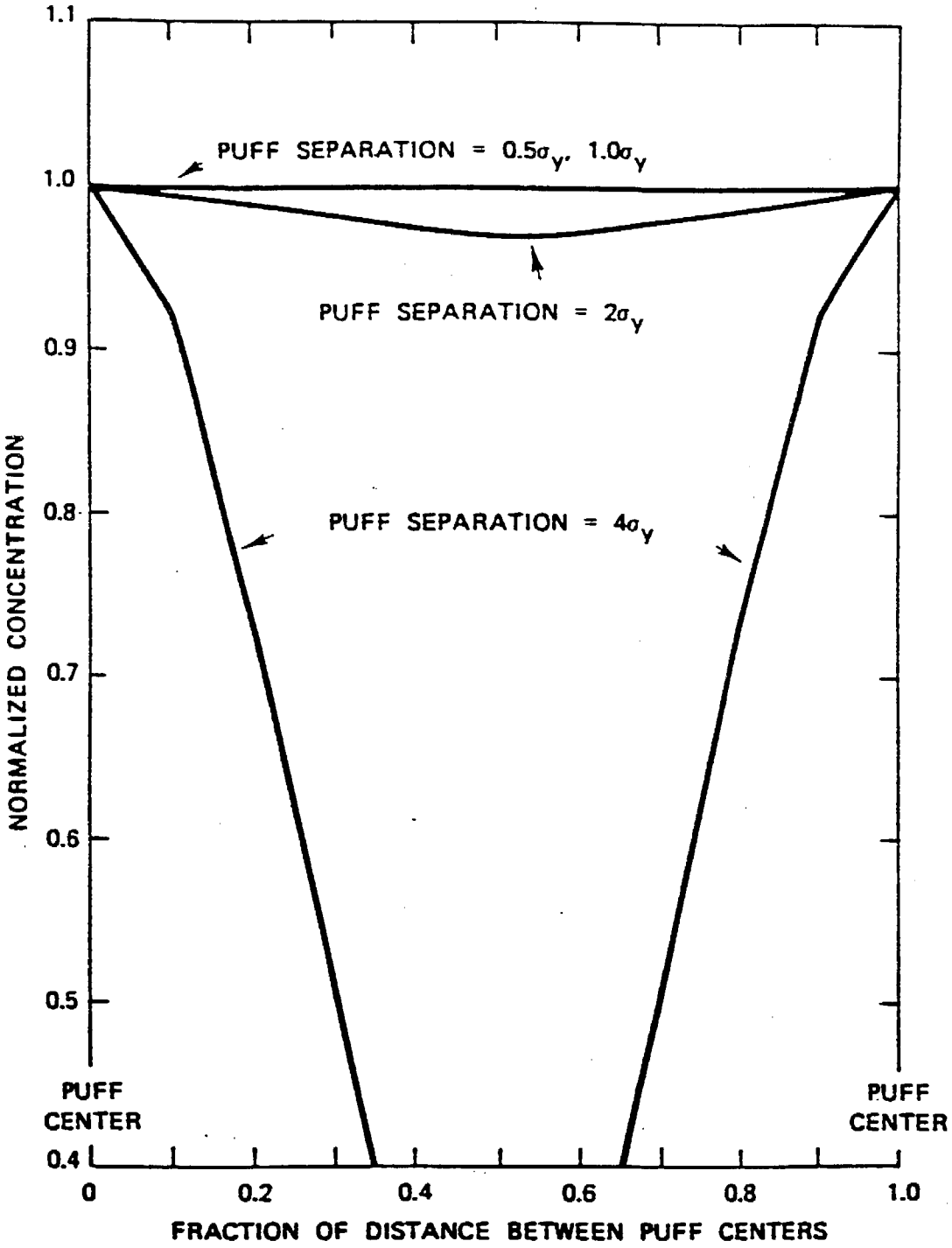

Figure 2.1-1. Normalized concentration between two puffs in a string of puffs of equal size and spacing. [From Ludwig et al. (1977)].

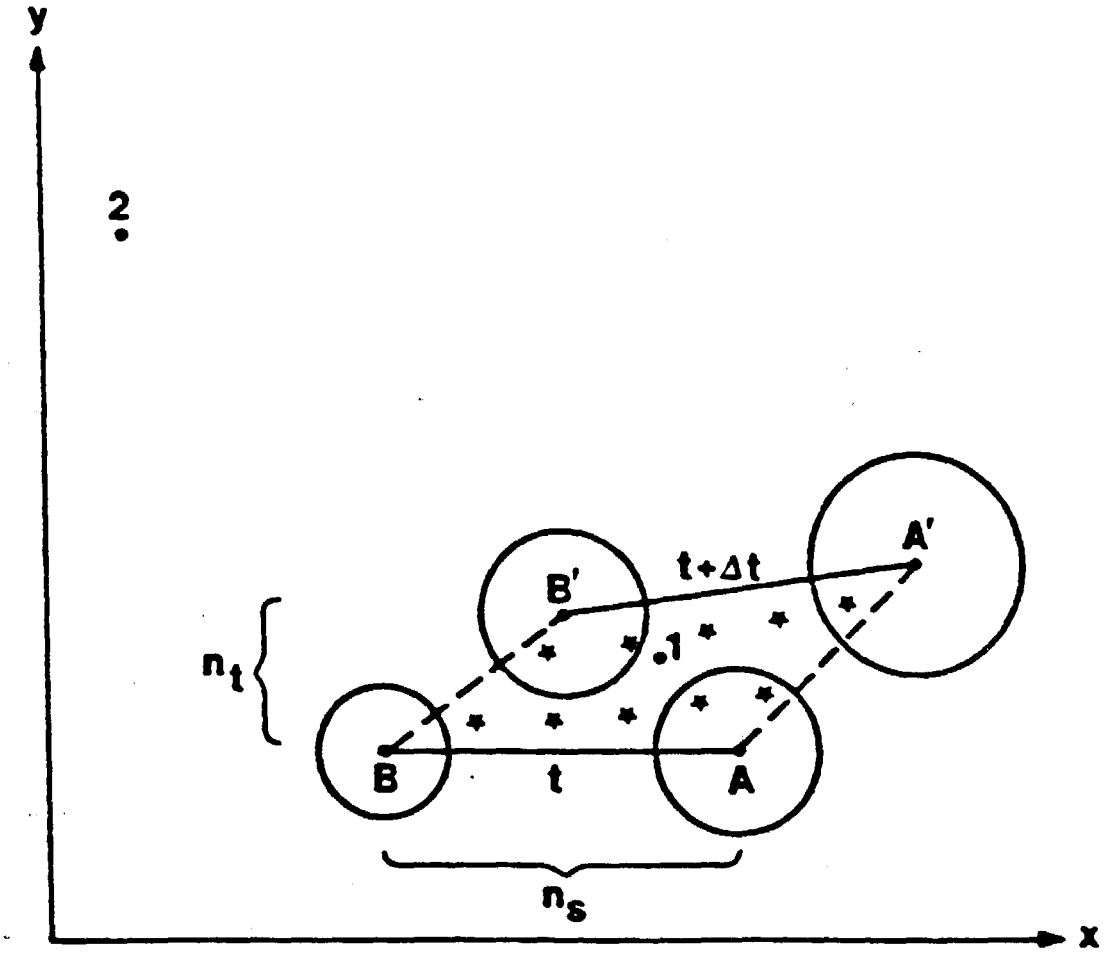

Figure 2.1-2. Illustration of the puff generation scheme of Zannetti (1981). The advected puffs (A -> A', B -> B') in the vicinity of Receptor 1 are not sufficient to resolve the plume. The mass from the original puffs is redistributed into n_t x n_s new puffs (asterisks) for sampling purposes. [From Zannetti (1981)].

high wind speed, neutral conditions (10 m/s, D stability), nearly 2200 puffs/hour are needed. The more stringent one σ_y criterion would double the number of puffs required.

Two alternatives to the conventional snapshot sampling function are discussed below. The first is based on the integrated sampling function in the MESOPUFF II model (Scire et al., 1984), with modifications for near-field applications. The second scheme uses a non-circular puff (slug) elongated in the direction of the wind to eliminate the need for frequent releases of puffs. The performances of the original and modified integrated sampling functions and the slug model are evaluated for unsteady and steady-state conditions. The proposed sampling scheme for the ARB model is a hybrid circular puff/elongated slug method taking advantage of the strengths of each algorithm.

2.1.1 Integrated Puff Sampling Function Formulation

The basic equation for the contribution of a puff at a receptor is:

$$C = \frac{Q}{2\pi\sigma_x\sigma_y} g \exp[-d_a^2/(2\sigma_x^2)] \exp[-d_c^2/(2\sigma_y^2)] \qquad (2.1\text{-}1)$$

$$g = \frac{2}{(2\pi)^{1/2}_z\sigma} \sum_{n=\infty}^{\infty} \exp[-(H_e + 2nh)^2/(2\sigma_z^2)] \qquad (2.1\text{-}2)$$

where C is the ground-level concentration (g/m^3),

Q is the pollutant mass (g) in the puff,

σ_x is the standard deviation (m) of the Gaussian distribution in the along-wind direction,

σ_y is the standard deviation (m) of the Gaussian distribution in the cross-wind direction,

σ_z is the standard deviation (m) of the Gaussian distribution in the vertical direction,

d_a is the distance (m) from the puff center to the receptor in the along-wind direction,

d_c is the distance (m) from the puff center to the receptor in the cross-wind direction,

g is the vertical term (m) of the Gaussian equation,

H_e is the effective height (m) above the ground of the puff center, and,

h is the mixed-layer height (m).

The summation in the vertical term, g, accounts for multiple reflections off the mixing lid and the ground. It reduces to the uniformly mixed limit of 1/h for $\sigma_z > 1.6$ h. In general, puffs within the convective boundary layer meet this criterion within a few hours after release.

For a horizontally symmetric puff, with $\sigma_x = \sigma_y$, Eqn. (2.1-1) reduces to:

$$C(s) = \frac{Q(s)}{2\pi\sigma_y^2(s)}\, g(s)\exp[-R^2(s)/(2\sigma_y^2(s))] \qquad (2.1\text{-}3)$$

where R is the distance (m) from the center of the puff to the receptor, and,

s is the distance (m) traveled by the puff.

The distance dependence of the variables in Eqn. (2.1-3) is indicated (e.g., C(s), $\sigma_y(s)$, etc.). Integrating Eqn. (2.1-3) over the distance of puff travel, ds, during the sampling step, dt, yields the time averaged concentration, $\bar{C}$.

$$\bar{C} = \frac{1}{ds}\int_{s_o}^{s_o + ds} \frac{Q(s)}{2\pi\sigma_y^2(s)}\, g(s)\exp[-R^2(s)/(2\sigma_y^2(s))]ds \qquad (2.1\text{-}4)$$

where s_o is the value of s at the beginning of the sampling step.

If it is assumed that the most significant s dependencies during the sampling step are in the R(s) and Q(s) terms, an analytical solution to this integral can be obtained. Figure 2.1-3 illustrates the movement of a puff from coordinates (x_1, y_1) to (x_2, y_2). Assuming the trajectory segment is a straight line, and transforming s to a dimensionless trajectory variable, p, the radial distance to the receptor at (x_r, y_r) is:

$$R(s) = [(x_1 - x_r + p\,dx)^2 + (y_1 - y_r + p\,dy)^2]^{1/2} \qquad (2.1\text{-}5)$$

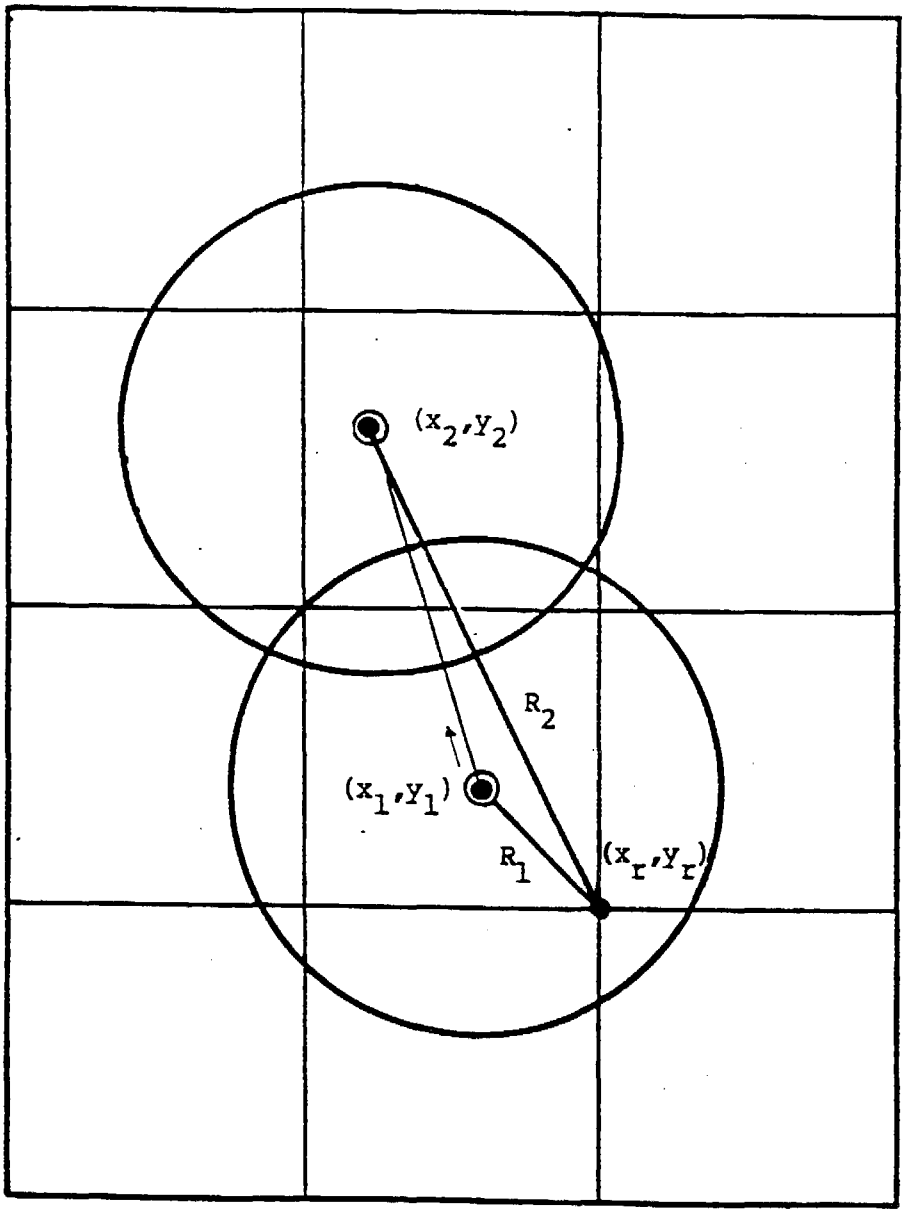

Figure 2.1-3. Illustration of the puff movement during the sampling step and the associated changes in the puff-receptor distance.

where p is zero at the beginning of the trajectory segment (i.e., at (x_1,y_1)),
p is one at the end of the trajectory segment (i.e., at (x_2,y_2)), and,
dx, dy are the incremental X and Y distances travelled by the puff
(i.e., $dx = x_2 - x_1$, and $dy = y_2 - y_1$).

The exponential variation of Q due to removal and chemical transformation processes is expressed as a linear function of the sampling interval:

$$Q(s) = Q(s_o) + p\,[Q(s_o + ds) - Q(s_o)] \qquad (2.1\text{-}6)$$

Using Eqn. (2.1-6), and transforming to p coordinates, Eqn. (2.1-4) becomes:

$$C = \frac{g}{2\pi\,\sigma_y^{\,2}} \left\{ Q(s_o) \int_0^1 \exp[-R^2(p)/(2\sigma_y^{\,2})]\,dp + \right.$$

$$\left. [Q(s_o + ds) - Q(s_o)] \int_0^1 p\,\exp[-R^2(p)/(2\sigma_y^{\,2})]\,dp \right\} \qquad (2.1\text{-}7)$$

The solution of the integrals in Eqn. (2.1-7) is expressed in terms of error functions and exponentials:

$$\bar{C} = \frac{g}{2\pi\,\sigma_y^{\,2}} \{Q(s_o)\,I_1 + [Q(s_o+ds) - Q(s_o)]\,I_2\} \qquad (2.1\text{-}8)$$

$$I_1 = \left[\frac{\pi}{2a}\right]^{1/2} \exp\left[\frac{b^2}{2a} - \frac{c}{2}\right] \left\{ \operatorname{erf}\left[\frac{a+b}{(2a)^{1/2}}\right] - \operatorname{erf}\left[\frac{b}{(2a)^{1/2}}\right] \right\} \qquad (2.1\text{-}9)$$

$$I_2 = \frac{-b\,I_1}{a} + \frac{1}{a} \exp\left[\frac{b^2}{2a} - \frac{c}{2}\right] \left\{ \exp\left[\frac{-b^2}{a}\right] - \exp\left[\frac{a+2b+b}{2a}\right] \right\} \qquad (2.1\text{-}10)$$

$$a = (dx^2 + dy^2)/\sigma_y^2 \qquad (2.1\text{-}11)$$

$$b = [dx\ (x_2 - x_r) + dy(y_2 - y_r)]/\sigma_y^2 \qquad (2.1\text{-}12)$$

$$c = [(x_2 - x_r)^2 + (y_2 - y_r)^2]/\sigma_y^2 \qquad (2.1\text{-}13)$$

The horizontal dispersion coefficient, σ_y, and the vertical term, g, are evaluated and held constant throughout the trajectory segment. In MESOPUFF II, σ_y and g are computed at the mid-point of the trajectory segment ($p = 0.5$). At mesoscale distances, the fractional change in the puff size during the sampling step is usually small, and the use of the mid-point values of σ_y and g is adequate. This assumption reduces the number of times that the dispersion coefficients and vertical reflection terms need be computed to one per sampling step (independent of the number of receptors). This optimization for mesoscale distances, however, may not be appropriate in the near-field, where the fractional puff growth rate can be rapid and plume height may vary. For this reason, the integrated sampling function has been also tested with receptor-specific values of σ_y and g, evaluated at the point of closest approach of the puff to each receptor. The results of the test runs of both puff models as well as the slug model described in the next subsection are discussed below.

2.1.2 Slug Formulation and Sampling Functions

In the slug model, the "puffs" consist of Gaussian packets of pollutant material stretched in the along-wind direction. A slug can be visualized as a group of overlapping circular puffs having very small puff separation distances. In fact, the slug represents the continuous emission of puffs, each containing the infinitesimal mass q dt. The length of the main body of the slug is $u\ \Delta t_e$, where u is the wind speed, and Δt_e is the time of emission of the pollutant. The concentration due to the presence of a slug can be described as:

$$C(t) = \frac{Fq}{(2\pi)^{1/2}\ u'\sigma_y}\ g\ \exp\left[\frac{-d_c^2}{2\sigma_y^2}\ \frac{u^2}{u'^2}\right] \qquad (2.1\text{-}14)$$

$$F = \frac{1}{2}\left\{\mathrm{erf}\left[\frac{d_{a2}}{\sqrt{2}\,\sigma_{y2}}\right] - \mathrm{erf}\left[\frac{-d_{a1}}{\sqrt{2}\,\sigma_{y1}}\right]\right\} \qquad (2.1\text{-}15)$$

where u is the vector mean wind speed (m/s),

u′ is the scalar wind speed [defined as $u' = (u^2 + \sigma_v^2)^{1/2}$ with σ_v = wind speed variance],

q is the source emission rate (g/s),

F is a "causality" function, and

g is the vertical coupling factor of Eqn. 2.1-2.

The quantities d_c and d_a are cross-slug (i.e., perpendicular to the slug axis) and along-slug distances, respectively, to the receptor. In particular, d_{a2} is the distance from slug end 2 (with $d_{a2} > 0$ in the direction of end 1), whereas the distance from slug end 1 is defined as $-d_{a1} \equiv d_{a2} - \ell_{xy}$, with ℓ_{xy} being the length of the slug projection in the x-y plane. The subscripts 1 and 2 on the dispersion coefficients refer to values at the oldest and youngest ends of the slug, respectively. The absence of a numerical subscript indicates a value defined at the receptor.

This "slug" formulation retains many of the important properties of the circular puff model, while significantly reducing puff overlap problems associated with snapshot sampling of circular puffs. The concentration distribution within the body of the slug, away from the slug endpoints, approaches that of the Gaussian plume result under the appropriate steady-state conditions. The concentrations near the endpoints of the slug (both inside and outside of the body of the slug) fall off in such a way that if adjacent slugs are present, the plume predictions will be reproduced when the contributions of those slugs are included (again, during steady-state conditions). Eqn. (2.1-14) can be explicitly shown to conserve mass. As with circular puffs, each slug is free to evolve independently in response to the local effects of dispersion, chemical transformation, removal, etc. However, unlike puffs, we constrain the end points of adjacent slugs to remain connected. This ensures continuity of a simulated plume without the gaps associated with puff or segmented plume models.

The "causality" function, F, accounts for edge effects near the endpoints of the slug. For long emission times such that $u\,\Delta t_e >> \sigma_x$, and points well inside the body of the slug, evaluation of the error functions in Eqn. (2.1-15) produces $F = 0.5(1 - (-1)) = 1$ (i.e., no edge effects). For receptors well

outside the slug, F becomes zero, indicating that the pollutant material has not yet reached the receptor or has already passed it by. Near the endpoints, the causality factor produces a leading/trailing Gaussian tail on the distribution.

The factor (u/u') allows low wind speed and calm conditions to be properly treated. As u approaches zero, the exponential crosswind term becomes unity and F approaches $-\text{erf}\{d_a/[(\sqrt{2}\,\sigma_y]\}/2$. Under these conditions, the radial concentration dependence of the distribution is determined by the causality factor. For u greater than a few meters per second, (u/u') is very close to one, so that this ratio becomes unimportant. The factors (u/u') and F make the slug model more "puff-like" than segmented plume models (e.g., Hales et al., 1977; Benkley and Bass, 1979). Unlike the slug model, segmented plume models generally do not properly treat low wind speed conditions or segment edge effects.

Eqn. (2.1-14) represents a "snapshot" description of the elongated puff at time t. Figure 2.1-4 displays the concentration isopleths of two such slug snapshots. As with the "snapshot" puff equation, Eqn. (2.1-14) must be integrated during the sampling step to produce a time-averaged concentration. In the case where the emission rate and meteorological conditions do not vary during the sampling step, a generalized analytical solution to the integral can be obtained for "emitting" slugs (i.e., the endpoint of the "youngest" end of the slug is at the source):

$$\bar{C} = \frac{\bar{F}q}{\sqrt{2\pi}\,u'\sigma_y}\, g\, \exp\left[\frac{-d_c^2}{2\sigma_y^2}\,\frac{u^2}{u'^2}\right] \qquad (2.1\text{-}16)$$

$$\bar{F} = \frac{1}{2}\,\text{erf}(\phi_2) + \frac{1}{2}\,\frac{\sqrt{2}\,\sigma_y}{u\Delta t_s}\left\{[\xi_e\,\text{erf}(\xi_e) - \xi_b\,\text{erf}(\xi_b)]\right.$$

$$\left. + \frac{1}{2}[\exp(\xi_e^2) - \exp(\xi_b^2)]\right\} \qquad (2.1\text{-}17)$$

where $$\xi_e = \frac{d_{a2} - u\Delta t_s}{\sqrt{2}\,\sigma_y} \qquad (2.1\text{-}18)$$

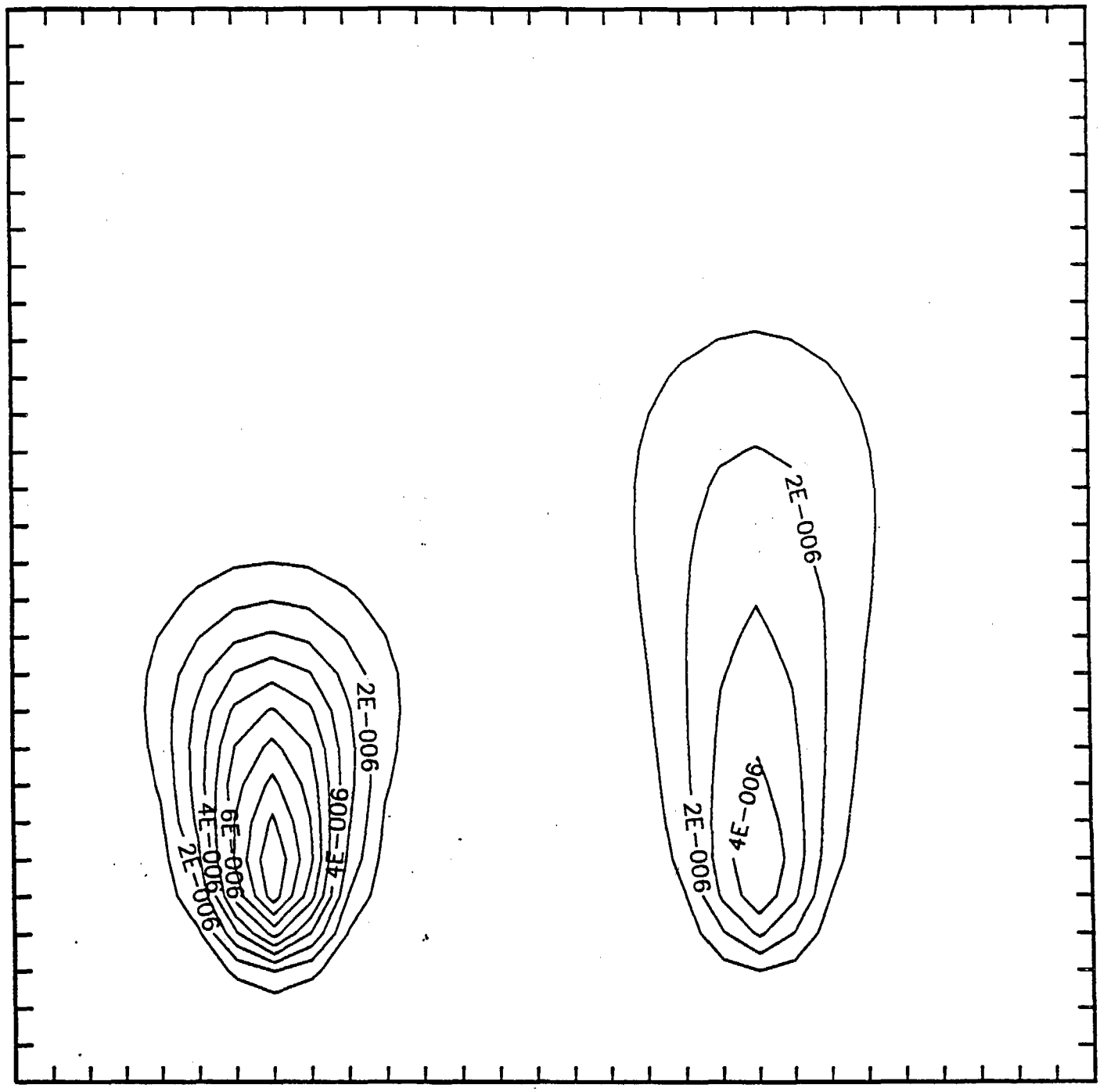

Figure 2.1-4. Isopleths of two slug "snapshots." The slug snapshot at left represents the slug at the beginning of a time step whereas the snapshot at right shows the instantaneous distribution at the end of the time step. During the time step, the slug experienced advection (to the right), diffusion, and some along-slug stretching due to wind shear.

represents the situation at the end of the time step Δt_s.

$$\xi_b = \frac{d_{a2}}{\sqrt{2}\sigma_y} \qquad (2.1\text{-}19)$$

represents the situation at the beginning of the time step,

$$\phi_2 = \frac{d_{a2}}{\sqrt{2}\sigma_{y2}} \qquad (2.1\text{-}20)$$

represents the steady state conditions at the source, and where Δt_s is the duration of the sampling step.

For Eqn. (2.1-16) to apply, the sampling interval must correspond to the emission interval, as is normally the case for fresh emissions. The value of σ_{y2} used is the initial lateral spread (if any) of the emissions at the source. For older slugs, the endpoint of the slug is no longer fixed at the source and the long axis of the slug is not likely to be along the advecting wind direction. An analytical integration of Eqn. (2.1-14) is not possible for these slugs unless restrictive conditions are imposed on the form of the puff growth equations. Because of the importance of generality in the puff growth equations, the time-averaged concentrations of older slugs are determined by numerical integration of Eqn. (2.1-14). As discussed in the next subsection, this integration can be accomplished at reasonable computation cost. Figure 2.1-5 shows the result of such integral averaging for the situation where the Figure 2.1-4 "snapshots" depict the start and end slug states of the averaging period.

The above development also ignores the effect of loss or production mechanisms; however, this can be handled in much the same "linearized" manner that MESOPUFF II invokes. This is accomplished by allowing the effective emission rate, q, to vary linearly over time as

$$q(t) = q_b + (q_e - q_b)\cdot(t/\Delta t_s) \qquad (2.1\text{-}21)$$

where q_b is the effective emission rate for the slug at the beginning of the time step (n.b., $q_b = q$ for fresh emissions),

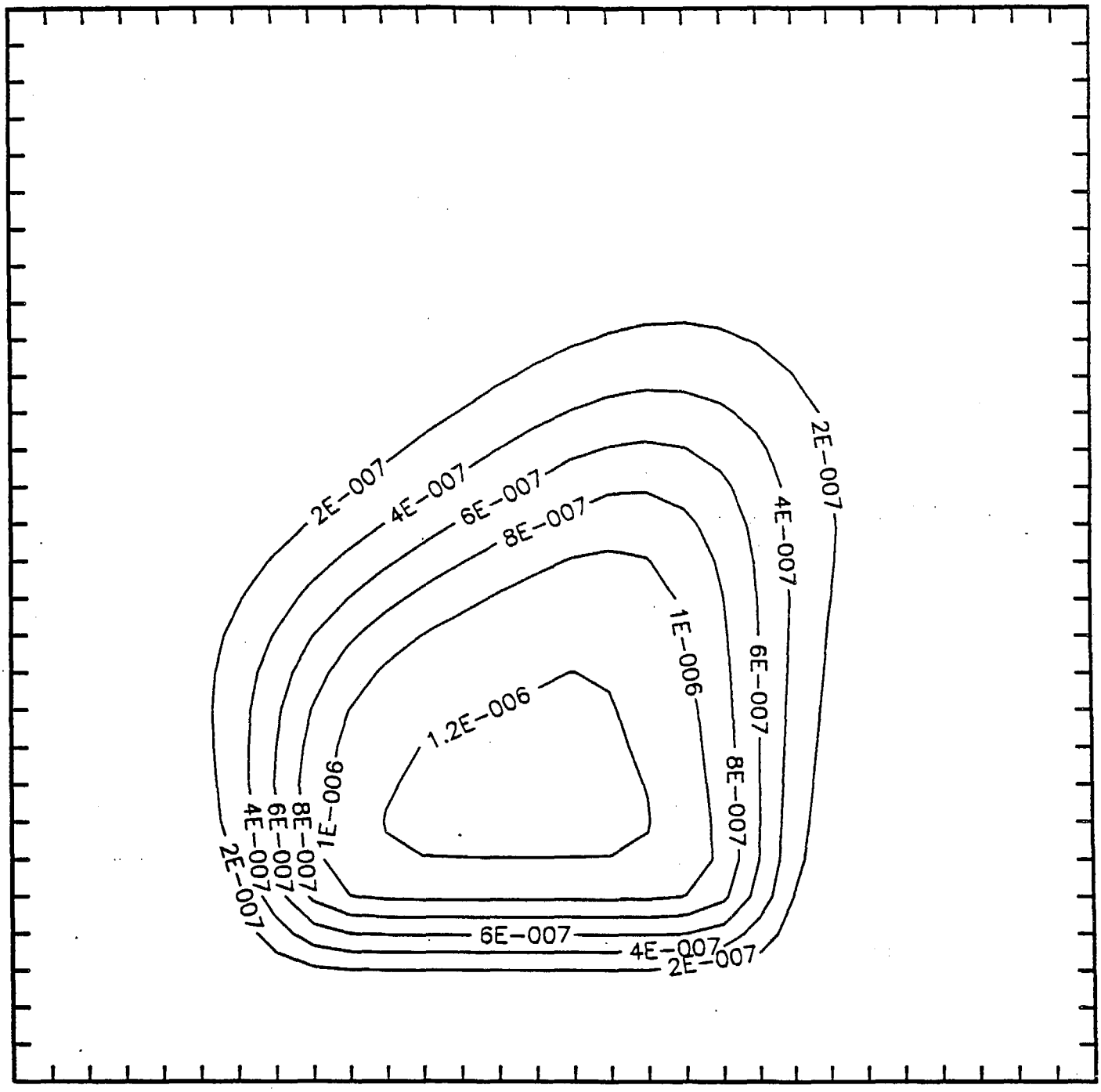

Figure 2.1-5 Receptor-time averaged concentrations resulting from the transport and evolution of the slug depicted in Figure 2.1-4 from its initial (left "snapshot") to final (right "snapshot") state. The tick marks on the border suggest the 2-d mesh of receptors considered.

q_e is the effective emission rate including loss or production which occurs during the time step, and

Δt_s is the duration of the time step.

The variable ξ is also the function

$$\xi = \frac{d_{a2} - u\Delta t_s \cdot (t/\Delta t_s)}{\sqrt{2}\sigma_y} \qquad (2.1\text{-}22)$$

of the dimensionless time variable $t/\Delta t_s$, where $0 \le t/\Delta t_s \le 1$, such that

$$\xi = \xi_b + (\xi_e - \xi_b)\cdot(t/\Delta t_s), \qquad (2.1\text{-}23)$$

and the causality function becomes

$$F(\xi) = \frac{1}{2}\{\mathrm{erf}(\phi_2) - \mathrm{erf}(\xi)\} \qquad (2.1\text{-}24)$$

Thus, the time averaging process yields

$$\bar{C} = \frac{g}{\sqrt{2\pi}u'\sigma_y}\left\{\exp\left[\frac{-d_c^2}{2\sigma_y^2}\cdot\frac{u^2}{u'^2}\right]\right\}\left\{q_b F_o + (q_e - q_b)F_1\right\} \qquad (2.1\text{-}25)$$

where F_o is just $\bar{F}$ from Eqn. 2.1-17 and

$$F_1 = \int_o^{\Delta t_s} \frac{dt}{\Delta t_s}(t/\Delta t_s)F(t) = \frac{1}{\Delta\xi}\int_{\xi_b}^{\xi_e} d\xi \frac{\xi - \xi_b}{\Delta\xi} F(\xi) \qquad (2.1\text{-}26)$$

with $\Delta\xi \equiv \xi_e - \xi_b = \dfrac{-u\Delta t_s}{\sqrt{2}\sigma_y}$

Substituting in Eqn. (2.1-24) then yields

$$F_1 = \frac{1}{4}\mathrm{erf}(\phi_2) - \frac{1/2}{(\Delta\xi)^2}\left\{\int_{\xi_b}^{\xi_e} d\xi\ \xi\ \mathrm{erf}(\xi) - \xi_b\int_{\xi_b}^{\xi_e} d\xi \mathrm{erf}(\xi)\right\} \qquad (2.1\text{-}27)$$

where $\int dx\ \mathrm{erf}(x) = x\ \mathrm{erf}(x) + \frac{1}{\sqrt{\pi}} \exp(-x^2)$ (2.1-28)

has already been used to obtain Eqn. (2.1-17) and where

$$\int dx\ x\ \mathrm{erf}(x) = \frac{1}{2}x^2 \mathrm{erf}(x) + \frac{1}{2}\frac{x}{\sqrt{\pi}} \exp(-x^2) - \frac{1}{4}\mathrm{erf}(x) \qquad (2.1\text{-}29)$$

is a special case of the more general expression developed by Geller and Ng (1971) in terms of the generalized hypergeometric function ${}_2F_2$.

Generalizing the problem of dealing with older slugs is trivial if one deals with a numerical integration (i.e., time average) of Eqn. (2.1-14). The time dependent expression q(t) given by Eqn. (2.1-21), simply replaces q and the numerical integration proceeds.

This numerical integration process has itself received special attention because it greatly influences the computing time needs of the slug model. First, all receptors lying outside of the slug's $\pm 3\sigma_y$ envelope during the entire averaging time interval are eliminated from consideration. Second, for those receptors remaining, integration time limits are computed such that sampling is not performed when the receptor is outside of the $\pm 3\sigma_y$ envelope. As the endpoints of the slug are advected separately such that the slug may "tumble", the algebra for finding the appropriate time limits involves the roots of cubic equations, but is otherwise straightforward and is not discussed further.

Invocation of the "frozen σ" methodology (i.e., σ_y and σ_z are fixed at receptor specific values throughout the averaging time period) creates another class of situations which can be integrated analytically; however, the most general case involves indefinite integrals of the form

$$\int dt\ \exp(-\beta^2 t^2)\mathrm{erf}(a + bt), \qquad (2.1\text{-}30)$$

which defy solution except in a few simple cases (e.g., a = 0 and b = β). In fact, integrability has proven not to be the sole criteria in these slug sampling problems. For example, the preceding work on linear time variation of loss (or production) mechanisms can also be evaluated for the more realistic

exponential process; however, the analytic forms are found to be very volatile on a computer because subtraction of large numbers to obtain small numbers is required.

One tractable case involves the quite physical scenario of a slug passing rapidly over a receptor and with slug endpoints sufficiently far away that the along-slug causality factor, F(t), is time independent. In this case the causality factor also becomes fixed and can be taken outside the integral and approximated as

$$\bar{F} = \frac{1}{2}(F_b + F_e) \quad , \tag{2.1-31}$$

which is just the average of values at the beginning and end of the time step. This approximation is, however, made only if F_b and F_e are within a specified fractional tolerance of each other. A similar procedure enables one to move the vertical coupling factor, g, outside the integral and replace it with the mean value $\bar{g}$. The tolerance factor for both causality and vertical coupling coefficient variation is currently set at a conservative 0.02 (i.e., 2%). Finally the variability of the lateral coupling term,

$$Y(t) = \exp\left[-\eta(t)^2\right] \quad , \tag{2.1-32}$$

where $\eta(t) = \dfrac{d_c(t)}{\sqrt{2}\,\sigma_y} \cdot \dfrac{u}{u'}$

and $d_c(t)$ is the time dependent crosswind distance, is checked and the integrals

$$I_m = \int_0^{\Delta t_s} \frac{dt}{\Delta t_s}(t/\Delta t_s)^m \, Y(t) \tag{2.1-33}$$

evaluated for m = 0 and 1.

These integrals can be accomplished to yield

$$I_0 = \frac{\sqrt{\pi}}{2}[\mathrm{erf}(\eta_e) - \mathrm{erf}(\eta_b)]/(\eta_e - \eta_b) \tag{2.1-34}$$

and

$$I_1 = \frac{1}{2}[\exp(-\eta_b^2) - \exp(-\eta_e^2)]/(\eta_e - \eta_b)^2 \qquad (2.1\text{-}35)$$

$$- \eta_b I_0/(\eta_e - \eta_b)$$

so that the final time-averaged concentrations can be written as

$$\bar{C} = \frac{\bar{g}\,\bar{F}}{\sqrt{2\pi}\,u'\sigma_y}\left\{q_b I_0 + (q_e - q_b) I_1\right\} \qquad (2.1\text{-}36)$$

as an alternative to numerical integration for the older slugs.

Computations are also performed for the vertically integrated counterparts to Eqs. (2.1-25 and 2.1-36) as these are required for evaluation of wet removal and wet fluxes at a ground level receptor; however, Gaussian normalization dictates that this is accomplished simply by replacing g with 1.0 in Eqn. (2.1-25) or $\bar{g}$ with 1.0 in Eqn. (2.1-36).

2.1.3 Sampling Function Testing

The slug model and two versions of the integrated (circular) puff model have been subjected to several sensitivity tests in order to:

- evaluate the performance of each formulation in reproducing the known steady-state plume solution under the appropriate emission and meteorological conditions;
- demonstrate and intercompare the models' capabilities under non-steady conditions;
- assess the cost-effectiveness of the different algorithms;
- demonstrate the consistency of the circular puff/elongated slug models and the feasibility of the proposed hybrid approach.

Tables 2.1-1 (a,b) and 2.1-2 (a,b) present the plume, puff, and slug results for two sets of steady-state emission and meteorological conditions. Plume centerline values are presented at receptors from 100 m to 10 km from the source. A constant emission rate of 1 g/s from a 10 m high source is assumed. The first set of results assume neutral (D class) stability conditions with 10 m/s winds. Stable (F class) conditions with 3 m/s winds are applied in the second set of runs. Puff model #1 employs the integrated puff sampling function with trajectory mid-point values of σ_y and g. The puff release rate and sampling rate were varied from 100/hr to 500/hr for the puff model #1 simulations. Puff model #2 uses the same integrated sampling function as #1, except receptor-specific values of σ_y and g are used instead of trajectory mid-point values. The puff release rate and sampling rate in the puff model #2 runs were both 1/hr. Operationally, the slug model would employ the efficient time-integrated relationship (Eqn. 2.1-16) for the slug originating at the source; however, these concentrations will always be slightly less than the plume concentrations, but do approach them asymptotically as $\Delta t_s \rightarrow \infty$. Instead, the slug model was evaluated by considering the slugs as being "old", and both the numerical integration technique of Eq. (2.1-14) and the approximate, factored form of Eq. (2.1-36) were considered. Both of these "old" slug methods gave predictions identical to the plume model for the four significant digits displayed. (It should be noted that numerical integration was not necessary in this special case of steady-state conditions, but was performed anyway to demonstrate the more general technique and allow its evaluation in terms of its consistency with the plume solution and its cost effectiveness).

The results indicate that a large number of puffs/samples are necessary to adequately reproduce the plume solution at near-field receptors when the puff model #1 assumptions are employed. The errors are associated with the use of the trajectory mid-point values of σ_y and g. This model is optimized for source-receptor distances on scales from tens to hundreds of kilometers, and is not cost effective for application close to the source. Puff model #2, using receptor-specific dispersion coefficients and the integrated sampling function, reproduces the plume solution exactly with a computational cost less than 1% of that required for puff model #1. In fact, its CPU requirements are competitive with those needed to solve the steady-state plume equation. The CPU costs of the slug model are comparable to the plume model when the

Table 2.1-1 (a)

Comparison of Plume, Puff, and Slug Models for Steady-State Conditions

(Wind Speed: 10 m/s, Stability Class: D, Stack Height: 10 m, Unlimited Mixing Height, Emission Rate: 1 g/s)

Distance	Plume Model	Puff Model #1		
		100 puffs/hr	300 puffs/hr	500 puffs/hr
(m)	(g/m^3)	100 samp./hr	300 samp./hr	500 samp./hr
100	8.273×10^{-5}	1.266×10^{-4}	1.749×10^{-4}	9.618×10^{-5}
200	1.204×10^{-4}	1.266×10^{-4}	1.295×10^{-4}	1.306×10^{-4}
300	8.270×10^{-5}	1.288×10^{-4}	8.341×10^{-5}	7.929×10^{-5}
400	5.711×10^{-5}	3.164×10^{-5}	5.183×10^{-5}	5.682×10^{-5}
500	4.145×10^{-5}	3.693×10^{-5}	3.976×10^{-5}	4.176×10^{-5}
600	3.144×10^{-5}	3.733×10^{-5}	3.212×10^{-5}	3.145×10^{-5}
700	2.469×10^{-5}	3.189×10^{-5}	2.529×10^{-5}	2.467×10^{-5}
800	1.995×10^{-5}	1.559×10^{-5}	2.002×10^{-5}	1.995×10^{-5}
900	1.648×10^{-5}	1.658×10^{-5}	1.644×10^{-5}	1.648×10^{-5}
1000	1.387×10^{-5}	1.654×10^{-5}	1.394×10^{-5}	1.393×10^{-5}
2000	4.863×10^{-6}	4.871×10^{-6}	4.853×10^{-6}	4.856×10^{-6}
3000	2.616×10^{-6}	2.613×10^{-6}	2.614×10^{-6}	2.612×10^{-6}
4000	1.702×10^{-6}	1.704×10^{-6}	1.699×10^{-6}	1.698×10^{-6}
5000	1.219×10^{-6}	1.219×10^{-6}	1.217×10^{-6}	1.217×10^{-6}
6000	9.284×10^{-7}	9.280×10^{-7}	9.270×10^{-7}	9.268×10^{-7}
7000	7.374×10^{-7}	7.372×10^{-7}	7.364×10^{-7}	7.359×10^{-7}
8000	6.040×10^{-7}	6.029×10^{-7}	6.023×10^{-7}	6.022×10^{-7}
9000	5.066×10^{-7}	5.060×10^{-7}	5.055×10^{-7}	5.053×10^{-7}
10000	4.329×10^{-7}	4.326×10^{-7}	4.324×10^{-7}	4.321×10^{-7}
Compaq-286 CPU time (s)	1.0	249.4	2054.3	5592.4

Table 2.1-1 (b)

Comparison of Plume, Puff, and Slug Models for Steady-State Conditions

(Wind Speed: 10 m/s, Stability Class: D, Stack Height: 10 m, Unlimited Mixing Height, Emission Rate: 1 g/s)

		CALPUFF MODULES	
Distance (m)	Plume Model (g/m^3)	Integrated* Puff Model (g/m^3)	Slug Model* (g/m^3)
100	8.273×10^{-5}	8.273×10^{-5}	8.273×10^{-5}
200	1.204×10^{-4}	1.204×10^{-4}	1.204×10^{-4}
300	8.270×10^{-5}	8.270×10^{-5}	8.270×10^{-5}
400	5.711×10^{-5}	5.711×10^{-5}	5.711×10^{-5}
500	4.145×10^{-5}	4.145×10^{-5}	4.145×10^{-5}
600	3.144×10^{-5}	3.144×10^{-5}	3.144×10^{-5}
700	2.469×10^{-5}	2.469×10^{-5}	2.469×10^{-5}
800	1.995×10^{-5}	1.995×10^{-5}	1.995×10^{-5}
900	1.648×10^{-5}	1.648×10^{-5}	1.648×10^{-5}
1000	1.387×10^{-6}	1.387×10^{-6}	1.387×10^{-6}
2000	4.863×10^{-6}	4.863×10^{-6}	4.863×10^{-6}
3000	2.616×10^{-6}	2.616×10^{-6}	2.616×10^{-6}
4000	1.702×10^{-6}	1.702×10^{-6}	1.702×10^{-6}
5000	1.219×10^{-6}	1.219×10^{-6}	1.219×10^{-6}
6000	9.284×10^{-7}	9.284×10^{-7}	9.284×10^{-7}
7000	7.374×10^{-7}	7.374×10^{-7}	7.374×10^{-7}
8000	6.040×10^{-7}	6.040×10^{-7}	6.040×10^{-7}
9000	5.066×10^{-7}	5.066×10^{-7}	5.066×10^{-7}
0000	4.329×10^{-7}	4.329×10^{-7}	4.329×10^{-7}
Compaq-286 CPU time (s)	1.0	1.8	1.2-5.7

* Same as plume model to four places of accuracy.

Table 2.1-2 (a)

Comparison of Plume, Puff, and Slug Models for Steady-State Conditions

(Wind Speed: 5 m/s, Stability Class: F, Stack Height: 10 m, Unlimited Mixing Height, Emission Rate: 1 g/s)

Distance	Plume Model	Puff Model #1		
		100 puffs/hr	300 puffs/hr	500 puffs/hr
(m)	(g/m^3)	100 samp./hr	300 samp./hr	500 samp./hr
100	6.495×10^{-7}	1.379×10^{-7}	1.379×10^{-7}	5.814×10^{-5}
200	1.017×10^{-4}	1.823×10^{-4}	1.159×10^{-4}	1.018×10^{-4}
300	2.075×10^{-4}	1.869×10^{-4}	2.033×10^{-4}	2.046×10^{-4}
400	2.255×10^{-4}	2.171×10^{-4}	2.313×10^{-4}	2.242×10^{-4}
500	2.076×10^{-4}	2.234×10^{-4}	2.027×10^{-4}	2.078×10^{-4}
600	1.816×10^{-4}	1.733×10^{-4}	1.818×10^{-4}	1.813×10^{-4}
700	1.567×10^{-4}	1.736×10^{-4}	1.575×10^{-4}	1.566×10^{-4}
800	1.357×10^{-4}	1.337×10^{-4}	1.351×10^{-4}	1.355×10^{-4}
900	1.184×10^{-4}	1.197×10^{-4}	1.185×10^{-4}	1.183×10^{-4}
1000	1.042×10^{-5}	1.062×10^{-5}	1.041×10^{-5}	1.040×10^{-5}
2000	4.154×10^{-5}	4.135×10^{-5}	4.153×10^{-5}	4.154×10^{-5}
3000	2.397×10^{-5}	2.401×10^{-5}	2.398×10^{-5}	2.394×10^{-5}
4000	1.644×10^{-5}	1.644×10^{-5}	1.641×10^{-5}	1.641×10^{-5}
5000	1.224×10^{-6}	1.224×10^{-6}	1.223×10^{-6}	1.222×10^{-6}
6000	9.612×10^{-6}	9.609×10^{-6}	9.592×10^{-6}	9.594×10^{-6}
7000	7.830×10^{-6}	7.832×10^{-6}	7.822×10^{-6}	7.818×10^{-6}
8000	6.596×10^{-6}	6.584×10^{-6}	6.581×10^{-6}	6.580×10^{-6}
9000	5.669×10^{-6}	5.661×10^{-6}	5.659×10^{-6}	5.658×10^{-6}
10000	4.950×10^{-6}	4.945×10^{-6}	4.939×10^{-6}	4.940×10^{-6}
Compaq-286 CPU time (s)	1.1	309.8	2566.7	7049.5

Table 2.1-2 (b)
Comparison of Plume, Puff, and Slug Models for Steady-State Conditions

(Wind Speed: 5 m/s, Stability Class: F, Stack Height: 10 m,
Unlimited Mixing Height, Emission Rate: 1 g/s)

		CALPUFF MODULES	
Distance (m)	Plume Model (g/m^3)	Integrated* Puff Model (g/m^3)	Slug Model* (g/m^3)
100	6.495×10^{-7}	6.495×10^{-7}	6.495×10^{-7}
200	1.017×10^{-4}	1.017×10^{-4}	1.017×10^{-4}
300	2.075×10^{-4}	2.075×10^{-4}	2.075×10^{-4}
400	2.255×10^{-4}	2.255×10^{-4}	2.255×10^{-4}
500	2.076×10^{-4}	2.076×10^{-4}	2.076×10^{-4}
600	1.816×10^{-4}	1.816×10^{-4}	1.816×10^{-4}
700	1.567×10^{-4}	1.567×10^{-4}	1.567×10^{-4}
800	1.357×10^{-4}	1.357×10^{-4}	1.357×10^{-4}
900	1.184×10^{-4}	1.184×10^{-4}	1.184×10^{-4}
1000	1.042×10^{-4}	1.042×10^{-4}	1.042×10^{-4}
2000	4.154×10^{-5}	4.154×10^{-5}	4.154×10^{-5}
3000	2.397×10^{-5}	2.397×10^{-5}	2.397×10^{-5}
4000	1.644×10^{-5}	1.644×10^{-5}	1.644×10^{-5}
5000	1.224×10^{-5}	1.224×10^{-5}	1.224×10^{-5}
6000	9.612×10^{-6}	9.613×10^{-6}	9.613×10^{-6}
7000	7.830×10^{-6}	7.830×10^{-6}	7.830×10^{-6}
8000	6.596×10^{-6}	6.596×10^{-6}	6.596×10^{-6}
9000	5.669×10^{-6}	5.669×10^{-6}	5.669×10^{-6}
10000	4.950×10^{-6}	4.950×10^{-6}	4.950×10^{-6}
Compaq-286 CPU time (s)	1.1	1.5	1.3-5.7

* Same as plume model to four places of accuracy.

analytic form is used, but is somewhat more costly than puff model #2 when the 40 iteration, numerical solver is selected. Additional test runs of the puff and slug models under a range of different meteorological conditions produced similar results.

The slug and puff (#2) models were also used to simulate a case of non-steady emissions. An emission rate of 1 g/s for a duration of one hour was modeled. Although a one-hour release was used in this demonstration run, either model is capable of handling arbitrary variations in emission rates, including those on time scales of less than one hour. B stability, 1 m/s winds were the assumed meteorological conditions. The results are presented in Figures 2.1-6 and 2.1-7 along with the steady-state plume solution. The puff and slug model results intercompare well (within a few percent, except at the tails of the distribution with very low concentration values). The puff/slug predictions approach the steady-state results when the center of the pollutant cloud passes the receptor, but clearly show the causality and edge effects of the approaching/passing distribution. The puff model lumps the pollutant mass into n packets (puffs), each with 1/n of the total emission (n = 100 in this test). The mass actually release from time t=0 to t=dt/n is packaged into the puff released at t=0. The puff lumping effect tends to result in a slightly premature arrival/departure of the pollutant, which is not seen in the case of steady emissions. In the non-steady runs, because the correct puff causality is obtained by increasing the puff release rate, the slug model is more computationally efficient.

In order to provide a cost-effective sampling scheme for a range of meteorological, emission, and source-receptor configurations, a hybrid circular puff/elongated slug scheme is proposed. The model will store information on the trailing endpoint of the emission cloud (required for the slug model) in addition to the data describing the leading edge (used in both the puff and slug models), at least initially, when the ratio $s_y/(u\ dt_e)$ is small. In the far-field, the initial elongation of the slug becomes unimportant, and puff sampling is nearly always the most efficient. For near-field receptors, however, if the emission rate changes rapidly, or a large wind direction change results in advection of a slug segment at a large angle to its long axis, the slug model is more cost effective. Therefore, internal checks will be performed to a select the most appropriate sampling

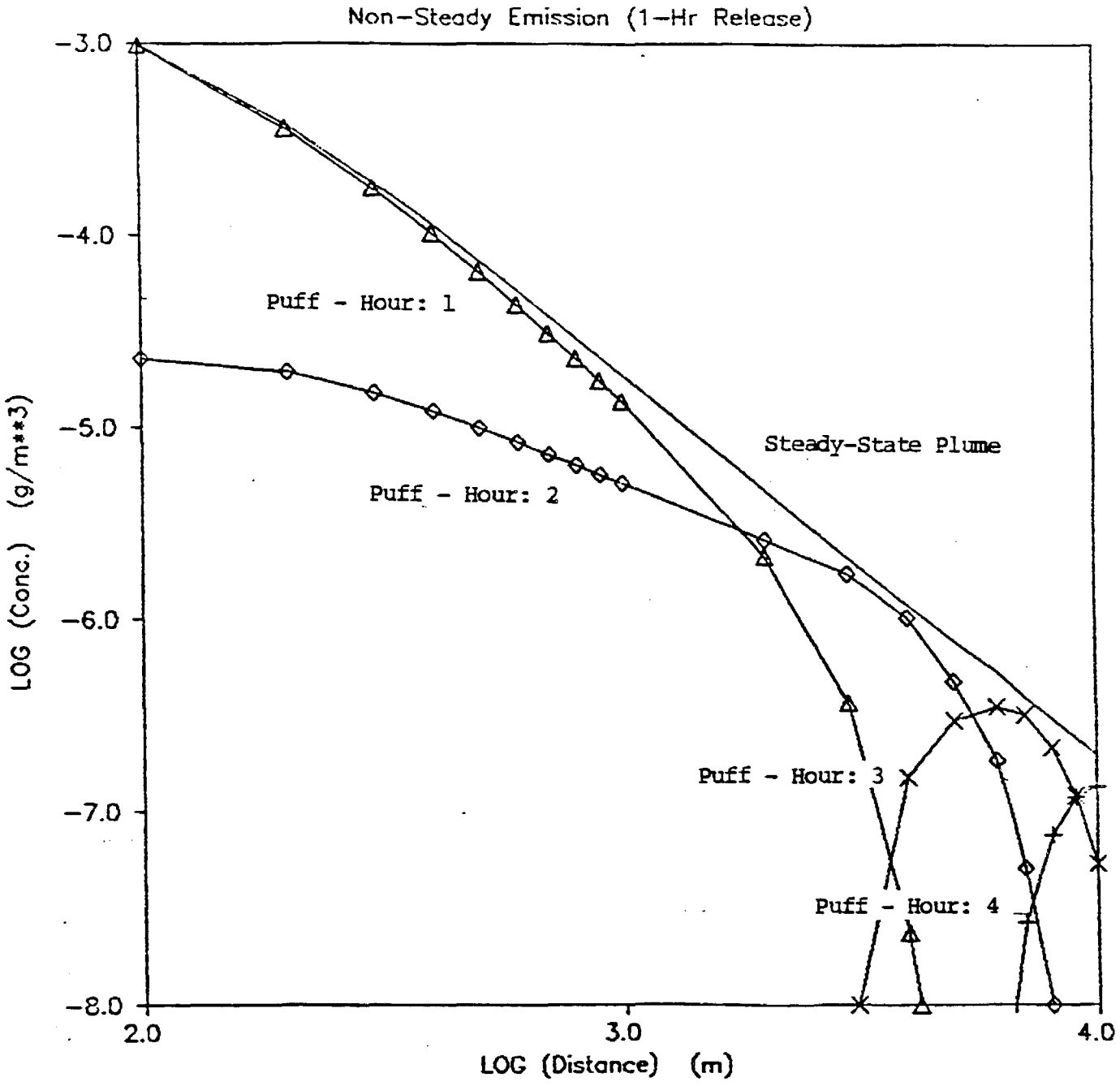

Figure 2.1-6. Concentration predictions of puff model #2 for non-steady emission conditions. Emission rate: 1 g/s, Emission duration: 1 hour, Wind speed: 1 m/s, Stability class: B, Stack height: 10 m, Mixing height: unlimited.

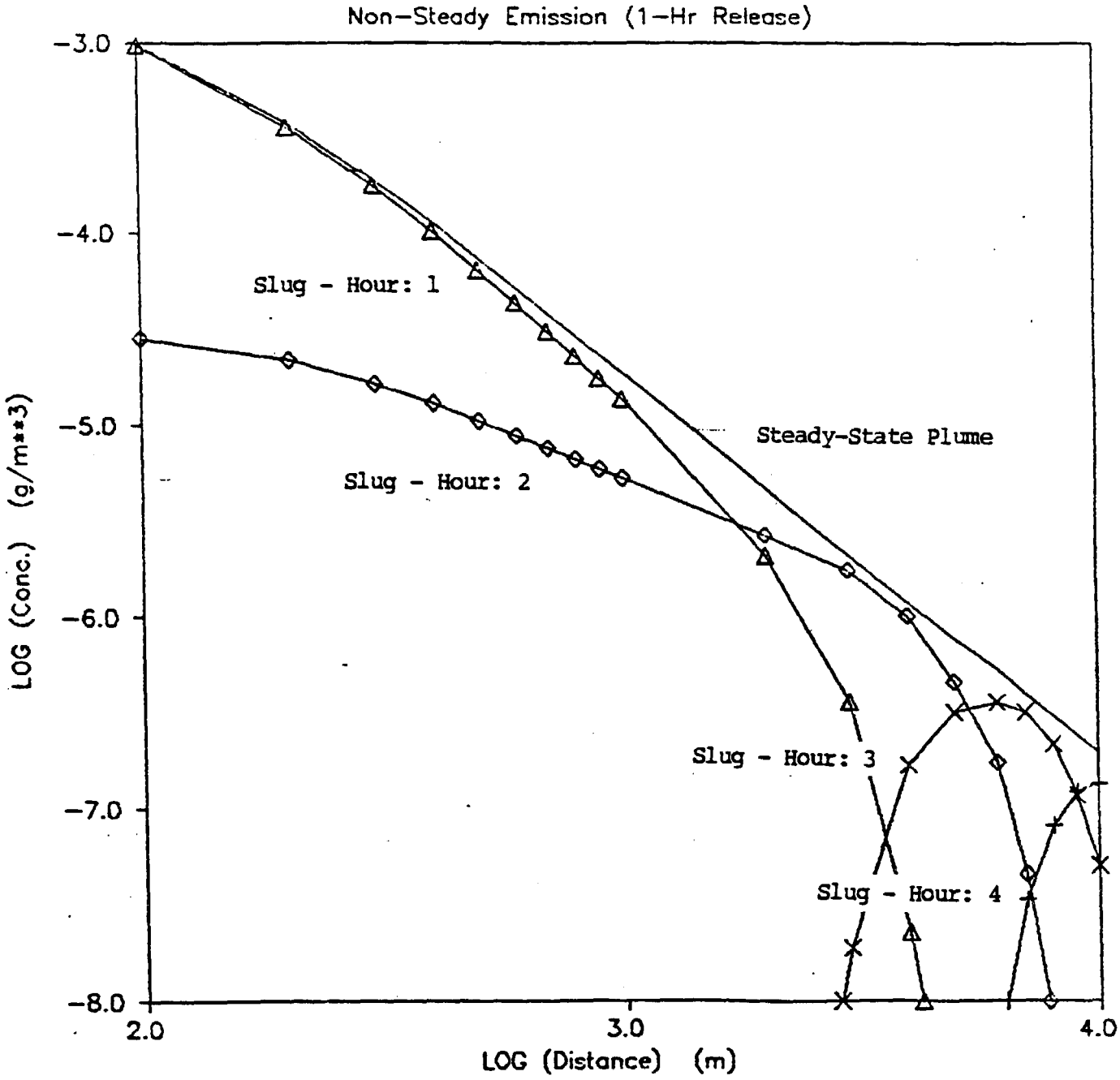

Figure 2.1-7. Concentration predictions of the slug model for non-steady emission conditions. Emission rate: 1 g/s, Emission duration: 1 hour, Wind speed: 1 m/s, Stability class: B, Stack height: 10 m, Mixing height: unlimited.

scheme. Although an all-slug or all-puff model could be engineered to produce appropriate results under all conditions, this hybrid approach, which takes advantage of the strengths of each algorithm, can produce the same results at lower computational cost.

2.2 Dispersion Coefficients

A key modeling consideration is the specification of the horizontal and vertical Gaussian dispersion coefficients, σ_y and σ_z. The dispersion coefficients n time steps from the source each consist of a number of different components:

$$\sigma_{y,n}^2 = \sigma_{yt}^2(\xi_{n-1} + \Delta\xi) + \sigma_{ys}^2 + \sigma_{yb}^2 \qquad (2.2\text{-}1)$$

where ξ_{n-1} is defined implicitly by the relation $\sigma_{yt}(\xi_{n-1}) = \sigma_{y,n-1}$ and ξ_o is defined implicitly by the relation $\sigma_{yt}^2(\xi_o) = \sigma_{yo}^2$, and

$$\sigma_{z,n}^2 = \sigma_{zt}^2(\xi_{n-1} + \Delta\xi) + \sigma_{zb}^2, \qquad (2.2\text{-}2)$$

where $\sigma_{zt}(\xi_{n-1}) = \sigma_{z,n-1}$ defines ξ_{n-1} implicitly and $\sigma_{zt}^2(\xi_o) = \sigma_{zo}^2$ defines ξ_o implicitly, and

where $\sigma_{y,n}$ $\sigma_{z,n}$ are the total horizontal and vertical dispersion coefficients at the end of n time steps,

σ_{yt} σ_{zt} are the functional forms of the components (m) of σ_y and σ_z due to atmospheric turbulence,

σ_{yb} σ_{zb} are the components (m) of σ_y and σ_z due to plume buoyancy,

σ_{yo} σ_{zo} are the initial values (m) of σ_y and σ_z due to the nature of the source (e.g., area source) or the rapid initial dilution associated with building downwash of point sources,

σ_{ys} is the component of the horizontal dispersion coefficient (m) due to vertical wind shear effects,

ξ_{n-1} is the pseudo-value based on the previous time step's total sigma,

$\Delta\xi$ is the incremental transport distance or time variable, and,

ξ_o is the initial pseudo-value of this variable and is defined implicitly and separately for y and z.

Thus, quadratic addition of initial dispersion components is assumed, but subsequent growth of the puff or slug is accomplished using the

pseudo-distance or pseudo-transport time approach. This pseudo-variable approach is necessary if current puff growth is to be dependent only on the current size of the puff and not on how it reached that size.

2.2.1 Atmospheric Turbulence Components

The basic strategy in the design of the dispersion module is to allow the use of the most refined data available in the calculation of σ_{yt} and σ_{zt} while providing for backup algorithms not requiring specialized data for situations in which these data are not available. Three levels of input data will be allowed:

(1) Direct measurements of turbulence, σ_v and σ_w, (Option 1)

(2) Micrometeorological scaling parameters u_*, w_*, L, and h, from CALMET or other meteorological model yielding internally computed estimates of the crosswind and vertical components of turbulence based on similarity theory, (Option 2), or

(3) Pasquill-Gifford-Turner (PGT) class and user choice of either ISC dispersion coefficients (Option 3) or the MESOPUFF II implementation of PGT rural dispersion coefficients (Option 4).

The general forms of σ_{yt} and σ_{zt} (Hanna et al., 1977) for Options (1) and (2) are:

$$\sigma_{yt} = \sigma_v \; t \; f_y(t/t_{ly}) \qquad (2.2\text{-}3)$$

$$\sigma_{zt} = \sigma_w \; t \; f_z(t/t_{lz}) \qquad (2.2\text{-}4)$$

where, σ_v is the standard deviation (m/s) of the horizontal crosswind component of the wind,

σ_w is the standard deviation (m/s) of the vertical component of the wind,

t is the travel time (s) of the plume to the receptor, and,

t_{ly}, t_{lz} are the horizontal and vertical Lagrangian time scales (s).

Equations (2.2-3) and (2.2-4) can be expressed in terms of the horizontal and vertical components (i_y and i_z) of the turbulence intensity using the following relationships.

$$i_y = \sigma_v/u \simeq s_\theta \qquad (2.2\text{-}5)$$

$$i_z = \sigma_w/u \simeq s_\phi \qquad (2.2\text{-}6)$$

where, u is the wind speed (m/s),

s_θ is the standard deviation (m/s) of the horizontal wind angle, and,

s_ϕ is the standard deviation (m/s) of the vertical wind angle.

The most desirable approach is to relate the dispersion coefficients directly to the measured turbulence velocity variances (σ_v and σ_w) or intensity components (i_y and i_z). However, it is important that the quality of the observational data be considered in the selection of the method for computing the dispersion coefficients. For example, inaccurate observations of i_z, which is difficult to measure, may lead to less accurate modeling results that predictions based on more routine data. It is recommended that the default selection be Option 2, which uses similarity theory and micrometeorological variables derived from routinely available meteorological observations and surface characteristics. Many laboratory experiments, field studies, and numerical simulations (e.g., Deardorff and Willis, 1975; Caughey, 1981; Lamb, 1981) have shown the importance and utility of convective scaling in the convective boundary layer. Convective scaling has been successfully applied to data collected at a wide variety of sites, including oceans, rural land surfaces (e.g., Hicks, 1985) and urban areas (Ching et al., 1983). Similarly, in the stable boundary layer, local scaling has been shown to apply (e.g., Hunt, 1982; Nieuwstadt, 1984). The micrometeorological model, (see Section 4) explicitly relates the aerodynamic and thermal characteristics of the surface to the sensible heat flux and momentum transfer rates that are used in the computation of the dispersion coefficients.

Weil (1985) and Briggs (1985) provide reviews on the use of similarity theory in diffusion models. In the convective boundary layer, Weil describes the turbulence characteristics in three layers:

(1) Surface layer - $z \leq 0.1\ h$ - σ_v ~ constant with height,
σ_w increases with height

(2) Mixed layer - $0.1h < z < 0.8h$ - σ_v ~ constant with height,
σ_w ~ constant with height

(3) Entrainment layer - $z > 0.8h$ - σ_v decreases with height,
σ_w decreases with height.

In the surface layer, Panofsky et al. (1977) propose the following relations.

$$\sigma_v = u_* \left[4 + 0.6(-h/L)^{2/3}\right]^{1/2} \qquad (2.2\text{-}7)$$

$$\sigma_w = u_* \left[1.6 + 2.9(-z/L)^{2/3}\right]^{1/2} \qquad (2.2\text{-}8)$$

where u_* is the surface friction velocity (m/s), and
L is the Monin-Obukhov length (m).

Hicks (1985) suggests the following for the mixed layer (0.1 to 0.8 h).

$$\sigma_v = \left(3.6\ u_*^2 + 0.35\ w_*^2\right)^{1/2} \qquad (2.2\text{-}9)$$

$$\sigma_w = \left(1.2\ u_*^2 + 0.35\ w_*^2\right)^{1/2} \qquad (2.2\text{-}10)$$

In the neutral boundary layer, Arya (1984) reports monotonically decreasing values of σ_v and σ_w throughout the mixed layer. Using Blackadar and Tennekes (1968) relationship for the neutral boundary layer height, Arya's results can be expressed as:

$$\sigma_v = 1.8 \exp(-0.9\ z/h) \qquad (2.2\text{-}11)$$

$$\sigma_w = 1.3 \exp(-0.9\ z/h) \qquad (2.2\text{-}12)$$

In the stable boundary layer, Nieuwstadt (1984) finds that σ_v and σ_w bear constant ratios with the local friction velocity.

$$\sigma_v/u_{*1} = C_v \qquad (2.2\text{-}13)$$

$$\sigma_w/u_{*1} = C_w \qquad (2.2\text{-}14)$$

where u_{*1} is the local friction velocity (m/s), and,
C_v and C_w are constants.

Hanna et al. (1986) suggest that $C_v \simeq 1.6$. C_w has a value $\simeq 1.3$ (Nieuwstadt, 1984). The local friction velocity, u_{*1}, can be expressed (Nieuwstadt, 1984) as:

$$u_{*1} = u_* (1 - z/h)^{3/4} \qquad (2.2\text{-}15)$$

The modeling requires a formulation that yields the proper values and vertical variations for σ_v and σ_w in the convective, neutral, and stable limits, and one that provides a mechanism for interpolating the results for intermediate conditions without physically unrealistic discontinuities. The following equations for the neutral-convective boundary layer are based on the data discussed above and satisfy these conditions. The formulation for the entrainment layer is based on data reported by Caughey (1982).

Surface Layer: $z \leq 0.1\ h$ $\qquad (L \leq 0)$

$$\sigma_v = \left[4\ u_*^2\ a_n^2 + 0.35\ w_*^2\right]^{1/2} \qquad (2.2\text{-}18)$$

$$\sigma_w = \left[1.6\ u_*^2\ a_n^2 + 2.9\ u_*^2\ (-z/L)^{2/3}\right]^{1/2} \qquad (2.2\text{-}19)$$

$$a_n = \exp\left[-0.9(z/h)\right] \qquad (2.2\text{-}20)$$

Mixed-Layer: $z = 0.1\text{-}0.8\ h$ $\qquad (L \leq 0)$

$$\sigma_v = \left[4\ u_*^2\ a_n^2 + 0.35\ w_*^2\right]^{1/2} \qquad (2.2\text{-}21)$$

$$\sigma_w = \left[1.15\ u_*^2\ a_n^2 + 0.35\ w_*^2\right]^{1/2} \qquad (2.2\text{-}22)$$

Entrainment Layer: $z > 0.8\ h$ $(L \leq 0)$

$$\sigma_v = \left[4\ u_*^2\ a_n^2 + 0.35\ w_*^2\right]^{1/2} \qquad (2.2\text{-}23)$$

for $z = 0.8$ to $1.0\ h$

$$\sigma_w = \left[1.15\ u_*^2\ a_n^2 + a_{c1}\ 0.35\ w_*^2\right]^{1/2} \qquad (2.2\text{-}24)$$

$$a_{c1} = \left[1/2 + (h-z)/(0.4h)\right] \qquad (2.2\text{-}25)$$

for $z = 1.0$ to $1.2\ h$

$$\sigma_w = \left[1.15\ u_*^2\ a_n^2 + a_{c2}\ 0.35\ w_*^2\right]^{1/2} \qquad (2.2\text{-}26)$$

$$a_{c2} = \left[1/3 + (1.2h-z)/(1.2h)\right] \qquad (2.2\text{-}27)$$

In the neutral-stable boundary layer, the following equations can be used to interpolate vertical profiles of σ_v and σ_w as a function of stability. As with the neutral-convective equations, they provide the proper values in the appropriate stability limits.

$$\sigma_v = u_* \left[\left(1.6\ C_s\ (z/L) + 1.8\ a_n\right)/(1 + z/L)\right] \qquad (L > 0) \qquad (2.2\text{-}28)$$

$$\sigma_w = 1.3\ u_* \left[\left(C_s\ (z/L) + a_n\right)/(1 + z/L)\right] \qquad (L > 0) \qquad (2.2\text{-}29)$$

$$C_s = (1 - z/h)^{3/4} \qquad (L > 0) \qquad (2.2\text{-}30)$$

In order to provide for non-zero plume growth rates above the mixing height and to prevent numerical problems associated with near-zero plume dimensions, minimum σ_v and σ_w values will be applied. Hanna et al. (1986) suggest an appropriate minimum one-hour average σ_v value is $\simeq 0.5$ m/s. This is significantly higher than σ_v expected based on PGT E and F stability curves. Appropriate default minimum values for σ_v and σ_w can be input by the user.

Equation (2.2-18) to (2.2-27) have been tested with the original data providing the basis for the Panofsky et al. (1977) and Hicks (1985) formulations. The results (summarized in Table 2.2-1) indicate that the modified equations compare well with the original equations and the observational data. The modified equations have the advantage of allowing a smooth and continuous transition to the neutral stability results of Arya (1984).

Irwin (1983) has evaluated several schemes for determining the f_y and f_z functions. It was concluded that a parameterization suggested by Draxler (1976) performed best overall.

$$f_y = \left[1 + 0.9\ (t/1000)^{1/2}\right]^{-1} \qquad (2.2\text{-}31)$$

$$f_z = \begin{cases} \left[1 + 0.9\ (t/500)^{1/2}\right]^{-1} & L < 0 \qquad (2.2\text{-}32) \\ \left[1 + 0.945\ (t/100)^{.806}\right]^{-1} & L > 0 \qquad (2.2\text{-}33) \end{cases}$$

At longer transport distances (e.g., > 10 km), an option is provided to switch to the Heffter (1965) equations (i.e., $\sigma_{yt} \simeq t$, $\sigma_{zt} \simeq t^{1/2}$).

The user may also wish to have puff growth determined on the basis of gridded input fields of PGT class. The approach is particularly useful if one is trying to compare the modeling results with steady-state regulatory model predictions or attempting to achieve compatibility with regulatory requirements. The user may select either ISC model (U.S. EPA, 1987) dispersion methodology (Option 3) or the MESOPUFF II (Scire et al., 1984) implementation of the PGT dispersion curves (Option 4).

Option 3 also requires the specification of gridded land use type, which in turn determines whether the ISC "rural" or "urban" dispersion curves are used. The "rural" dispersion equations and parameters are presented in Tables 2.2-2 and 2.2-3 for σ_y and σ_z respectively and are based on parameterizations of the PGT curves. The "urban" dispersion equations and parameter values are based on Briggs' (as reported in Gifford, 1976) parameterizations of the St.

Table 2.2-1

Comparison of Panofsky et al. (1977)/Hicks (1985)
σ_v, σ_w Formulations with Equations 2.2-(18-27)

Panofsky et al. data	Observed σ_v vs. Panofsky	Observed σ_v vs. Eqns. 2.2-(18-27)	Panofsky σ_v vs. Eqns. 2.2-(18-27)
Average	(1.14, 1.20)	(1.14, 1.21)	(1.20, 1.21)
Corr. Coef.	.81	.84	.992
Average Bias	.07	.07	.00
Average Abs. Error	.10	.09	.02
RMSE	.13	.12	.02

Hicks 1985 data	Observed σ_v vs. Hicks	Observed σ_v vs. Eqns. 2.2-(18-27)	Hicks σ_v vs. Eqns. 2.2-(18-27)
Average	(1.17, 1.12)	(1.17, 1.06)	(1.12, 1.06)
Corr. Coef.	.79	.77	.998
Average Bias	-.05	-.11	.06
Average Abs. Error	.20	.23	.06
RMSE	.27	.30	.08

Hicks 1985 data	Observed σ_w vs. Hicks	Observed σ_w vs. Eqns. 2.2-(18-27)	Hicks σ_w vs. Eqns. 2.2-(18-27)
Average	(.98, 1.01)	(.98, .98)	(1.01, .98)
Corr. Coef.	.91	.91	.998
Average Bias	.03	.00	-.03
Average Abs. Error	.12	.11	.03
RMSE	.15	.14	.04

Table 2.2-2

Parameters Used to Calculate Pasquill-Gifford σ_y *

Pasquill Stability Category	σ_y (meters) = 465.11628 (x) tan (TH) ** TH = 0.017453293 (c - d ln x)	
	c	d
A	24.1670	2.5334
B	18.3330	1.8096
C	12.5000	1.0857
D	8.3330	0.72382
E	6.2500	0.54287
F	4.1667	0.36191

* Source: U.S. EPA (1987).

** Where σ_y is in meters and x is in kilometers.

Table 2.2-3

Parameters Used to Calculate Pasquill-Gifford σ_z *

Pasquill Stability Category	x (km)	σ_z (meters) = a x^b	
		c	d
A***	< .10	122.800	0.94470
	0.10 - 0.15	158.080	1.05420
	0.16 - 0.20	170.220	1.09320
	0.21 - 0.25	179.520	1.12620
	0.26 - 0.30	217.410	1.26440
	0.31 - 0.40	258.890	1.40940
	0.41 - 0.50	346.750	1.72830
	0.51 - 3.11	453.850	2.11660
	>3.11	**	**
B***	< .20	90.673	0.93198
	0.21 - 0.40	98.483	0.98332
	> 0.40	109.300	1.09710
C***	All	61.141	0.91465
D	< .30	34.459	0.86974
	0.31 - 1.00	32.093	0.81066
	1.01 - 3.00	32.093	0.64403
	3.01 - 10.00	33.504	0.60486
	10.01 - 30.00	36.650	0.56589
	> 30.00	44.053	0.51179

* Source: U.S. EPA (1987).

*** If the calculated value of σ_z exceeds 5000 m, σ_z is set to 5000 m.

Table 2.2-3
(Continued)

Parameters Used to Calculate Pasquill-Gifford σ_z*

Pasquill Stability Category	x (km)	σ_z (meters) = a x^b c	d
E	< .10	24.260	0.83660
	0.10 - 0.30	23.331	0.81956
	0.31 - 1.00	21.628	0.75660
	1.01 - 2.00	21.628	0.63077
	2.01 - 4.00	22.534	0.57154
	4.01 - 10.00	24.703	0.50527
	10.01 - 20.00	26.970	0.46713
	20.01 - 40.00	35.420	0.37615
	> 40.00	47.618	0.29592
F	< .20	15.209	0.81558
	0.21 - 0.70	14.457	0.78407
	0.71 - 1.00	13.953	0.68465
	1.01 - 2.00	13.953	0.63227
	2.01 - 3.00	14.823	0.54503
	3.01 - 7.00	16.187	0.46490
	7.01 - 15.00	17.836	0.41507
	15.01 - 30.00	22.651	0.32681
	30.01 - 60.00	27.074	0.27436
	> 60.00	34.219	0.21716

*Source: U.S. EPA (1987).

Louis dispersion data analyzed by McElroy and Pooler (1968) and are presented in Tables 2.2-4 and 2.2-5 for σ_y and σ_z respectively.

If the use of PGT stability-dependent dispersion curves is selected (Option 4), the puff growth functions are of the form:

$$\sigma_y = a_y x^{b_y} \quad (2.2\text{-}34)$$

$$\sigma_z = a_z x^{b_z} \quad (2.2\text{-}35)$$

where a_y, b_y, a_z, b_z are the stability dependent coefficients presented in Table 2.2-6.

2.2.2 Plume Buoyancy Components

The effect of plume buoyancy on the dispersion coefficients are parameterized in terms of the plume rise (Pasquill, 1976; Irwin, 1979).

$$\sigma_{yb} = \Delta H/3.5 \quad (2.2\text{-}36)$$

$$\sigma_{zb} = \Delta H/3.5 \quad (2.2\text{-}37)$$

where ΔH is the plume rise (m).

2.2.3 Initial Plume Size

The initial size of puffs emitted by area sources is determined by user-specified initial dispersion coefficients, σ_{yo} and σ_{zo}. The area source option allows the emissions from a number of smaller sources in a given area (e.g., a grid cell) to be combined into a single source. The area source emissions are immediately spread over an area described by σ_{yo} and σ_{zo}. The subsequent growth of the area source puff is computed in the same manner as the point source puffs.

Point source emissions subject to building downwash effects experience a rapid initial growth due to the high building-induced turbulence intensity in

Table 2.2-4

Briggs Formulas Used to Calculate McElroy-Pooler σ_y*

Pasquill Stability Category	σ_y (meters)**
A	$0.32 \times (1.0 + 0.0004\ x)^{-1/2}$
B	$0.32 \times (1.0 + 0.0004\ x)^{-1/2}$
C	$0.22 \times (1.0 + 0.0004\ x)^{-1/2}$
D	$0.16 \times (1.0 + 0.0004\ x)^{-1/2}$
E	$0.11 \times (1.0 + 0.0004\ x)^{-1/2}$
F	$0.11 \times (1.0 + 0.0004\ x)^{-1/2}$

*Source: U.S. EPA (1987).

**where x is in meters.

Table 2.2-5

Briggs Formulas Used to Calculate McElroy-Pooler σ_z *

Pasquill Stability Category	σ_z (meters) **
A	$0.24\ x\ (1.0 + 0.001\ x)^{+1/2}$
B	$0.24\ x\ (1.0 + 0.001\ x)^{+1/2}$
C	$0.20\ x$
D	$0.14\ x\ (1.0 + 0.0003\ x)^{-1/2}$
E	$0.08\ x\ (1.0 + 0.0015\ x)^{-1/2}$
F	$0.08\ x\ (1.0 + 0.0015\ x)^{-1/2}$

* Source: U.S. EPA (1987).

** where x is in meters.

Table 2.2-6

MESOPUFF II Growth Rate Coefficients a_y, b_y, a_z, b_z*

Stability Class	a_y	b_y	a_z	b_z
A	0.36	0.9	0.00023	2.10
B	0.25	0.9	0.058	1.09
C	0.19	0.9	0.11	0.91
D	0.13	0.9	0.57	0.58
E	0.096	0.9	0.85	0.47
F	0.063	0.9	0.77	0.42

*Source: Scire et al. (1984)

the lee of the building. A building downwash model (described in Section 2.3) is used to internally compute initial plume dimensions for downwashed point source emissions as a function of building dimensions, stack height, momentum flux, and meteorological conditions.

2.2.4 Vertical Wind Shear Component

The presence of vertical wind shear tends to enhance the effective lateral dispersion of a plume. Although operating on a continuous basis, this process can be visualized as consisting of two steps: (1) distortion of the plume by changes in the wind direction or speed with height, followed by (2) vertical mixing of the distorted plume. Through the vertical mixing process, the vertical shear enhances the lateral spread of the plume. Pasquill (1976) suggests that the crosswind spread of the plume at large downwind distances (e.g., > 20 km) can be roughly approximated as ~ 0.75 x $d\theta$, where x is the downwind distance (m), and $d\theta$ is the change in the wind direction (radians) over the entire depth of the plume. The shear-induced crosswind spread is converted to an effective standard deviation, σ_{ys}, by the Gaussian relationship 2.15 σ_{ys} = (crosswind spread half-width), or:

$$\sigma_{ys}^2 = 0.03\ (x\ d\theta)^2 \qquad (2.2\text{-}38)$$

2.3 Building Downwash

The dispersion and buoyant rise of plumes released from short stacks can be significantly modified by the presence of buildings or other obstacles to the flow. Hosker (1984) provides a description of the flow patterns in three regions near buildings. Figure 2.3-1 shows (1) a displacement zone upwind of the buildings, where the flow is influenced by the high pressure along the upwind building face, (2) a cavity zone characterized by recirculating flow, high turbulence intensity, and low mean wind speed, and (3) a turbulent wake region where the flow characteristics and turbulence intensity gradually approach the ambient values.

The parameterization of building downwash in CALPUFF is appropriate for use in the turbulent wake region and is based on the procedures used in the ISCST model. ISCST contains two building downwash algorithms:

- Huber-Snyder model (Huber and Snyder, 1976; Huber, 1977). In ISCST, this model is applied when the source height is greater than the building height (H_b) plus one-half of the lesser of the building height or projected width (L). It applies either a full building wake effect or none at all, depending on the effective height of the emitted plume.
- Schulman-Scire model (Scire and Schulman, 1980; Schulman and Hanna, 1986). This model applies a linear decay factor to the building-induced enhancement of the dispersion coefficients, accounts for the effect of downwash on plume rise, and uses wind direction-specific building dimensions. It is used in ISCST for stacks lower in height than H_b + 0.5 L.

The differences in the treatment of downwash between ISCST and CALPUFF include the following.

- The height threshold determining which model is used is an input variable. This option allows the user to apply one of the models for all stacks, which has the desirable effect of eliminating the discontinuity of the ISCST approach at stack

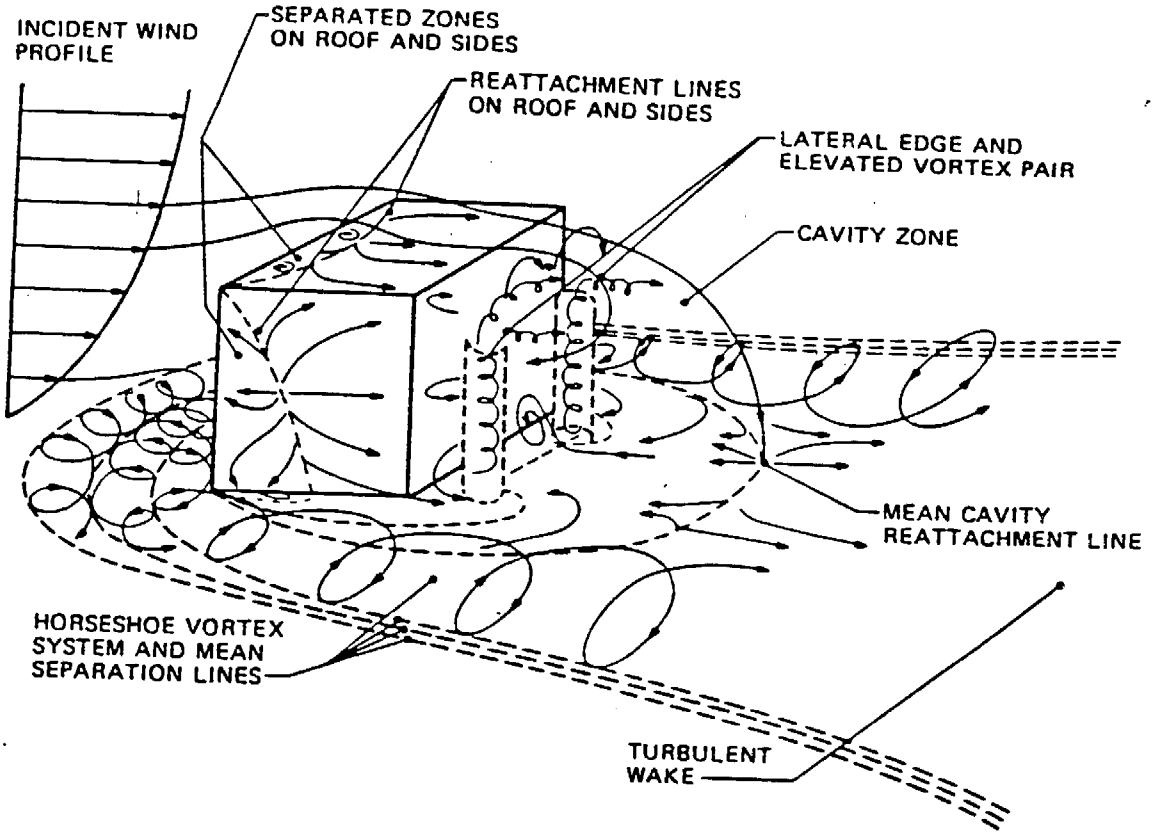

Figure 2.3-1. Flow near a sharp-edged building in a deep boundary layer. [From Hosker, (1984)]

heights of H_b + 0.5 L. Thus, in CALPUFF, the Huber-Snyder technique is used for stacks greater than $H_b + T_{bd}$ L, where T_{bd} has a default value of 0.5. A zero value of T_{bd} indicates the Huber-Snyder method is used for all stacks, and a value of 1.5 results in the Schulman-Scire method being always used.

- Wind direction specific building dimensions are allowed with the Huber-Snyder technique.

- In cases where the controlling building height varies as a function of wind direction, the model will allow the Huber-Snyder techniques to be applied for some wind directions (using wind direction specific values) and the Schulman-Scire model in other cases.

2.3.1 Huber-Snyder Downwash Procedure

If the stack height exceeds $H_b + T_{bd}L$, the Huber-Snyder algorithm is applied. The first step is to compute the effective plume height, H_e, due to momentum rise at a downwind distance of two building heights. If H_e exceeds H_b + 1.5 L (where H_b and L are the wind direction specific values), building downwash effects are assumed to be negligible. Otherwise, building-induced enhancement of the plume dispersion coefficients is evaluated. For stack heights, H_s, less than $1.2H_b$, both σ_y and σ_z are enhanced. Only σ_z is enhanced for stack heights above 1.2 H_b (but below H_b + 1.5 L).

A building is defined as a squat building if the projected building width, H_w, exceeds the building height (i.e., $H_w \geq H_b$). A tall building is defined as one for which $H_w < H_b$. Because both the controlling building height and projected width can vary with wind direction, the definition of a building as squat or tall can also vary by direction. For a squat building, the enhanced σ_z is:

$$\sigma_z' = 0.7\ H_b + 0.067\ (x - 3H_b) \qquad 3H_b < x < 10H_b \qquad (2.3\text{-}1)$$

where x is the downwind distance (in meters).

For a tall building,

$$\sigma_z' = 0.7\ H_w + 0.067\ (x - 3H_b) \qquad 3H_b < x < 10H_b \qquad (2.3\text{-}2)$$

If the ratio H_s/H_b is less than or equal to 1.2, the horizontal dispersion coefficient, σ_y, is enhanced. For a squat building with a projected width to height ratio (H_w/H_b) less than 5, the equation for σ_y is:

$$\sigma_y' = 0.35\ H_w + 0.067\ (x - 3H_b) \qquad 3H_b < x < 10H_b \qquad (2.3\text{-}3)$$

For buildings with (H_w/H_b) greater than 5, two options are provided for σ_y.

$$\sigma_y' = 0.35\ H_b + 0.067\ (x - 3H_b) \qquad 3H_b < x < 10H_b \qquad (2.3\text{-}4)$$

or,

$$\sigma_y' = 1.75\ H_b + 0.067\ (x - 3H_b) \qquad 3H_b < x < 10H_b \qquad (2.3\text{-}5)$$

Eqn. (2.3-4) results in higher centerline concentrations than Eqn. (2.3-5), and is considered as an upper bound estimate of the impacts of the source. The ISCST manual suggests that Eqn. (2.3-5) is most appropriate if the source is located within 2.5 H_b of the end of the building. Eqn. (2.3-4) is a better estimate if the source is located near the center of the building. However, in practice, the more conservative Eqn. (2.3-4) is usually used for regulatory applications regardless of the position of the stack.

For a tall building, the equation for σ_y is:

$$\sigma_y' = 0.35\ H_w + 0.067\ (x - 3H_b) \qquad 3H_b < x < 10H_b \qquad (2.3\text{-}6)$$

2.3.2 Schulman-Scire Downwash Procedure

The main features of the Schulman-Scire algorithm are that the effects of building downwash on reducing plume rise are incorporated, and the enhancement of σ_z is a gradual function of effective plume height rather than a step function. As note above, in CALPUFF, both schemes use wind direction specific building dimensions.

The plume rise equations incorporating building downwash effects are discussed in Section 2.4.4. Many studies have shown that plume rise is decreased during downwash conditions. The increased mechanical turbulence in the building wake leads to enhanced plume dispersion (reflected in the enhanced dispersion coefficients), which causes a rapid dilution of the plume. This dilution reduces the rate of rise of the plume and results in lower plume heights. As discussed in Section 2.4.4, the initially high dilution rate is modeled by applying an initial "dilution radius" to the plume. The inclusion of downwash effects in the plume rise equations is a key part of the Schulman-Scire downwash method.

The second component of the model is the linear decay function which is applied to the enhancement of σ_z. The vertical dispersion coefficient is determined as:

$$\sigma_z'' = A\,\sigma_z' \qquad (2.3\text{-}7)$$

where σ_z' is determined from Eqns. (2.3-1) and (2.3-2), and,

$$A = \begin{cases} 1 & H_e \le H_b \\ (H_b - H_e)/(2L) + 1 & H_b < H_e \le H_b + 2L \\ 0 & H_b + 2L < H_e \end{cases} \qquad (2.3\text{-}8)$$

2.4 Plume Rise

The plume rise relationships in the CALPUFF model are generalized to apply to a variety of source types and plume characteristics. The following effects are included in the plume rise algorithm:

- Plume buoyancy and momentum
- Stable atmospheric stratification
- Partial penetration of the plume into an elevated stable inversion layer
- Building downwash and stack-tip downwash effects
- Vertical wind shear

2.4.1 Basic Plume Rise Equations

The basic point source plume rise relationships are based on the Briggs (1975) equations. The plume rise due to buoyancy and momentum during neutral or unstable conditions, z_n is:

$$z_n = \left[3F_m x/(\beta_j^2 u_s^2) + 3Fx^2/(2\beta_1^2 u_s^3)\right]^{1/3} \qquad (2.4\text{-}1)$$

where F_m is the momentum flux (m^4/s^2),
F is the buoyancy flux (m^4/s^3),
u_s is the stack height wind speed (m/s),
x is the downwind distance (m),
β_1 is the neutral entrainment parameter (~ 0.6),
β_j is the jet entrainment coefficient ($\beta_j = 1/3 + u_s/w$), and,
w is the stack gas exit speed (m/s).

The distance to final plume rise, x_f, is:

$$x_f = \begin{cases} 3.5\, x^* & F > 0 \qquad (2.4\text{-}2) \\ 4D\,(W + 3u_s)^2/(u_s w) & F = 0 \qquad (2.4\text{-}3) \end{cases}$$

$$x^* = \begin{cases} 14\ F^{5/8} & F \le 55\ m^4/s^3 \quad (2.4\text{-}4) \\ 34\ F^{2/5} & F > 55\ m^4/s^3 \quad (2.4\text{-}5) \end{cases}$$

where D is the stack diameter (m).

During stable conditions, the final plume rise, z_{sf}, is determined by:

$$z_{sf} = \left[3F_m/(\beta_j^2 u_s S^{1/2}) + 6F/(\beta_2^2 u_s S)\right]^{1/3} \quad (2.4\text{-}6)$$

where β_2 is the stable entrainment parameter (~ 0.6),

S is a stability parameter $\left[(g/T_a)(d\theta/dz)\right]$,

T_a is the ambient temperature (deg. K), and,

$d\theta/dz$ is the potential temperature lapse rate (deg. K/m).

Transitional plume rise during stable conditions is computed by Eqn. (2.4-1) up to the point at which $z_n = z_{sf}$. For low wind speed and calm conditions, the following equation (Briggs, 1975) is used to compute the plume centerline rise:

$$z_{sf} = 4\ F^{1/4}/S^{3/8} \quad (2.4\text{-}7)$$

2.4.2 Stack-tip Downwash

If the ratio of the stack gas exit speed to the ambient wind speed is less than 1.5, the plume may be drawn into the lee of the stack. Briggs (1973) suggests modifying the stack height to adjust for this stack-tip effect:

$$h_s' = \begin{cases} h_s + 2D(w/u_s - 1.5) & w/u_s < 1.5 \quad (2.4\text{-}8) \\ h_s & w/u_s \ge 1.5 \quad (2.4\text{-}9) \end{cases}$$

where h_s' is the adjusted stack top height.

2.4.3 Partial Plume Penetration

During neutral and unstable conditions, the puff may penetrate into the elevated stable layer above the boundary layer. If the top of the plume $[(1 + \beta_1)z_n]$, exceeds the mixed layer height, h, the partial penetration model of Briggs (1975) is used to evaluate the effective plume height and the fraction of mass injected into the stable layer. The effective plume rise is estimated as the minimum of z_n predicted by Eqn. (2.4-1) and the following:

$$z_n = \left[1.8 z_b^{\,3} + 3F/(\beta'^{\,2} u_s S)\right]^{1/3} \qquad (2.4\text{-}10)$$

where z_b is the distance from the adjusted stack top (h_s') to the top of the mixed-layer (h), i.e., $z_b = h - h_s'$, and,

β' is an entrainment parameter (~ 0.4).

The fraction, P, of the puff's mass that penetrates into the stable layer aloft is:

$$P = \begin{cases} 0.0 & z_b/z_n \geq 1.5 \qquad (2.4\text{-}11) \\ 1.5 - z_b/z_n & 0.5 < z_b/z_n < 1.5 \qquad (2.4\text{-}12) \\ 1.0 & z_b/z_n \leq 0.5 \qquad (2.4\text{-}13) \end{cases}$$

The mass injected into the upper layer, $Q_u = P\ Q_t$, and the mass in the boundary layer is $Q_m = (1 - P)Q_t$, where Q_t is the total pollutant mass in the puff.

If the stack height exceeds the mixed-layer height, then the stable plume rise equations (2.4-6) and (2.4-7) are used to compute the plume rise.

2.4.4 Building Downwash

Wind tunnel observations of plume dispersion and plume rise indicate that plume rise can be significantly reduced by building downwash. Huber and Snyder (1982) found that during downwash conditions, plume rise was reduced by

one-third below the value obtained in the absence of the building. In an analysis of plume rise observations, Rittmann (1982) found lower plume rise than predicted by the 2/3 law (a form of Eqn. 2.4-1) for smaller sources which are most likely to be affected by downwash. Several studies (e.g., Bowers and Anderson, 1981; Scire and Schulman, 1981; Thuillier, 1982) with the original version of the ISC building downwash algorithm, which did not account for the effects of building downwash or plume rise, sometimes significantly underestimated peak concentrations during downwash conditions.

The increased mechanical turbulence in the building wake which leads to enhanced plume dispersion, causes a rapid dilution of the plume. This dilution reduces the rate of rise of the plume and leads to lower plume heights. One method of treating the initially high dilution rate is to assume an initial "dilution radius" for the plume (Scire and Schulman, 1979). This technique is incorporated in the Buoyant Line and Point Source (BLP) model (Schulman and Scire, 1980) and a modified version of the ISC model. It has been shown (Schulman and Hanna, 1986), to produce more realistic estimates of ground-level concentrations during building downwash conditions.

The plume rise of a downwashed plume with $\sigma_{yo} \leq \sigma_{zo}$ during neutral-unstable conditions is given by:

$$z_s^3 + (3R_o z_d/\beta_1 + 3R_o^2/\beta_1^2)z_d = \left[3F_m x/(\beta_j^2 u_s^2) + 3Fx^2/(2\beta_1 2u_s^3)\right] \quad (2.4\text{-}14)$$

where R_o is the dilution radius $\left[R_o = (2)^{1/2}\sigma_{zo}\right]$. The factor of $(2)^{1/2}$ converts the Gaussian dispersion coefficient into an effective top-hat distribution for the plume rise calculations.

Final stable plume rise is:

$$z_d^3 + (3R_o z_d/\beta_2 + 3R_o^2/\beta_2^2)z_d = \left[3F_m/(\beta_j^2 u_s S^{1/2}) + 6F/(\beta_2^2 u_s S)\right] \quad (2.4\text{-}15)$$

Transitional plume rise during stable conditions is computed with Eqn. (2.4-14) until the final plume height predicted by Eqn. (2.4-15) is obtained.

When horizontal mixing of the plume in the building wake causes $\sigma_{yo} > \sigma_{zo}$, it is necessary to account for the elongated shape of the plume. The

plume can be represented as a finite line source. The plume rise for a line source of length L during neutral-unstable conditions is:

$$z_d^3 + \left[3L/(\pi\beta_1)\right]z_d^2 + \left[3R_o z_d/\beta_1 + 6R_o L/(\pi\beta_1^2) + 3R_o^2/\beta_1^2\right]z_d = \left[3F_m x/(\beta_j^2 u_s^2) + 3Fx^2/(2\beta_1^2 u_s^3)\right] \quad (2.4\text{-}16)$$

and, for final stable plume rise:

$$z_d^3 + \left[3L/(\pi\beta_1)\right]z_d^2 + \left[3R_o z_d/\beta_1 + 6R_o L/(\pi\beta_1^2) + 3R_o^2/\beta_1^2\right]z_d = \left[3F_m/(\beta_j^2 u_s S^{1/2}) + 6F/(\beta_2^2 u_s S)\right] \quad (2.4\text{-}17)$$

The effective line length, L,. is $(2\pi)^{1/2}$ $(\sigma_{yo}-\sigma_{zo})$ if $\sigma_{yo} > \sigma_{zo}$. Otherwise, L = 0, and Eqns. (2.4-16) and (2.4-17) reduce to Eqns. (2.4-14) and (2.4-15).

As described in Section 2.3, the enhanced dispersion coefficients, σ_{zo} and σ_{yo}, vary with stack height, momentum rise, and building dimensions. The variation of R_o with for several stack heights is illustrated in Figure 2.4-1. As σ_{zo} and σ_{yo} approach zero (i.e., building downwash effects become negligible), Eqns (2.4-14) to (2.4-17) approach the unmodified Briggs equations. The effect of R_o and L is always to lower the plume height, thereby tending to increase the predicted maximum ground-level concentration.

2.4.5 Vertical Wind Shear

The variation of wind speed with height is usually accounted for in plume rise algorithms by the use of the stack height wind speed in the plume rise equations. Most formulations assume that the wind speed is constant above the stack top. This assumption is reasonable for mid-sized and tall stacks. However, the variation of wind speed above the stack top can have a significant effect on reducing the plume rise of buoyant releases from short stacks imbedded in the surface (shear) layer of the atmosphere (Scire and Schulman, 1979). Assuming the vertical wind speed profile above the stack can be approximated as $u(z) \simeq u_s\ (z/h_s)^p$, where u_s is the wind speed at the stack

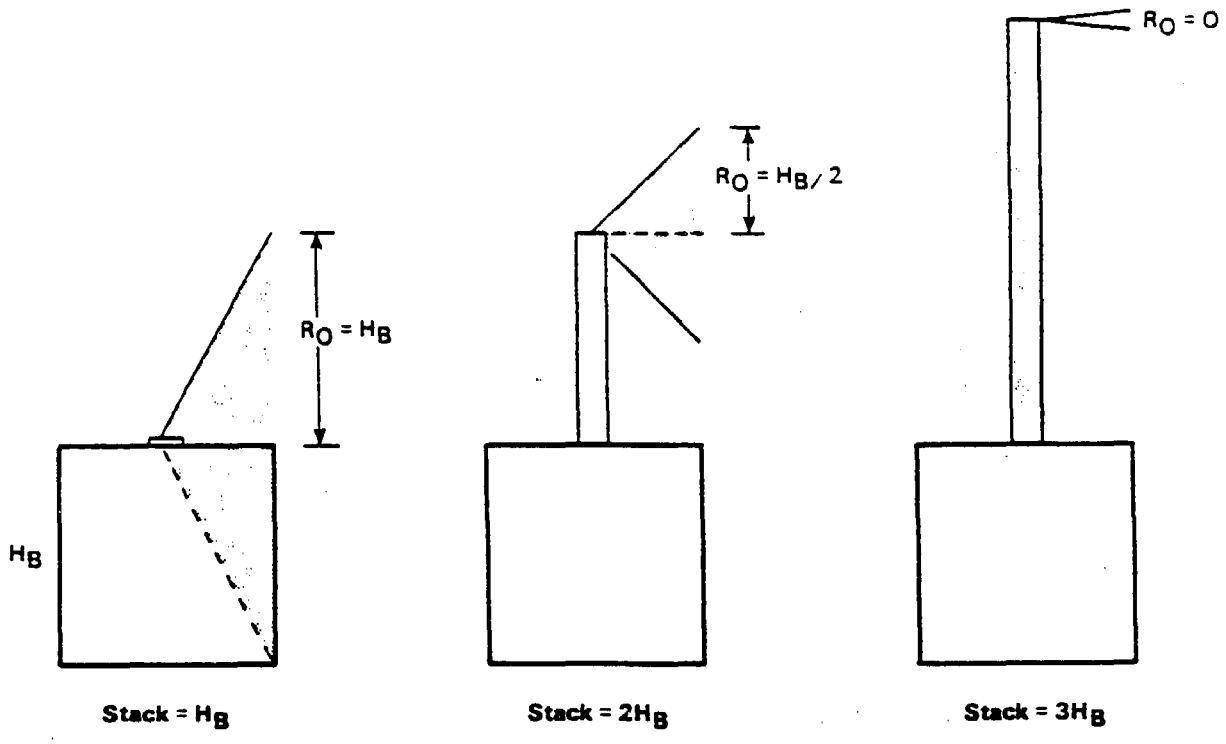

Figure 2.4-1. Illustration of the initial dilution radius, R_o, as a function of stack height for a squat building (from Schulman and Scire (1981)). Momentum plume rise is neglected in the figure.

top, h_s, and u(z) is the wind speed at height z, the plume rise from a short stack can be represented during neutral and unstable conditions as:

$$z_w = \left[[e^2/(6+2p)](F\, z_m^{3p})/(\beta_1^2\, u_m^3) \right]^{1/e} x^{2/e} \qquad (2.4\text{-}18)$$

$$e = 3 + 3p \qquad (2.4\text{-}19)$$

where p is the wind speed power law exponent.

During stable conditions, the final plume height is:

$$z_w = \left[[2\ (3+p) z_m^{\,p}\ F]/(\beta_2^2\, u_m\, S) \right]^{1/(3+p)} \qquad (2.4\text{-}20)$$

The wind shear exponent can be estimated from the atmospheric stability class or computed from the vertical wind data generated from the wind field model. It should be noted that Eqns. (2.4-18) and (2.4-20) both reduce to the Briggs buoyant plume rise equations when there is no wind shear above the stack top (i.e., p = 0).

The assumption of $u(z) \simeq u_s\ (z/h_s)^p$ is most valid for short stacks where the shear effect is expected to be the greatest. However, it breaks down for taller stacks. Therefore, Eqns. (2.4-18) and (2.4-20) are used to provide an upper limit of the plume height for short stacks, i.e., that the actual plume height be taken as the minimum of the predictions of the shear, downwash, and no-shear predictions, as appropriate.

2.5 Overwater and Coastal Dispersion

There are important differences in the structures of the marine and continental boundary layers which can have significant effects on plume dispersion in the overwater and coastal environments. These differences arise for three basic reasons (LeMone, 1978):

- Water has a high heat capacity and is partially transparent to solar radiation, resulting in a relatively small diurnal temperature range (~ 0.5 deg. C).

- The sea surface is generally more uniform and less aerodynamically rough than typical land surfaces.

- There is a constant source of moisture in the marine boundary layer.

As a result of these differences, the sensible heat flux over the open water is typically more than an order of magnitude less than over land. The absence of a strong sensible heat flux to drive the marine mixed-layer and the small surface roughness result in relatively low mixing heights that offer the potential for significant plume trapping effects. LeMone (1978) indicates that the typical marine mixing depth is only about 500 m. Data from three offshore and coastal experiments reported by Hanna et al. (1985) (two of which were conducted in California) show many hours with mixing heights less than 100 m.

Another result is that the diurnal and annual variations of stability over water are completely unrelated to the typical overland behavior. For example, North Sea observations of water and air temperatures reported by Nieuwstadt (1977) (Figure 2.5-1) show that temperature inversions typically persist most of the day in June, while unstable conditions occur all day in January. During other times of the year, the overwater diurnal stability cycle is out of phase with the overland cycle (i.e., stable over water during the day and unstable at night).

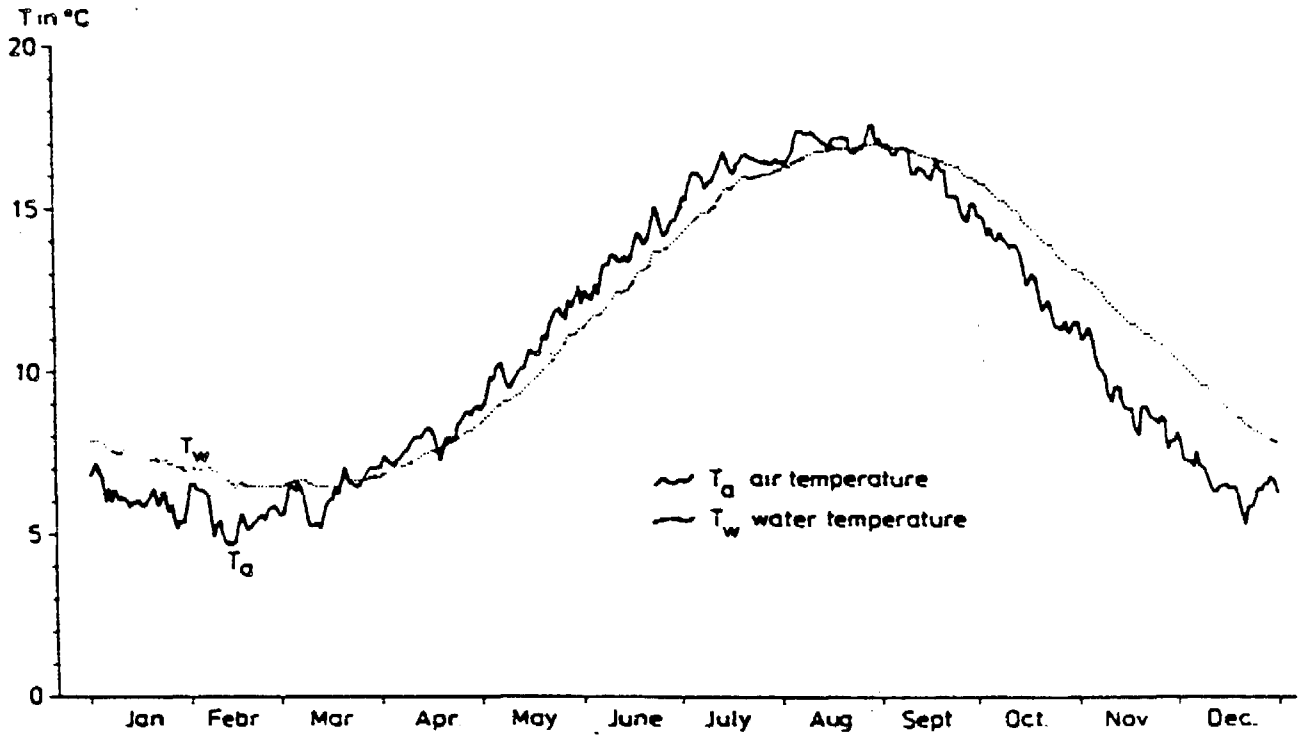

Figure 2.5-1. Daily average air and water temperatures measured in the North Sea (from Nieuwstadt (1977)).

The techniques used in the CALMET meteorological model for determining overwater mixing height, stability, and turbulence levels based on the air-sea temperature difference, wind speed, and the specific humidity have been discussed in Scire et al. (1990). These methods are applied by CALMET to the portions of the modeling domain over water. At the land-sea interface, rapid changes in the dispersion characteristics may occur which can significantly affect the ground-level concentrations from coastal sources. The puff model formulation is well-suited to accommodate these spatial changes in the coastal transition zone.

A typical situation during stable onshore flow conditions is shown in Figure 2.5-2. A narrow plume imbedded in the stable layer above the shallow mixed-layer is intercepted by a growing Thermal Internal Boundary Layer (TIBL). The growth of the TIBL is caused by the sensible heat flux associated with solar heating of the land surface. The convective overland conditions can rapidly bring the elevated pollutant to the ground, causing locally high ground-level concentrations. Many coastal fumigation models assume immediate mixing of the pollutant intercepted by the TIBL to the ground (e.g., Lyons and Cole, 1973, Misra, 1980). Deardorff and Willis (1982), based on laboratory experiments, suggest the importance of turbulent fluctuations in the TIBL height and indicate the plume does not become well-mixed immediately. In the Offshore and Coastal Dispersion (OCD) model, Hanna et al. (1985) use the minimum concentration predicted by a virtual source technique or that predicted by the Deardorff and Willis model to describe shoreline fumigation.

In CALPUFF, the land-sea interface is resolved on the scale of the computational grid. The CALPUFF model provides the turbulence and dispersion characteristic of the overwater as well as the overland boundary layers. The transition from marine to continental dispersion rates is assumed to occur at the coastal boundary determined from the gridded land use data. Once a puff included with a marine layer encounters the overland mixed layer height, the puff growth is changed for that appropriate for the marine layer to the overland dispersion rates.

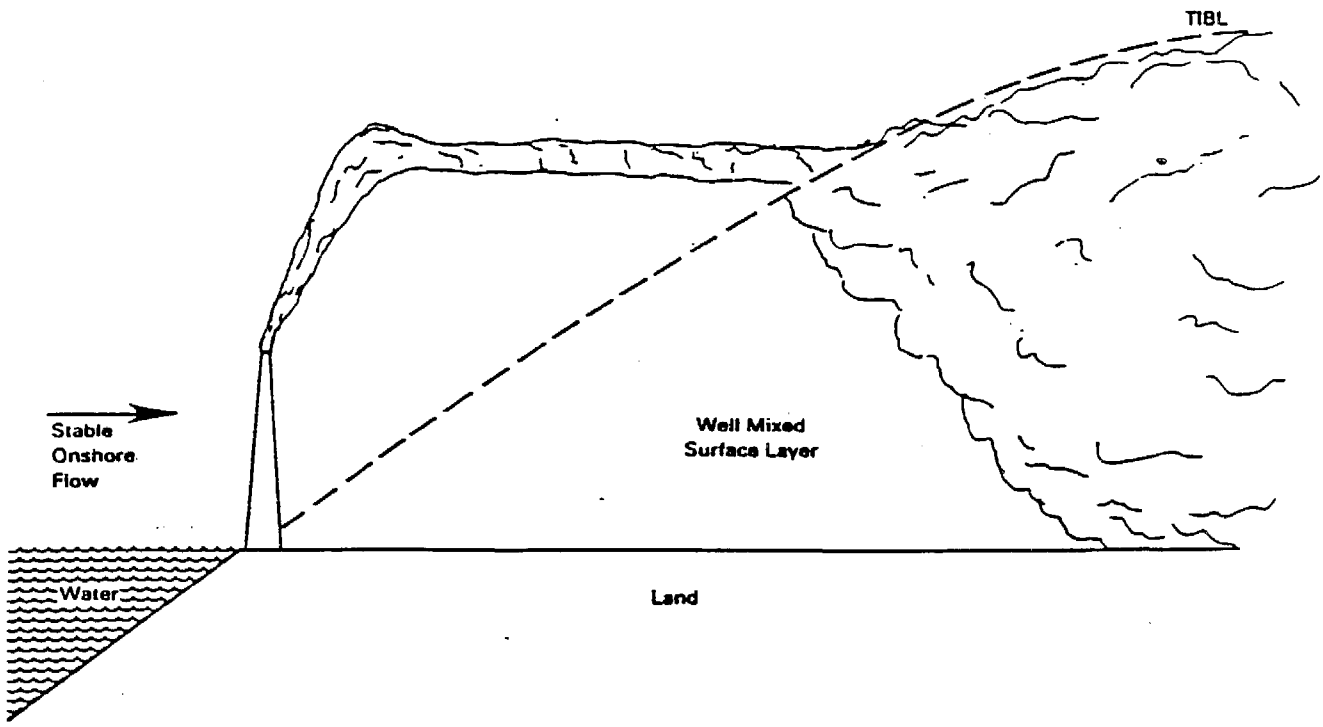

Figure 2.5-2. Schematic illustration of a typical coastal fumigation condition (from Hanna et al., (1985)).

2.6 Complex Terrain

CALPUFF responds to the presence of terrain on two scales. The effect of terrain that extends over a scale large enough to be resolved by the grid used in the flow field model will be manifest in the boundary conditions for the flow field. A puff embedded in this flow will either rise with the flow along the surface of the terrain, or it will be steered by the flow along the terrain, depending on the degree of stratification. Concentration estimates are calculated along the trajectory of the puff as if the terrain beneath it were flat. Effects of terrain that are not resolved by the grid used in the flow field model are treated in a separate subroutine, CTSG (COMPLEX TERRAIN ALGORITHM FOR SUB-GRID SCALE FEATURES).

CTSG accepts the flow field produced by the flow model (both the wind and temperature structure) in the vicinity of a terrain feature as the incident flow toward that feature. It then proceeds to simulate changes in the flow and in the rate of dispersion that are induced by that terrain feature. At the core of CTSG is the modeling approach adopted in CTDM, the complex terrain model developed in EPA's Complex Terrain Model Development program. Our goal in designing CTSG is to produce a puff algorithm that contains those elements of the CTDM approach that have the greatest impact on ground-level concentrations.

Figure 2.6-1 illustrates the intended role of CTSG in the CALPUFF system. In the upper panel of the figure, a cross-section of steep terrain rising with distance inland from a coast is depicted. The vertical dashed lines show the boundaries of a grid used by the wind-field model. The idealized terrain consists of a nearly uniform slope over much of the grid-square, plus a secondary feature right at the coast. At night, one might imagine a puff of material traveling down this slope in a drainage flow toward the secondary feature. The interaction of the puff with this secondary feature would be simulated by CTSG.

In the lower panel, the puff is shown as it is "seen" in the modeling system. The wind model provides the transport speed and direction for the puff, and concentrations are computed at receptors beneath the puff as if the terrain were flat. However, the secondary feature is now represented as an

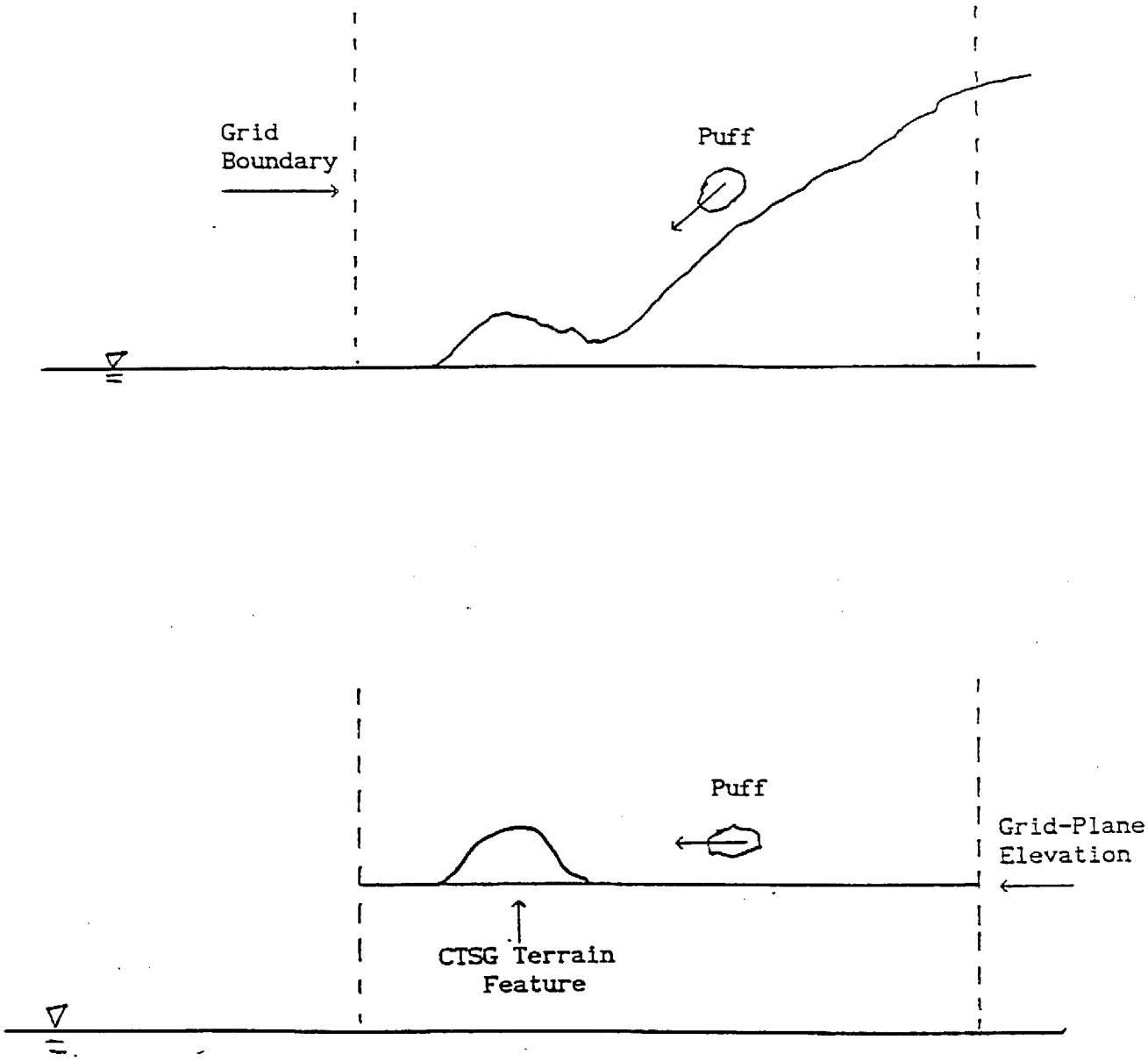

Figure 2.6-1. Depiction of the intended use of CTSG. The lower panel illustrates the portion of the terrain present in the upper panel that can be simulated by CTSG, and it illustrates the relationship between the gridded terrain, the modeled winds, and the CTSG terrain feature.

obstacle to the flow, and CTSG produces concentrations at receptors on this feature using methods developed for CTDM.

2.6.1 Modeling Regions

A central feature of CTDM adopted for use in CTSG is the dividing-streamline concept. The flow is taken to be composed of two layers. In the upper layer, the approach flow has sufficient energy to transport a fluid parcel up and over the hill against a stable potential density gradient. In the lower layer, the flow is constrained to travel around the hill. This concept was suggested by theoretical arguments of Drazin (1961) and Sheppard (1956) and was demonstrated through laboratory experiments by Riley et al. (1976), Brighton (1978), Hunt and Snyder (1980), Snyder (1980), and Snyder and Hunt (1984).

H_d, the dividing-streamline height (m), is obtained from profiles of wind speed (m/s) and temperature (as the Brunt-Vaisala frequency, N (1/s)). H_d is computed for each hill by locating the lowest height at which the kinetic energy of the approach flow just balances the potential energy attained in elevating a fluid parcel from this height to the top of the hill. The statement that defines this balance is:

$$.5\ u^2(H_d) = \int_{H_d}^{H} N^2(z)\ [H - z]dz \qquad (2.6\text{-}1)$$

where $h(H_d)$ is the wind speed at $z = H_d$, H is the elevation of the top of the hill, and N(z) is the Brunt-Vaisala frequency at height z. In practice, the value of H_d is obtained by rewriting the integral on the right-hand side (RHS) of Equation 2.6-1 as a sum over layers of constant N. For layer n,

$$RHS_n = RHS_{n+1} + \int_{z_n}^{z_{n+1}} N_n^2\ (H-z)dz = N_i^2\ (H-z_{mn})\ (z_{n+1} - z_n). \qquad (2.6\text{-}2)$$

where z_{mn} denotes the mean height of the layer, $0.5\ (z_{n+1} + z_n)$. The layer that contains H_d is found by comparing the LHS of Equation 2.6-1 at each

measurement height n with the corresponding RHS_n. If LHS_n exceeds RHS_n, then H_d must lie below z_n, and so the process is repeated until the lowest level is found for which the LHS becomes less than the RHS. This then identifies the layer that contains H_d.

H_d is then computed within this layer by assuming that the wind speed follows a linear profile. Denote this as layer j, where the elevations at the top and bottom of the layer are z_{j+1} and z_j, respectively. Denote u(z) in the layer as

$$u(z) = a_j + b_j z$$

then equation 2.6-1 becomes

$$\frac{1}{2} (a_j + b_j H_d)^2 = N_j^2 (H - 1/2[z_{j+1} + H_d]) (z_{j+1} - H_d) + RHS_{j+1} \qquad (2.6\text{-}3)$$

where the last term, RHS_{j+1}, denotes the value of the RHS from z_{j+1} to the top of the hill. Equation 2.6-3 is quadratic in H_d, and is readily solved for H_d.

Once H_d is computed for a hill, the stratification length scale for the flow above H_c is computed as u_m/N_m where u_m and N_m are average values between H_d and the first measurement level above the top of the hill. This length scale characterizes the degree of stratification of the flow above H_d. Note that N_m is computed from the temperature difference across the layer.

Puff material above H_d, the dividing-streamline height, experiences an altered rate of diffusion in the deformed flow field over the hill. It is this change in the effective dispersion that leads to increased ground-level concentrations (GLC's) observed over hills when H_d is zero. When H_d is not zero, only that portion of the puff that lies above H_d as the puff encounters the hill travels over the hill. The puff is modeled as if it were sheared off at H_d so that material nearer the center of the puff may reach the surface without further dilution. The theory of diffusion of narrow plumes embedded in a deforming flow field (Hunt and Mulhearn, 1973) provides the basis for estimating GLC values in the upper layer (subroutine UPPER).

Puff material below H_d is deflected around the hill, being embedded in a horizontal two-dimensional flow. The stagnation streamline in this flow forms the boundary of the hill and therefore separates portions of the puff which travel around one side or the other. The center of the puff is able to impinge on the hillside only if the puff is centered on the stagnation streamline, and lies below H_d. Concentration estimates from subroutine LOWER are based on the analysis of Hunt et al. (1979) which indicates that the GLC near the impingement point is essentially that obtained by sampling the puff (in the absence of the hill) along the stagnation streamline at the elevation of the receptor. As the puff encounters the hill, the lateral distribution of material in the puff is separated along the stagnation streamline, and each segment is allowed to travel around the hill with complete reflection at the plane z=0 as well as y=Yd (stagnation streamline), i.e., the hillside. Figure 2.6-2 illustrates how the puff material is treated in CTSG. For the sake of illustration, the outline of a continuous series of puffs is portrayed as a plume and the height of the center of the plume exceeds H_d.

Three regions are identified in the figure. Boundaries between these three regions are defined differently in the upper and lower layers, as discussed later. For illustration, we will consider the boundaries identical, as drawn in Figure 2.6-2. The distinction between the upper flow and the lower flow as described above is strictly applied in region 2. Prior to this, in region 1, the portion of the puff above H_d has not reached the hill (at $z = H_d$) and so the vertical structure remains continuous. Concentrations are estimated as if receptors in this region were positioned on poles. Receptors below H_d in region 1 are placed on poles to simulate an impingement calculation. The pole height is equal to the height of the receptor above the base of the hill, and the lateral position of the pole is shifted to the location of the stagnation streamline. In essence, the flow below H_d in region 1 is turned much as it is in region 2, but no reflection from the side of the hill is included. Receptors may also be located above H_d in region 1. Figure 2.6-3 depicts a situation in which departures in shape between the actual terrain feature and the simplified hill used in CTSG cause ground-level receptors to be placed above H_d in region 1. In this case receptor 2 is also modeled as a receptor-on-a-pole, but the height of this pole is set to H_d, and its lateral position is the same as that of the

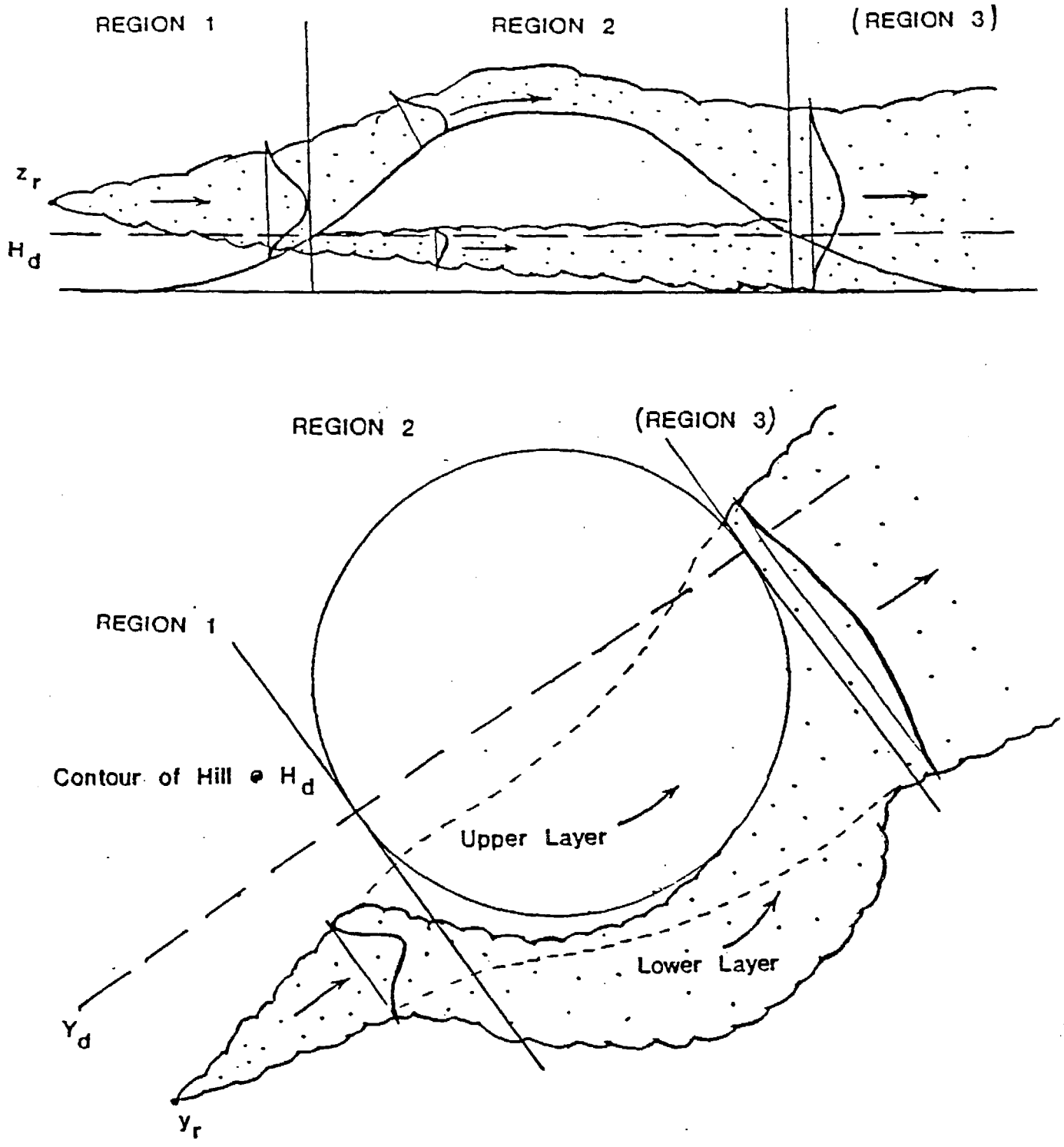

Figure 2.6-2. Illustration of modeling regions and partitioning of the flow above and below the dividing-streamline height H_d.

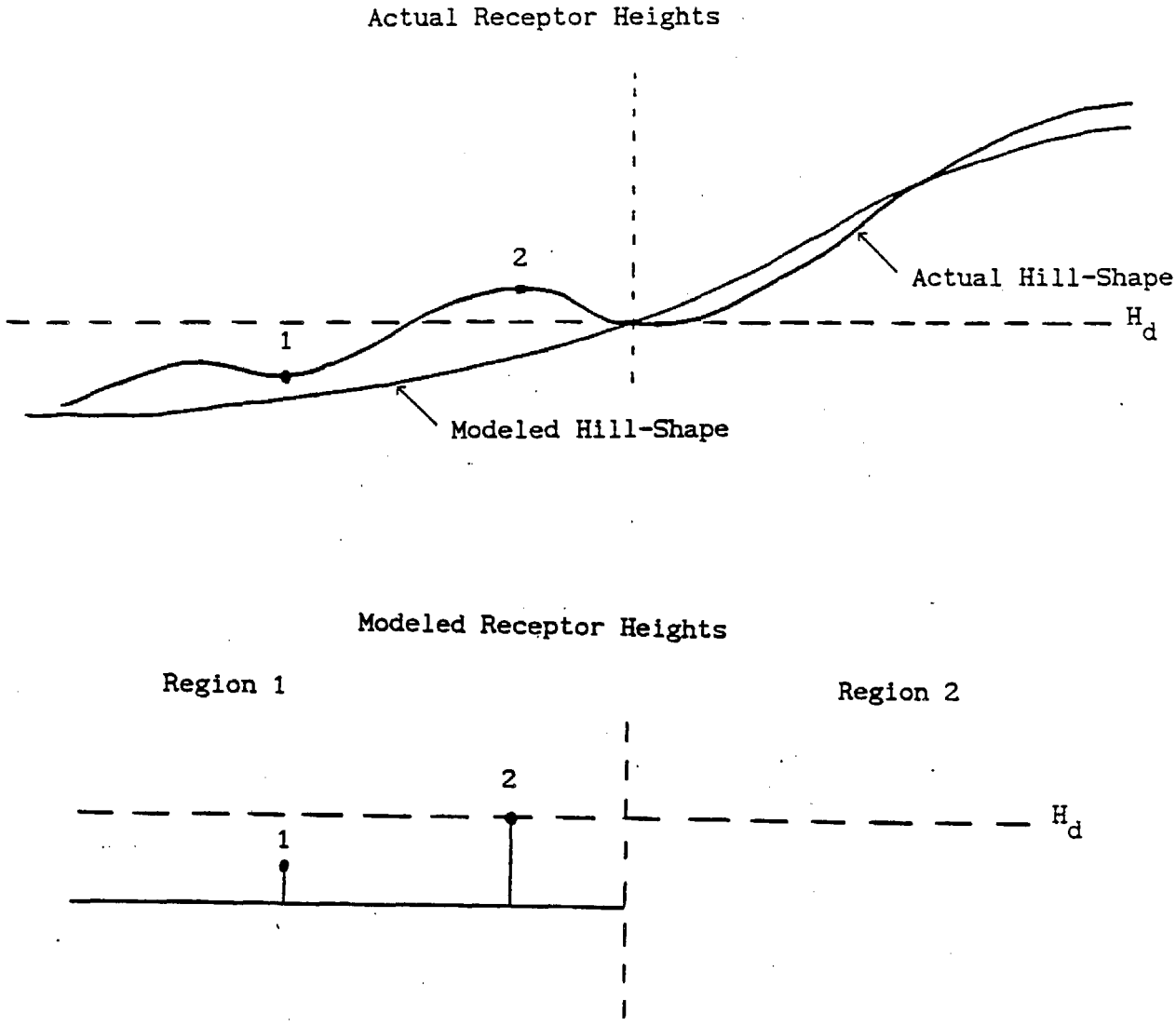

Figure 2.6-3. Treatment of height of receptors located upwind of the impingement point (Region 1).

receptor. This approach assumes that flow above H_d is deflected in the vertical, but not in the lateral direction. No alterations are made to the dispersion rates. Differences in the way receptors in region 1 are treated can be summarized as follows: the flow above H_d is considered to be terrain-following in the vertical, with no horizontal deflection, and the flow below H_d is considered to be terrain-following in the horizontal, with no vertical deflection. Note that the stagnation streamline defines the boundary that shifts the flow left or right in the horizontal. Subroutine PUFFC performs these calculations in region 1. Details of the model for regions 2 and 3 are provided in the following sub-sections.

The CTSG algorithm may be invoked whenever concentration estimates are needed at receptors that are located on terrain elements that are not resolved by the grid in the flow-field model. It specifies the relationship between a single puff and all receptors on a single terrain feature for the current averaging/transport time-period. Consequently, CTSG is called for each puff/terrain-element pair during each time-step. Some reduction in execution time is be gained by screening out puff/terrain-element pairs for combinations of puff size and position, relative to those of the terrain feature, that exhibit minimal terrain influence. These combinations are then modeled as if the terrain were absent.

2.6.2 Description of Terrain Features

CTSG uses simple analytical obstacle shapes to represent sub-grid scale terrain features. Below H_d, CTSG uses an elliptical cylinder to represent the hill. The axes and orientation of this ellipse represent the overall scale and orientation of the terrain feature at the minimum of the elevation of the puff, or H_d. Above H_d, CTSG uses a Gaussian shape to represent the hill. The height of the Gaussian hill is equal to the difference in height from the peak of the hill to H_d. The horizontal length scales and orientation of the hill are chosen so that the lateral extent of the Gaussian hill at one half its height is representative of the scale of the terrain feature half way between H_d and the top of the hill. When the major axis of the hill lies along the x-axis of the coordinate system, these shapes are defined by

$$\text{ellipse:} \qquad 1 = \left(\frac{x}{a}\right)^2 + \left(\frac{y}{b}\right)^2$$

$$\text{Gaussian:} \qquad h = H\, e^{-(x/L_x)^2} e^{-(y/L_y)^2} \tag{2.6-4}$$

where (a,b) are the semi-axis lengths of the horizontal cross-section of the elliptical cylinder below H_d, and (L_x, L_y) are the Gaussian length scales along the two axes of the hill above H_d. For each puff, hill, and value of H_d, the model selects a particular elliptic cylinder and Gaussian-shaped hill.

To do this, the user must describe each terrain feature as an inverse polynomial hill (Figure 2.6-4). For each axis, the shape that must be fit to the height-profile of the terrain feature has the functional form:

$$\text{ht} = \text{relief} \left[\frac{1 - (|x|/\text{axmax})^{\text{expo}}}{1 + (|x|/\text{scale})^{\text{expo}}} \right] \tag{2.6-5}$$

where "ht" is the elevation of a point on the hill above the grid-plane, "|x|" is the unsigned distance from the center of the hill to the inverse polynomial profile at the elevation "ht", "axmax" is the value of "|x|" at which "ht" equals zero (the base of the hill), "relief" is the height of the hill above the grid-plane, "scale" is the length scale of the polynomial function which is half the span of the function at one half the peak of the function, and "expo" is the power (exponent) of the function.

Given this description of the hill, CTSG solves for "x" at specific elevations "ht" along each axis of the hill to obtain the semi-axes for the elliptic cylinder and the Gaussian hill:

$$\text{axis (ht)} = \text{scale} \left[\frac{1 - \text{ht/relief}}{\text{ht/relief} + (\text{scale/axmax})^{\text{expo}}} \right]^{1/\text{expo}} \tag{2.6-6}$$

Below H_d, the height used to obtain the axes of the elliptic cylinder is the minimum of H_d and the puff height. Above H_d, the length scales are obtained

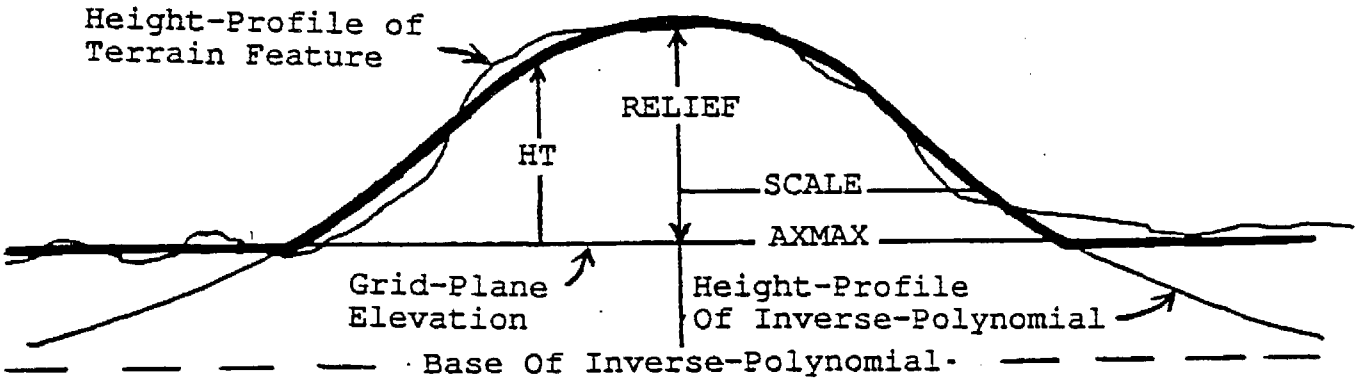

Figure 2.6-4. Profile of a terrain feature along one of its two axes. A best-fit inverse polynomial function describes this profile to CTSG.

halfway between H_d and the top of the hill, and the corresponding length scales for the Gaussian hill are formed by multiplying these scales by 1.20. The factor 1.20 is obtained by demanding that the Gaussian Hill and the polynomial hill function have the same span at an elevation halfway between H_d and the top of the hill (Figure 2.6-5).

2.6.3 Upper Layer

An estimate of the concentration (g/m^3) at a receptor at the surface of a hill in region 2, due to a plume whose initial position is (z_p, y_p), is given by

$$C(t_R, y_R, 0; t_o) = qF_zF_y/[2\pi u\sigma_{ze}\sigma_{ye}] \qquad (2.6\text{-}7)$$

where t_R is the travel-time (s) from the source to the receptor, t_o is the travel-time along the plume centerline from the source to the upwind base of the hill (if H_d is non-zero, t_o is the time to the point where the flow first encounters the hill at an elevation equal to the lesser of z_p and H_d), y_R is the cross-wind location (m) of the receptor, q is the mass flux (g/s), F_z and F_y are the vertical and horizontal distribution functions, u is the mean wind speed (m/s) at the elevation of the center of the plume, and σ_{ze} and σ_{ye} are the effective dispersion parameters (m) given by

$$\sigma_{ze}^2 = \sigma_{zo}^2 + [\sigma_{z*}/T_z]^2 \qquad \sigma_{ye}^2 = \sigma_{yo} + [\sigma_{y*}/T_y]^2 \qquad (2.6\text{-}8)$$

The subscript o denotes a value obtained at $t = t_o$ and the subscript * denotes

$$\sigma_{x*}^2 = \sigma_x^2(t_R) - \sigma_x^2(t_o) \qquad \text{(for x = y or z)} \qquad (2.6\text{-}9)$$

T_z and T_y are factors that contain the effects of the distortion of the flow over the hill on the rates of vertical and lateral diffusion.

In the case of a puff, the sampling function allows us to rewrite the concentration estimate for a receptor on the surface (Equation 2.6-7) as

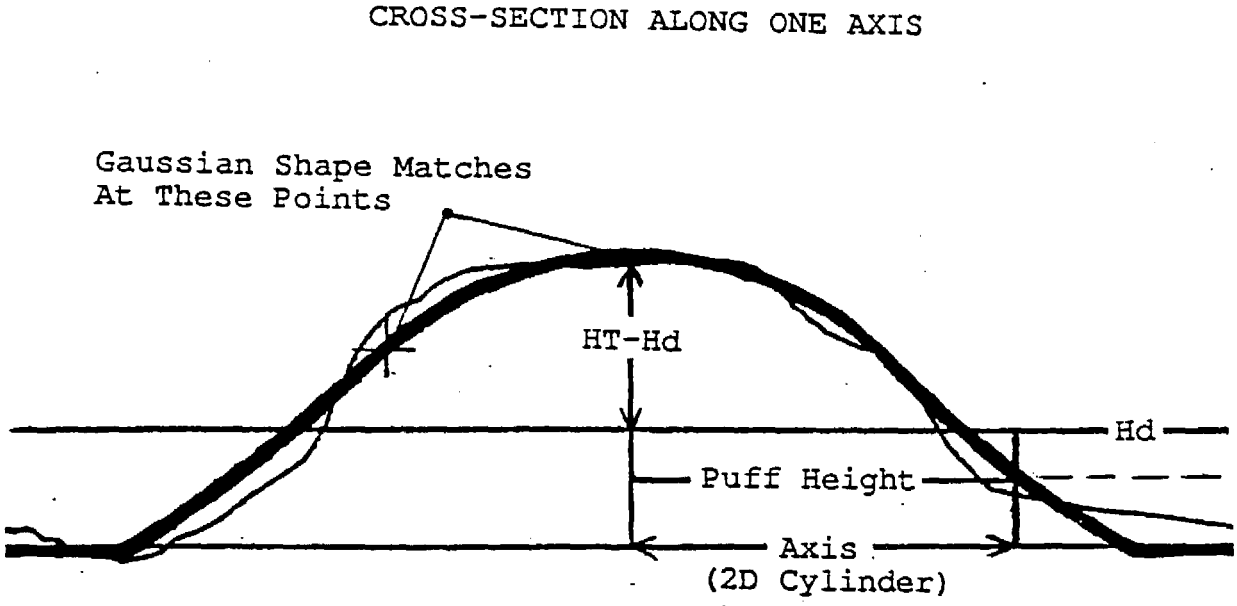

Figure 2.6-5. Use of hill profile function within CTSG. The model extracts the length scales for a Gaussian profile above H_d, and an elliptical cylinder below H_d.

$$GLC = \frac{Q}{t_2-t_1} \frac{F_y(t_R)\, F_z(t_R)}{4\,\pi\, u\, \sigma_{ze}\, \sigma_{ye}} \left\{ \mathrm{erf}\left(\frac{t_2-t_R}{\sqrt{2}\,\sigma_{ye}/u} \right) - \mathrm{erf}\left(\frac{t_1-t_R}{\sqrt{2}\,\sigma_{ye}/u} \right) \right\} \quad (2.6\text{-}10)$$

where Q is now the total mass of material (g) in the puff.

The distribution functions are given by

$$F_y = \exp(-.5\,[y_{Re} - y_p]^2/\sigma_{ye}^2)$$

$$F_z = \exp(-.5\,[z_p - H_d]^2/\sigma_{ze}^2)\ \mathrm{erfc}(\sigma_{z*}[H_d - z_p]/[2T_z\,\sigma_{ze}\,\sigma_{zo}]) \quad (2.6\text{-}11)$$

$$+ \exp(-.5\,[z_p + H_d]^2/\sigma_{ze}^2)\ \mathrm{erfc}(\sigma_{z*}\,[H_d + z_p]/[2T_z\,\sigma_{ze}\,\sigma_{zo}])$$

F_y contains information on the deflection in the trajectory over the hill as well as information on changes in the diffusivity. The effective lateral position of the receptor relative to the centerline of the plume is altered by the deformation in streamlines over the hill, and the effective rate of growth of the plume is altered as well. Hence, an effective receptor location (y_{Re}) and an effective lateral plume size (σ_{ye}) are used to compute the horizontal distribution function. F_z also contains the change in diffusivity in the effective vertical plume size, σ_{ze}, and it includes complete reflection from the surface of the hill (marked by H_d) for only that material which lay above H_d at $t = t_o$. "Cutting" the plume at $z = H_d$ and allowing reflection from this surface gives rise to the combination of exponential and error function products in Equation 2.6-11. A full discussion of the development of these equations is contained in Strimaitis et al. (1988).

These expressions do not include the effect of an elevated inversion on the vertical distribution of the puff. When a mixing lid is present, the F_z function contains many more terms to simulate multiple reflections. The derivation of F_z with a mixing lid is an extension not found in CTDM.

For a mixing lid of height z_L, the vertical distribution function in a puff just upwind of the hill is given by

$$F_{zo} = \exp\left(-.5\,[z_p - z]^2/\sigma_{zo}^2\right) + \exp\left(-.5\,[z_p + z]^2/\sigma_{zo}^2\right)$$

$$+ \sum_{i}^{\infty} \left\{\exp\left(-.5\,[2iz_L - z_p - z]^2/\sigma_{zo}^2\right) + \exp\left(-.5\,[2iz_L - z_p + z]^2/\sigma_{zo}^2\right)\right\}$$

$$+ \sum_{i}^{\infty} \left\{\exp\left(-.5\,[2iz_L - z_p - z]^2/\sigma_{zo}^2\right) + \exp\left(-.5\,[2iz_L + z_p + z]^2/\sigma_{zo}^2\right)\right. \quad (2.6\text{-}12)$$

Over the hill, the vertical distribution function (evaluated for a receptor at the surface of the hill--H_d) due to a point source located at a height "z" just upwind of the hill is given by

$$F_{zh} = 2\left\{\exp\left(-.5\,[z - H_d]^2/\sigma_{z^*}^2/T_z^2\right)\right.$$

$$+ \sum_{i}^{\infty} \exp\left(-.5\,[2i\,(z_L - H_d) - (z - H_d)]^2/\sigma_{z^*}^2/T_z^2\right)$$

$$+ \sum_{i}^{\infty} \left.\exp\left(-.5\,[2i\,(z_L - H_d) + (z - H_d)]^2/\sigma_{z^*}^2/T_z^2\right)\right\} \quad (2.6\text{-}13)$$

Therefore, the total influence of the vertical distribution of puff material just upwind of the hill on the concentration at a receptor on the surface of the hill is obtained by integrating the product of these two distributions from $z = H_d$ to $z = z_L$. The resulting F_z is given by

$$F_z = .5\left\{\sum_{i=1}^{\infty}\sum_{j=1}^{\infty} A_j B(E_j, E^+_{oi}) + \sum_{i=2}^{\infty}\sum_{j=1}^{\infty} A_j B(E_j, E^-_{oi})\right\} \quad (2.6\text{-}14)$$

where

$$A_j = \text{MIN}\,(2, j)$$

$$E_j = 2\,[j - 1]\,[z_L - H_d] \quad (2.6\text{-}15)$$

$$E^+_{oi} = 2\,z_L\,[i - 1] + z_p \qquad E^-_{oi} = 2\,z_L\,[i - 1] - z_p$$

and

$$B(E,E_o) = \exp(-.5[E-E_o+H_d]^2/\sigma_{ze}^2)\ \{\mathrm{erf}(K[\sigma_{ze}^2[z_L-H_d]-D1) + \mathrm{erf}(K\ D1)\}$$

$$+ \exp(-.5[E+E_o-H_d]^2/\sigma_{ze}^2)\ \{\mathrm{erf}(K[\sigma_{ze}^2[z_L-H_d]-D2) + \mathrm{erf}(K\ D2)\} \quad (2.6\text{-}16)$$

$$+ \exp(-.5[E+E_o+H_d]^2/\sigma_{ze}^2)\ \{\mathrm{erf}(K[\sigma_{ze}^2[z_L-H_d]+D3) - \mathrm{erf}(K\ D3)\}$$

$$+ \exp(-.5[E-E_o-H_d]^2/\sigma_{ze}^2)\ \{\mathrm{erf}(K[\sigma_{ze}^2[z_L-H_d]+D4) - \mathrm{erf}(K\ D4)\}$$

where

$$K = T_z\ /\ [\sqrt{2}\ \sigma_{ze}\ \sigma_{zo}\ \sigma_{z*}]$$

$$D1 = \sigma_{z*}^2\ [E_o - H_d]\ /\ T_z^2\ + \sigma_{zo}^2\ E$$

$$D2 = \sigma_{z*}^2\ [E_o - H_d]\ /\ T_z^2\ -\ \sigma_{zo}^2\ E \quad (2.6\text{-}17)$$

$$D3 = \sigma_{z*}^2\ [E_o + H_d]\ /\ T_z^2\ - \sigma_{zo}^2\ E$$

$$D4 = \sigma_{z*}^2\ [E_o + H_d]\ /\ T_z^2\ + \sigma_{zo}^2\ E$$

Each term in the sum in Equation 2.6-14 is a product of the exponential function and error functions as in Equation 2.6-11, representing the multiple reflections at H_d and z_L. Clearly, not all of the terms in the sum are needed. The inner sum over index j represents reflections between H_d and z_L once the puff moves over the hill, whereas the outer sum over index i represents reflections between 0 and z_L before the puff reaches the hill. The algorithm that evaluates these sums continues to include greater values of the index until the fractional change in F_z is reduced to less than 1%. The distribution of material in the vertical becomes well-mixed when σ_z reaches 1.6 z_L. At this point, F_z in Equation 2.6-14 reduces to

$$F_z = \sqrt{2\pi}\ \sigma_z/z_L \quad (2.6\text{-}18)$$

These equations take on a more familiar form when H_d is zero and when z_L is infinite. In that limit D1 = D4, D2 = D3, and inspection of the exponential factors reveals that the indices (i,j) must be equal to obtain non-zero terms. Further inspection of the error functions shows that the only non-zero term is that for i = j = 1, so that

$$F_z(H_d = 0, z_L = \infty) = 2 \exp(-.5[z_p/\sigma_{ze}]^2) \qquad (2.6\text{-}19)$$

which is the form commonly used for flat terrain.

Evaluation of the F_z and F_y distribution functions requires the use of a flow model that provides streamlines for stratified flow over a hill. The effective lateral receptor location, y_{Re}, and the effective puff dimensions, σ_{ze} and σ_{ye}, depend on the properties of the flow. These properties are provided by the flow algorithm contained in CTDM. This algorithm incorporates an approximate solution to the linearized equation of motion for steady-state Boussinesq flow over a Gaussian-shaped hill. It is formulated as a "backwards-looking" solution in which the deflection of a streamline that passes through a given point over a hill is provided. Hence, the algorithm answers the question: "Where did the streamline that passes through the point (x,y,z) come from?" rather than the question: "Where does the streamline that passes through the point (x,y,z) in the flow upwind of a hill go as the flow is deflected by the presence of the hill?" As such, the relationship between the lateral position of the center of the puff in the absence of terrain-deflections (y_p), and the "original" lateral position (y_{Re}) of the streamline that passes through the receptor is directly obtained form the flow algorithm because the receptor position on the hill (x_R, y_R, z_R) is known. The description of the flow algorithm is contained in the CTDM user's guide (Paine et al., 1987).

Evaluation of σ_{ze} and σ_{ye} is more complicated. As indicated in Equation 2.6-8, these effective puff dimensions require the quantities σ_{z*}/T_z and σ_{y*}/T_y, which depend on the rate of puff growth in the absence of the hill and on the amount of distortion to the flow induced by the hill. These are estimated on the basis of the theory for a narrow plume embedded in a flow with axisymmetric strain developed by Hunt and Mulhearn (1973). Their results show that the spread of material in a straining flow is approximately equal to

$$\sigma_{zd}^2(t) = \frac{1}{S^2(t)} \int_o^t S_t^2(t')2K_z(t')\,dt'$$

(2.6-20)

$$\sigma_{yd}^2(t) = \frac{1}{S_y^2(t)} \int_s^t S_y^2(t')\,2K_y(t')\,dt'$$

where K_z and K_y are the diffusivities, S_z and S_y are functions of the strain in the flow, and σ_{yd} and σ_{zd} describe the size of a deformed plume. Because we assume that the strain is negligible away from the hill, Equation 2.6-20 can be rewritten as

$$\sigma_z^2(t) = \frac{1}{S_z^2(t)} \left[\sigma_{zo}^2 + \int_{to}^t S_z^2(t')2K_z(t')dt' \right]$$

(2.6-21)

$$\sigma_y^2(t) = \frac{1}{S_y^2(t)} \left[\sigma_{yo}^2 + \int_{to}^t S_y^2(t')2K_y(t')dt' \right]$$

The expressions in brackets are equivalent to the quantities σ_{ze}^2 and σ_{ye}^2 defined by Equation 2.6-8, so that

$$\frac{\sigma_{z*}^2}{T_z^2} = \frac{\sigma_z^2(t) - \sigma_{zo}^2}{T_z^2} = \int_{to}^t S_z^2(t')2K_z(t')dt'$$

(2.6-22)

$$\frac{\sigma_{y*}^2}{T_y^2} = \frac{\sigma_y^2(t) - \sigma_{yo}^2}{T_y^2} = \int_{to}^t S_y^2(t')2K_y(t')dt'$$

The strain functions are given by

$$S_z(t) = \exp(1 - Th(t)) \qquad S_y(t) = \exp(1 - Tl(t)) \tag{2.6-23}$$

where Th and Tl are deformation factors. Th is the ratio of streamline spacing in the vertical in the deformed flow to that in the undistorted flow. Tl is the corresponding ratio for streamline spacing in the lateral direction (normal to the flow). The inverse of the product of these two factors at any point in the flow equals the speed up factor, Tu. These factors are computed from the flow model contained in CTDM. The integrals in Equation 2.6-22 are evaluated numerically along the trajectory of the center of the puff. Vertical and lateral diffusivities (m^2/s) in the absence of the terrain are found from the dispersion coefficients as

$$2K(t) = d(\sigma^2)/dt \tag{2.6-24}$$

where σ denotes either σ_y or σ_z. The effect of the terrain on the diffusivity is assumed to be restricted to the change in the vertical turbulence over the hill. We write the dispersion coefficient as the product of the turbulence and a function of time (in the absence of terrain). Over the hill, the vertical turbulence velocity is assumed to increase with wind speed as in the "inner layer" theory, and the lateral turbulence velocity is assumed constant as in the "rapid distortion" theory (e.g., see Britter et al. (1981) for a discussion of these theories). These assumptions tend to accentuate the effect of the hill in the diffusion calculation. The integrands of Equation 2.6-22 become

$$S_z^2\, 2K_z = \exp(1 - Th)\, T_u^2 \frac{d(\sigma_z^2)}{dt}$$

$$S_y^2\, 2K_y = \exp(1 - Tl) \frac{d(\sigma_y)^2}{dt} \tag{2.6-25}$$

Due to the computations required to obtain Th, Tl, and Tu, these factors are evaluated at no more than 25 points along the streamline that passes through the center of the puff. Linear interpolation between these points is then used in the numerical integration required to evaluate Equation 2.6-22 for each receptor. The range of points is centered at the mid-point of the

intersections of the puff trajectory (without deflection) and the ellipse that marks the boundary of the portion of the hill below H_d, and cover a distance equal to one and one-half times the distance between points of intersection of the line y = 0 (the centerplane of the flow over the hill) and the ellipse. If the undeflected trajectory of the puff does not intersect the ellipse, then the distortion factors are set to unity and the hill has no effect on σ_z and σ_y. Note that the hill also has no effect on σ_z or σ_y when the growth rate of the puff is virtually zero. This is not to say that the hill has no effect on concentrations, however, because the flow distortion over the hill results in $y_{Re} \neq y_R$, and the dividing-streamline height still allows puff material at $z = H_d$ to contact the surface of the hill.

2.6.4 Lower Layer

The equation for estimating the concentration (g/m^3) at a receptor at the surface of a hill in region 2, due to a plume whose initial position is (z_r, y_r), is given by

$$C(t_R, Y_d, z_R; t_o) = q\, F_z\, F_y \,/\, [2\, \pi\, u\, \sigma_z\, \sigma_y] \qquad (2.6\text{-}26)$$

where Y_d is the cross-wind location (m) of the lateral dividing-streamline which coincides with the side of the hill, z_R is the elevation of the receptor on the surface of the hill, F_z and F_y are the vertical and horizontal distribution functions, u is the mean wind speed (m/s) at the elevation of the center of the plume, and σ_z and σ_y are the dispersion parameters (m) at t_R. Note that unlike Equation 2.6-7 for the upper layer, changes to the rate of diffusion that are induced by the hill in the lower layer are considered small.

In the case of a puff, the sampling function allows us to rewrite the concentration estimate for a receptor on the surface (Equation 2.6-26) as

$$GLC = \frac{Q}{t_2 - t_1} \frac{F_y(t_R)\, F_z(t_R)}{4\, \pi\, u\, \sigma_z\, \sigma_y} \left\{ \text{erf}\left(\frac{t_2 - t_R}{\sqrt{2}\sigma_y / u} \right) - \text{erf}\left(\frac{t_1 - t_R}{\sqrt{2}\sigma_y / u} \right) \right\} \qquad (2.6\text{-}27)$$

The distribution functions are given by

$$F_y = \exp\left(-.5\left[Y_d - y_p\right]^2/\sigma_y^2\right)\left[1 \pm \mathrm{erf}\left(\left[Y_d - y_p\right]\sigma_{y*}/\left[\sqrt{2}\,\sigma_{yo}\,\sigma_y\right]\right)\right] \qquad (2.6\text{-}28)$$

$$F_z = .5\,\exp\left(-.5\left[z_p - z_R\right]^2/\sigma_z^2\right)\left[\mathrm{erf}\left(\left[b1-b2-b3\right]*K\right) + \mathrm{erf}\left(\left[b1+b2+b3\right]*K\right)\right]$$

$$+ .5\,\exp\left(-.5\left[z_r + z_R\right]^2/\sigma_z^2\right)\left[\mathrm{erf}\left(\left[b1-b2+b3\right]*K\right) + \mathrm{erf}\left(\left[b1+b2-b3\right]*K\right)\right]$$

where

$$K = \frac{1}{\sqrt{2}\,\sigma_z\,\sigma_{zo}\,\sigma_{z*}} \qquad b1 = H_d\,\sigma_z^2 \qquad (2.6\text{-}29)$$

$$b2 = z_R\,\sigma_{zo}^2 \qquad b3 = z_p\,\sigma_{z*}^2$$

The notation is the same as that in section 2.6.3. The only new quantity introduced in these equations is Y_d. As in CTDM, it is found by solving for the two-dimensional streamline pattern about an ellipse. The description is contained in the CTDM user's guide (Paine et al., 1987). Note that the CTDM adjustment to wind speed and direction for measurements made close to terrain has not been implemented in CTSG. The purpose of this adjustment is to estimate the "undisturbed" mean flow from measurements made within the region of disturbed flow near a terrain feature. Because CTSG makes use of the winds from the wind field model, the presence of the subgrid scale terrain features has not perturbed these winds.

F_y contains information about the amount of material on each side of the hill and about how the puff is sampled in the lateral direction. The lateral offset is the distance from the centerline to Y_d, reflecting the notion that all receptors lie along the side of a hill, coincident with the lateral dividing-streamline position. Furthermore, material may be split on either side, and complete reflection of material is allowed along this surface, giving rise to the form of the product of the exponential and error functions

in Equation 2.6-28. Note that the sign of the error function (taking the sign of its argument into account) is positive when both the receptor and the trajectory of the center of the puff lie on the same side of Y_d. If all of the material were to reside on one side of Y_d at to, then F_y would equal either 2 or 0, depending on whether the receptor were on the same side or on the other side of Y_d as the puff.

F_z contains information about the amount of material below H_d at t_o, and about how this material is sampled in the vertical. The form is a product of an exponential function and error functions in which the sampling height z_R is most evident in the exponential function, and the effects of splitting the plume at H_d is contained in the error functions. A full discussion of the development of these equations is contained in Strimaitis et al. (1988).

These expressions do not include the effect of an elevated inversion on the vertical distribution of the puff. When a mixing lid is present, the F_z function contains many more terms to simulate multiple reflections and the result is similar to that discussed in 2.6.3:

$$F_z = .5 \left\{ \sum_{i=1}^{\infty} \sum_{j=1}^{\infty} B(E_j^+, E_{oi}^+) + \sum_{i=1}^{\infty} \sum_{j=2}^{\infty} B(E_j^-, E_{oi}^+) \right. \tag{2.6-30}$$

$$\left. + \sum_{i=2}^{\infty} \sum_{j=1}^{\infty} B(E_j^+, E_{oi}^-) + \sum_{i=2}^{\infty} \sum_{j=2}^{\infty} B(E_j^-, E_{oi}^-) \right\}$$

where

$$E_j^+ = 2(j-1)z_L + z_R$$

$$E_j^- = 2(j-1)z_L - z_R \tag{2.6-31}$$

$$E_{oi}^+ = 2(i-1)z_L + z_p$$

$$E_{oi}^- = 2(i-1)z_L - z_p$$

and

$$B(E,E_o) = \exp(-.5[E_o-E]^2/\sigma_z^2)\{\mathrm{erf}(K[b1 - b2 - b3]) + \mathrm{erf}(K[b1 + b2 + b3])\}$$

$$+ \exp(-.5[E_o+E]^2/\sigma_z^2)\{\mathrm{erf}(K[b1 + b2 - b3]) + \mathrm{erf}(K[b1 - b2 + b3])\} \quad (2.6\text{-}32)$$

where

$$K = \frac{1}{\sqrt{2}\ \sigma_z\sigma_{zo}\sigma_{z^*}} \qquad b1 = H_d\sigma_z^2$$

$$b2 = E\ \sigma_{zo}^2 \qquad b3 = E_o\ \sigma_{z^*}^2 \quad (2.6\text{-}33)$$

The form of the "B-function" is identical to F_z (Equation 2.6-28) for the case of no limit to vertical mixing. Differences arise in the use of (E,E_o) rather than (z_R,z_p), so that the presence of the mixing lid is manifest in Equation 2.6-31.

The outer sum over the index i accounts for reflections between the mixing lid and the surface before the puff reaches the hill. The inner sum over the index j accounts for reflections that may occur as material diffuses above H_d when the puff passes the hill. The inner summation will generally produce non-zero terms only for j = 1, unless a mixing height only slightly greater than H_d is found. This circumstance may not occur at all, given the definition of H_d and z_L. In evaluating the sums, terms are included for greater values of each index until the fractional change in F_z is reduced to less than 1%. The distribution of material in the vertical becomes well-mixed when σ_z reaches 1.6 z_L. At this point, F_z in equation 2.6-27 reduces to

$$F_z = \sqrt{2\pi}\ \sigma_z/z_L \quad (2.6\text{-}34)$$

2.6.5 Operational Characteristics

The best way to illustrate the behavior of CTSG is to present concentrations obtained for a specific application, and to compare these with what would have been obtained if the terrain feature had been ignored. We take this approach in this section by simulating ground-level concentration patterns at receptors on a hill for the situation in which a single puff moves across the hill along a curved trajectory.

The hill chosen for this exercise is twice as long as it is wide, with its major dimension oriented north-south. The relief height of the hill is set to 100 m, and its dimensions at its base are 2264 m by 1132 m. The polynomial function describing its shape is characterized by the following parameters:

relief (m)	100
expo (1,2)	2, 2
scale (1,2) (m)	800, 400
axmax (1,2) (m)	1132, 566
xc, yc (m)	0, 0
thetah (deg)	0
zgrid (m)	25

Note that (xc,yc) are the coordinates of the center of the hill, thetah is the angle (CW) from north to the major axis of the hill, and zgrid is the elevation of the grid-plane above sea level.

The incident flow for this hill consists of a height-profile in which wind speeds are constant at 1.5 m/s, and the temperature gradient is constant with a Brunt-Vaisala frequency of 0.0167 s^{-1}. For the 100 m tall hill, this profile produces a dividing-streamline height of 10.18 m. The mixing height is set at 2000 m.

For this demonstration, the following formulas were used to specify the dispersion parameters:

$$\sigma_z = \sqrt{\sigma_{zi}^2 + (i_z t \mathcal{F}_z)^2}$$

$$\mathcal{F}_z = 1/(1 + .945(t/100)^{.806})$$

where $\sigma_{zi} = 5$ m and $i_z = 0.1$; and

$$\sigma_y = \sqrt{\sigma_{yi}^2 + (i_y t \mathcal{F}_y)^2}$$

$$\mathcal{F}_y = 1/(1 + .9\sqrt{t/1200})$$

where $\sigma_{yi} = 50$ m and $i_y = .25$.

These equations result in a puff size that produces significant concentrations on the ground in the absence of the hill, since the puff height is set at 45 m (MSL), or 20 m above the local grid elevation. Hence, the center of the puff is approximately 10 m above H_d for this demonstration.

The puff initially lies to the southwest of the hill. Its movement is tracked in timesteps of 5 minutes, so that it takes several timesteps to move across the hill. The wind direction shifts by 10 degrees each time-step, from an initial direction of 270 degrees. The puff contains 600 g of material.

The 1-hour average "foot-print" of concentrations produced by the movement of this puff is shown in Figure 2.6-6. The left panel illustrates simulated concentrations in the absence of the hill, and the right panel illustrates concentrations simulated by CTSG when terrain is present. The base of the hill function is outlined as an ellipse in each of these panels. Major features of CTSG are immediately apparent in these concentration patterns. Peak concentrations over the crest of the hill are larger by almost a factor of two, and puff material below H_d travels around the hill on either side. Note that some detail in the contours arises from discrete receptor locations. Even though 325 receptors were used (one at each intersection of the 100 m tic-marks), there is not enough coverage to produce smooth contours everywhere.

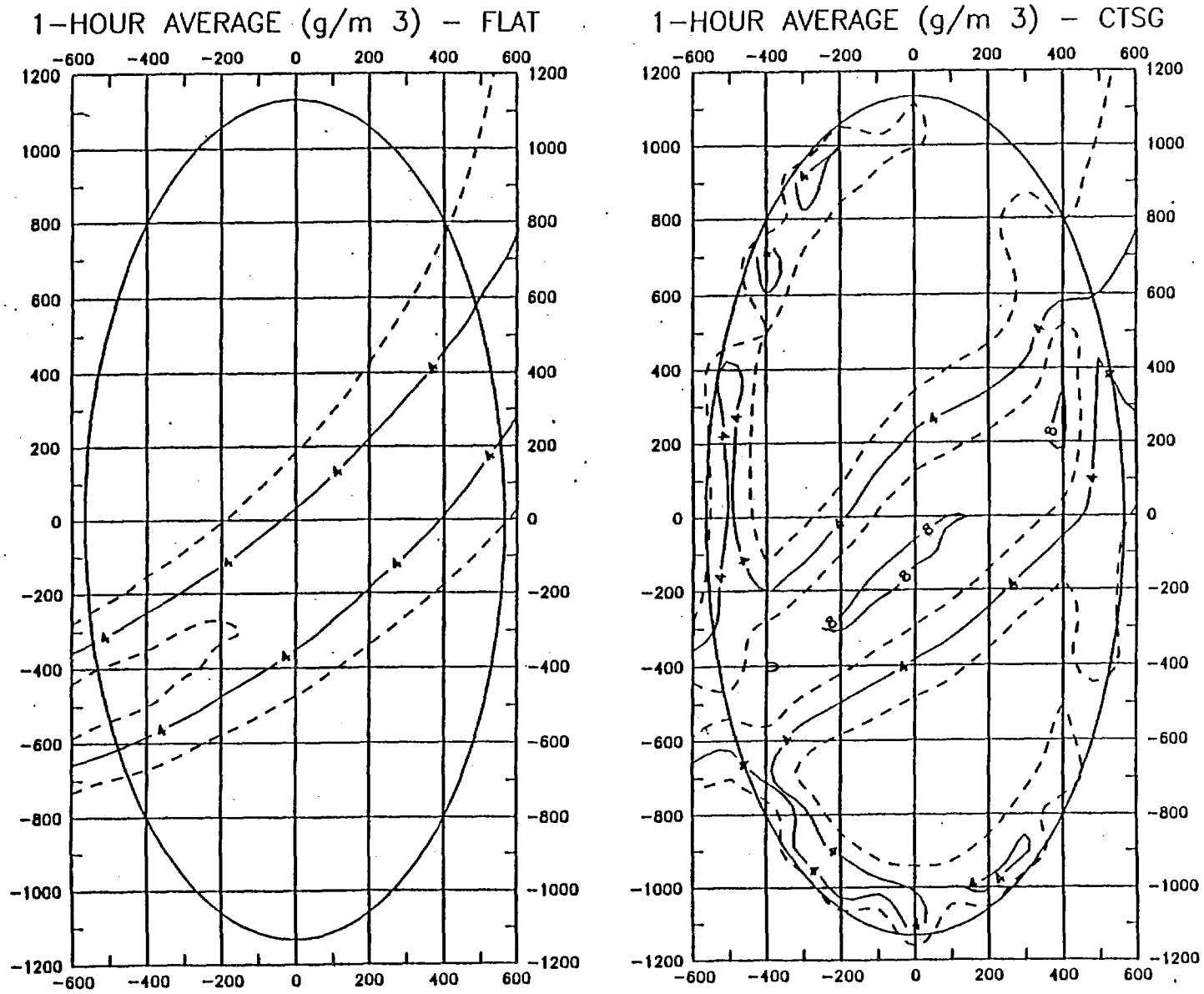

Figure 2.6-6. Concentrations (g/m^3) produced by CTSG (both with and without the hill), averaged over a period of one hour. The single puff that was simulated traveled over the hill in approximately 25 minutes during the hour.
(Contour interval = 2 g/m^3; grid units = m).

The "foot-prints" of the puff during each of the time-steps in which the puff was over the hill are shown in Figures 2.6-7 (a-f) corresponding to time-steps 3 through 8. These figures illustrate how CTSG partitions the puff during each step according to the relative position of the center of the puff, the dividing streamline height (H_d), and the position of the stagnation streamline. It is important to note that this partition does not increase the number of puffs in the model. Although the distribution becomes fragmented in the mathematics, all information remains referenced to a circular puff of a prescribed size. When a variable such as the flow direction changes between steps as it does in this example, the concentrations are obtained as if the current properties of the flow existed for all time, and the puff is partitioned according to those properties. Hence, the stagnation streamline in this demonstration differs from one step to another, and so the separation distance between the trajectory of the center of the puff and the stagnation streamline also differs from one step to another.

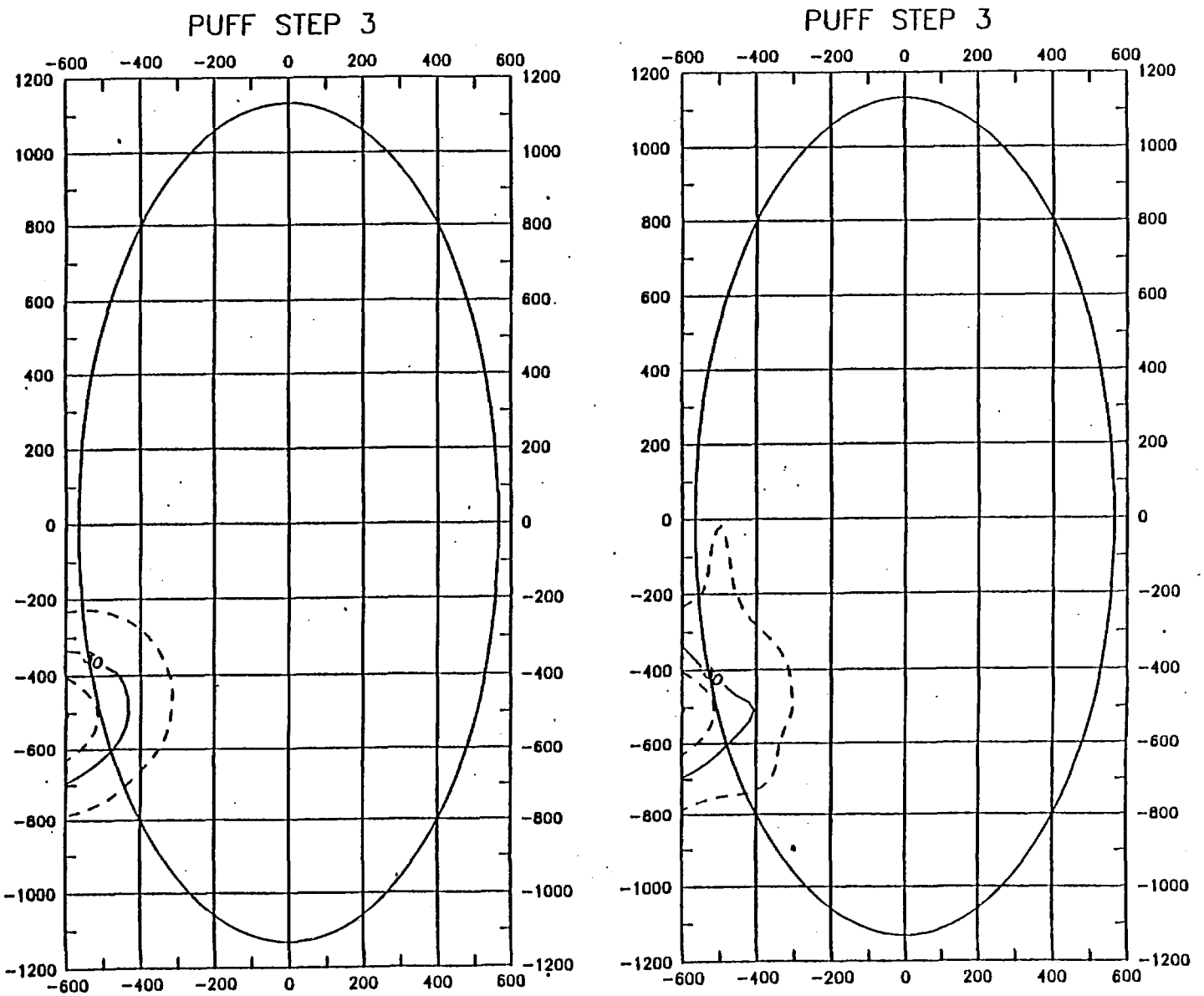

Figure 2.6-7a. Concentrations (g/m^3) produced by CTSG (both with and without the hill) during 5-minute time-step number 3. (Contour interval = 20 g/m^3; grid units = m).

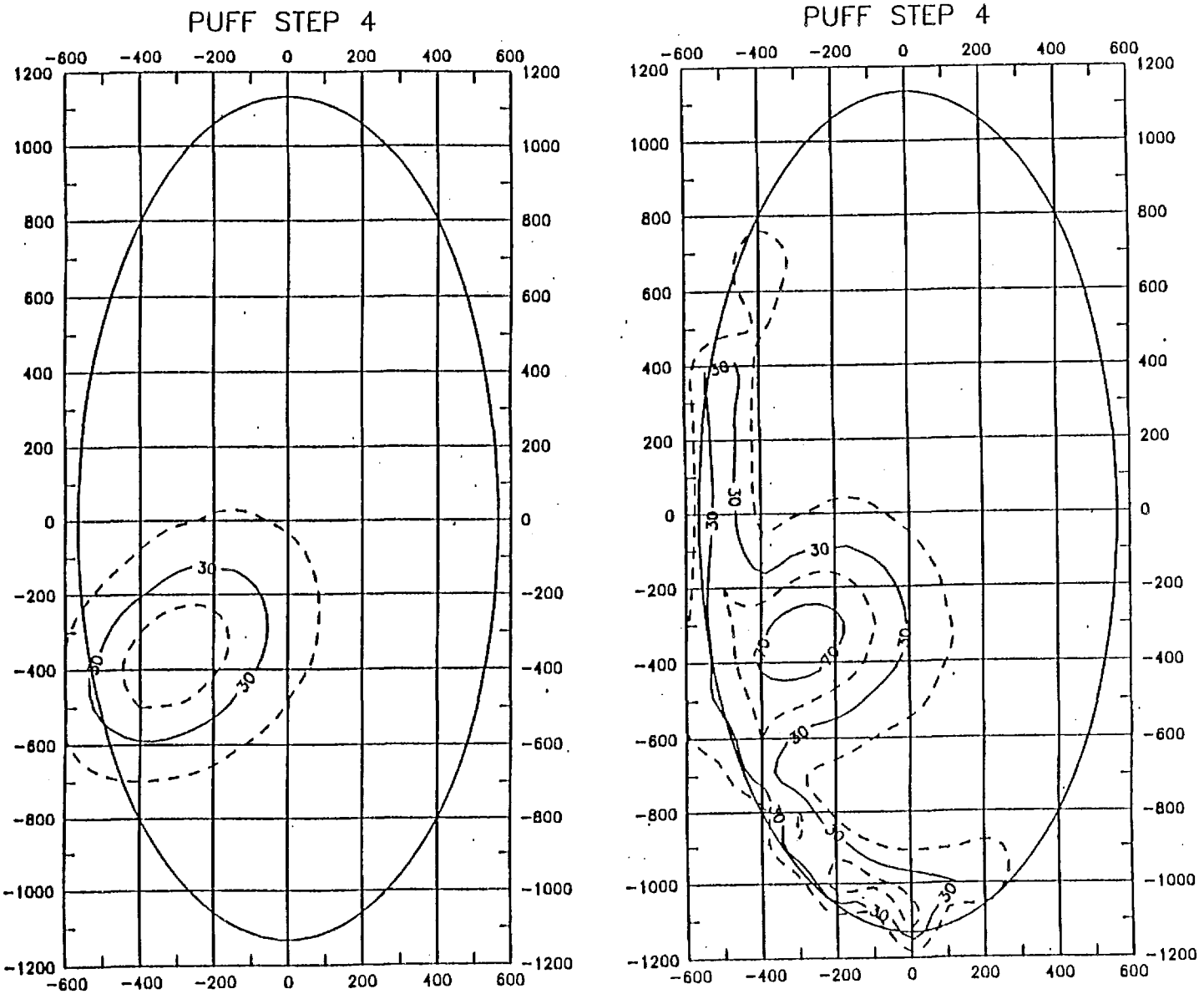

Figure 2.6-7b. Concentrations (g/m^3) produced by CTSG (both with and without the hill) during 5-minute time-step number 4. (Contour interval = 20 g/m^3; grid units = m).

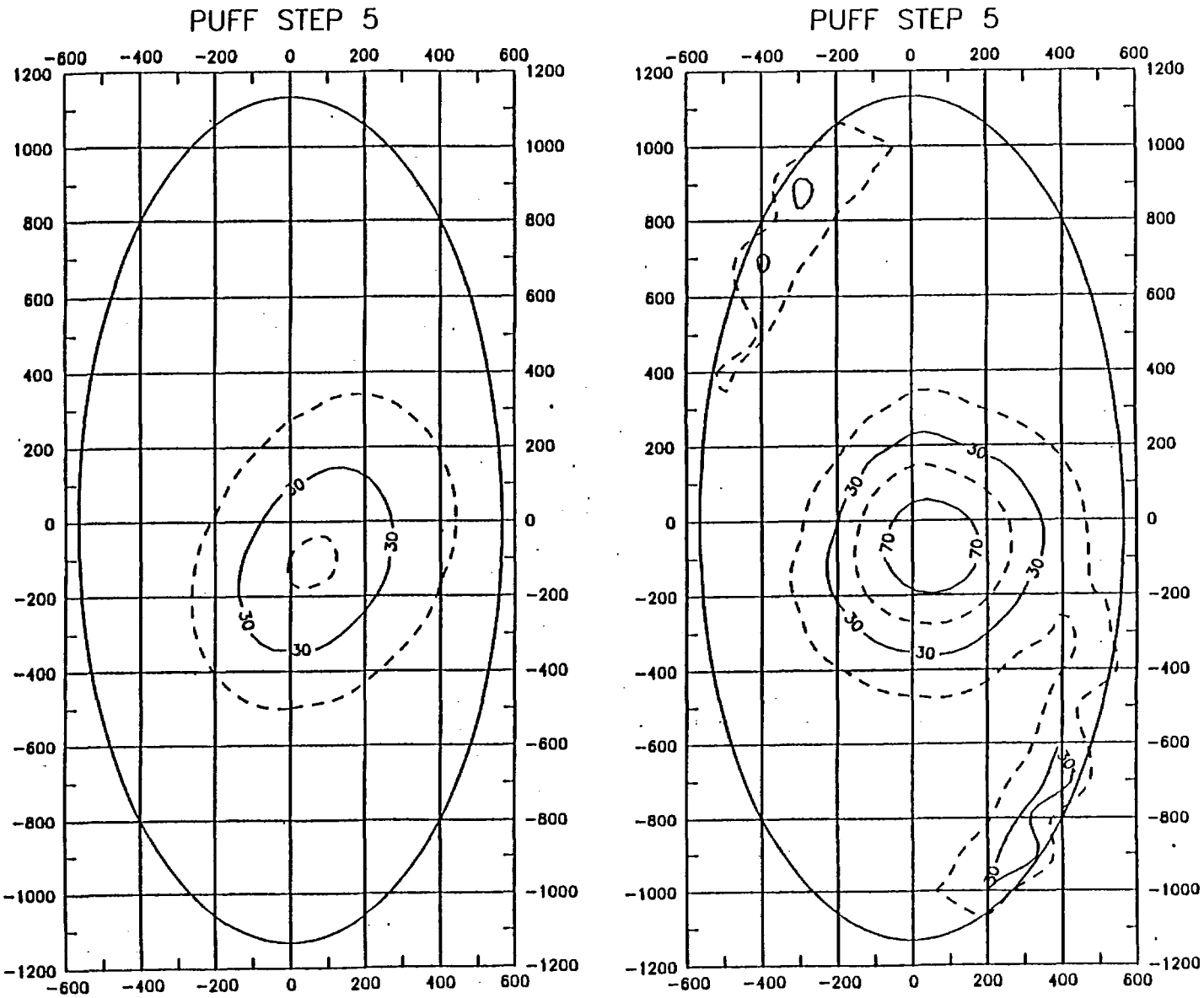

Figure 2.6-7c. Concentrations (g/m^3) produced by CTSG (both with and without the hill) during 5-minute time-step number 5. (Contour interval = 20 g/m^3; grid units = m).

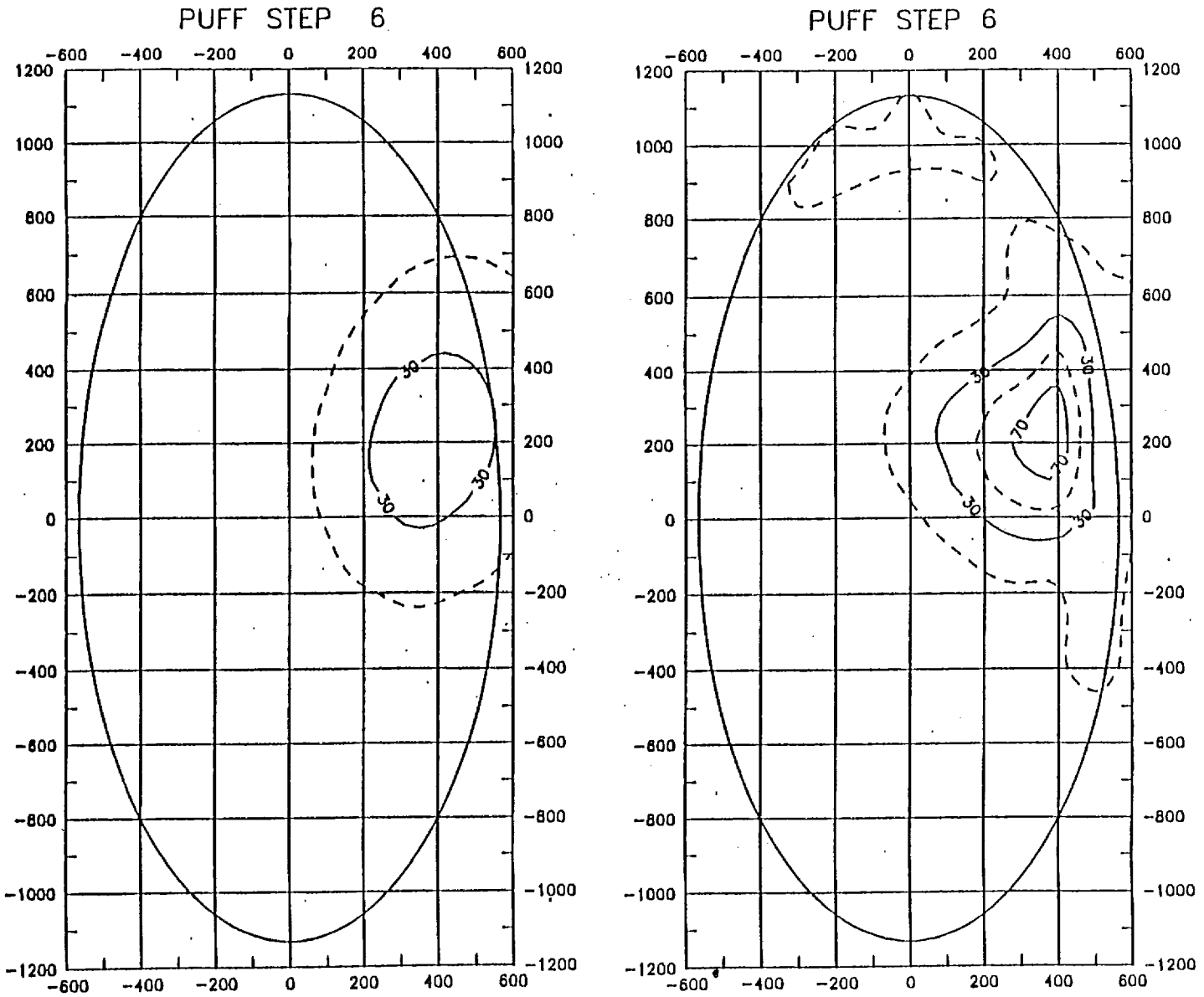

Figure 2.6-7d. Concentrations (g/m^3) produced by CTSG (both with and without the hill) during 5-minute time-step number 6. (Contour interval = 20 g/m^3; grid units = m).

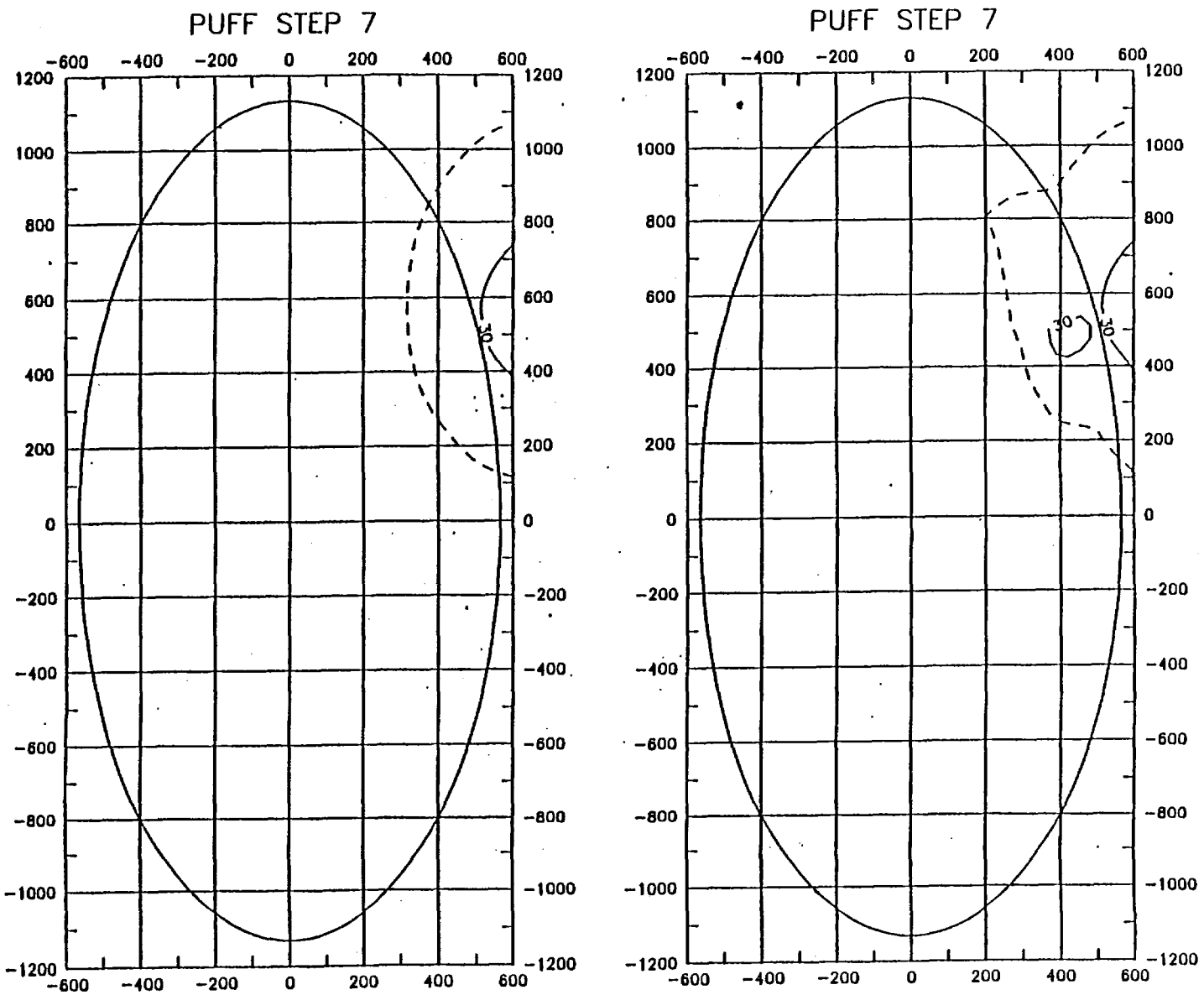

Figure 2.6-7e. Concentrations (g/m^3) produced by CTSG (both with and without the hill) during 5-minute time-step number 7.
(Contour interval = 20 g/m^3, grid units ...)

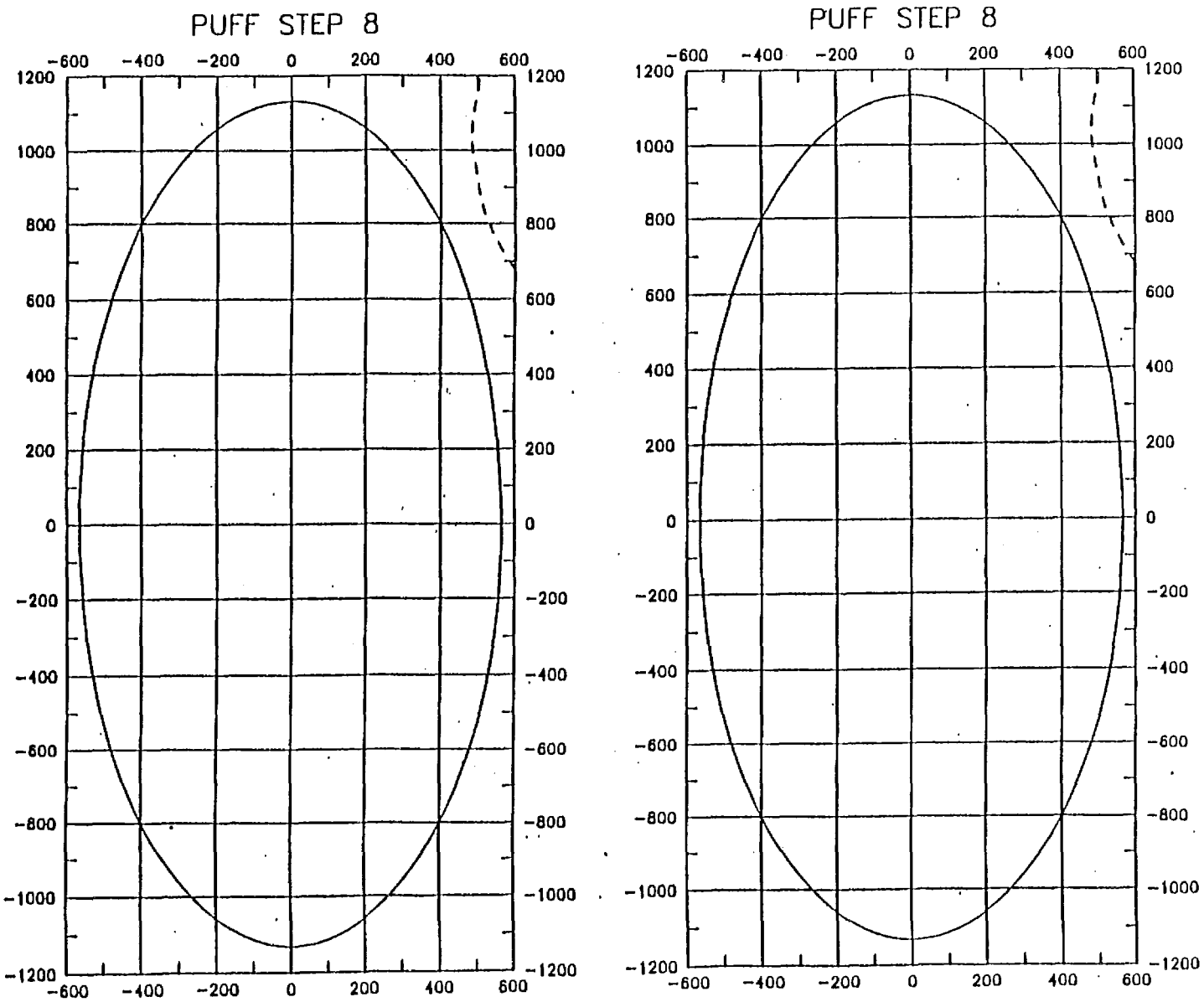

Figure 2.6-7f. Concentrations (g/m^3) produced by CTSG (both with and without the hill) during 5-minute time-step number 8. (Contour interval = 20 g/m^3; grid units = m).

2.7 Dry Deposition

Many complex processes are involved in the transfer and deposition of pollutants at the surface. Sehmel (1980) compiled a list (Table 2.7-1) of some of the most important factors that are known to influence dry deposition rates. The variables listed include the properties of the depositing material (e.g., particle size, shape, and density; gas diffusivity, solubility, and reactivity), the characteristics of the surface (e.g., surface roughness, vegetation type, amount, and physiological state), and atmospheric variables (e.g., stability, turbulence intensity). Hicks (1982) noted the important differences controlling the deposition of large particles (e.g., gravitational settling, inertial impaction) and those controlling gases (e.g., turbulence, molecular diffusion). Deposition of small particles is complicated by the fact that they may be influenced by the processes affecting both gases and large particles.

A commonly used measure of deposition is the deposition velocity, v_d, defined as:

$$v_d = F/\chi_s \qquad (2.7\text{-}1)$$

where, v_d is the deposition velocity (m/s),
F is the pollutant deposition flux ($g/m^2/s$), and,
χ_s is the pollutant concentration (g/m^3).

Due to the number and variability of the factors influencing dry deposition rates, reported deposition velocities exhibit considerable variability. For example, SO_2 deposition velocity measurements summarized by Sehmel (1980) range over two orders of magnitude (Figure 2.7-1). Particle deposition velocities (Slinn et al., 1978) show an even greater variability (Figure 2.7-2). Although it is not practical to include in the deposition model the effects of all of the variables listed in Table 2.7-1, it is possible, based on the atmospheric, surface, and pollutant properties to parameterize many of the most important effects. The CALPUFF deposition module provides three options reflecting different levels of detail in the treatment of dry deposition.

Table 2.7-1

Factors Influencing Dry Deposition Rates

Micrometeorological Variables	Depositing Material	Surface Variables
Aerodynamic roughness	Particles	Accommodation
- Mass transfer		- Exudates
(a) Particles	Agglomeration	- Trichomes
(b) Gases	Diameter	- Pubescence
- Heat	Density	- Wax
- Momentum	Diffusion	Biotic surfaces
Atmospheric stability	- Brownian	Canopy growth:
Diffusion, effect of:	- Eddy equal to	- Dormant
- Canopy	(a) Particle	- Expanding
- Diurnal variation	(b) Momentum	Senescent
- Fetch	(c) Heat	Canopy structure:
Flow separation:	- Effect of canopy on	- Areal density
- Above canopy	Diffusiophoresis	- Bark
- Below canopy	Electrostatic effects	- Bole
Friction velocity	- Attraction	- Leaves
Inversion layer	- Repulsion	- Porosity
Pollutant concentration	Gravitational settling	- Reproductive structure
Relative humidity	Hygroscopicity	- Soils
Seasonal variation	Impaction	- Stem
Solar radiation	Interception	- Type
Surface heating	Momentum	Electrostatic properties
Temperature	Physical properties	Leaf-vegetation:
Terrain	Resuspension	- Boundary layer
- Uniform	Shape	- Change at high winds
- Nonuniform	Size	- Flutter
Turbulence	Solubility	- Stomatal resistance
Wind velocity	Thermophoresis	Non-biotic surfaces
Zero-plane displacements		pH effects on:
- Mass transfer	Gases	- Reaction
(a) Particles		- Solubility
(b) Gases	Chemical activity	Pollutant penetration and distribution in canopy
- Heat	Diffusion:	Prior deposition loading
- Momentum	- Brownian	Water
	- Eddy	
	Partial pressure in equilibrium with surface	
	Solubility	

From: Sehmel (1980)

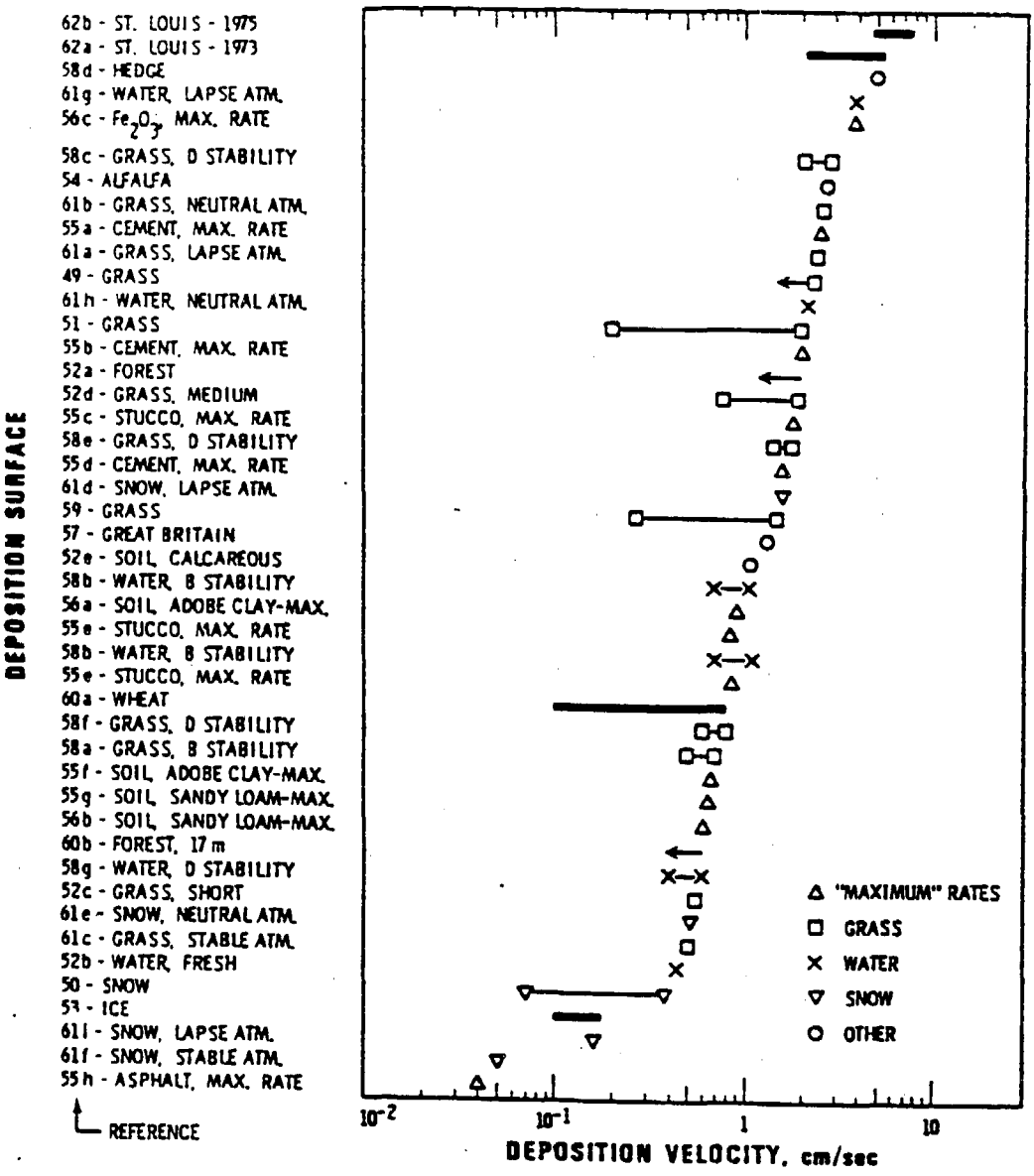

Figure 2.7-1. Summary of observed SO_2 deposition velocities (from Sehmel (1980)).

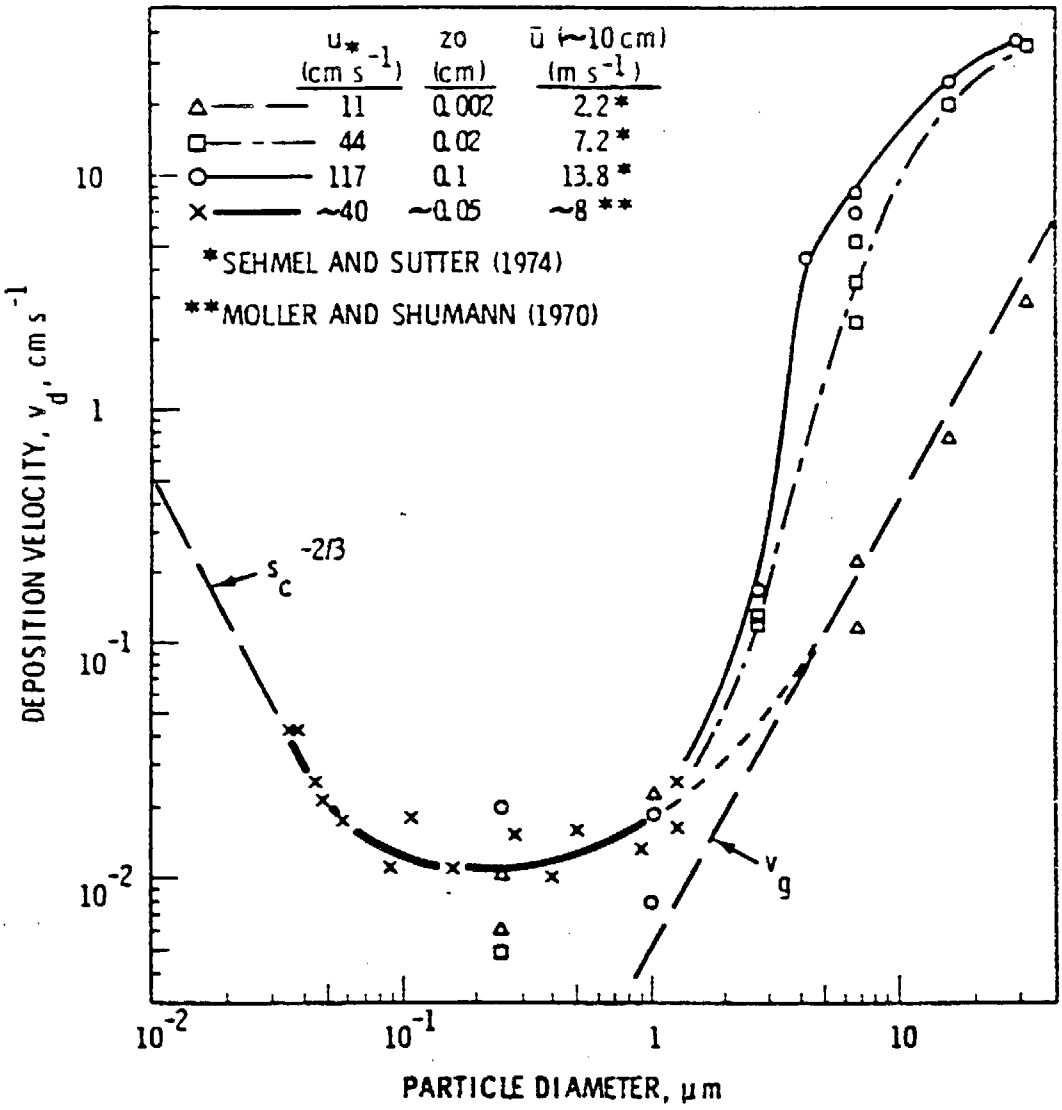

Figure 2.7-2 Observed deposition velocities as a function of particle size for 1.5 g/cm^3 density particles. Measured by Sehmel and Sutter (1974) and Moller and Schumann (1970). Figure from Slinn et al. (1978).

- Full treatment of spatially and temporally varying gas/particle deposition rates predicted by a resistance deposition model.

- User-specified 24-hour cycles of deposition velocities for each pollutant. This option allows a "typical" time dependence of deposition to be incorporated, but does not include any spatial dependencies.

- No dry deposition. A switch is incorporated into the model to by-pass all the dry deposition calculations. This option will provide for faster model execution for screening runs or pollutants not experiencing significant deposition.

The user specifies a flag in the control file for each pollutant which determines if dry deposition is treated and the specific method used to compute the deposition velocities (see Input Group 2, Section 4.2.1).

If the resistance deposition model is used, the user must input values for several parameters describing the characteristics of the pollutant (e.g., solubility, reactivity, diffusivity for gases, the size distribution for particles) (see Input Group 7 and 8) which are used in the computation of the resistances. In addition, several reference parameters and a flag indicating the state of unirrigated vegetation (i.e., stressed, unstressed, or inactive) are required (see Input Group 9).

If any pollutant is flagged as using "user-specified" deposition velocities, the user must prepare a data file with a 24-hour diurnal cycle of deposition velocities for each flagged species (see Section 4.2.5).

2.7.1 Vertical Structure and Mass Depletion

The CALPUFF dry deposition model is based on an approach which expresses the deposition velocity as the inverse of a sum of "resistances" plus, for particles, gravitational settling terms. The resistances represent the opposition to transport of the pollutant through the atmosphere to the surface. Slinn et al. (1978) describe a multilayer resistance model for dry

deposition. As illustrated in Figure 2.7-3, the atmosphere can be divided into four layers for purposes of computing dry deposition rates. For gases, an additional (vegetation) layer is included.

(A) Layer Aloft. The top layer is the region above the current mixing height. It contains pollutant material either injected directly from tall stacks, or dispersed upward during previous turbulent activity. Due to the low rate of turbulent mixing in this layer, its pollutant is essentially cutoff from the surface. Therefore, this material is not subject to dry deposition until it becomes entrained into the mixed-layer.

(B) Mixed-Layer. The top of the mixed-layer defines the depth of the turbulent boundary layer. Layer B extends down to a reference height within the atmospheric surface layer. Pollutant mixing is dominated by turbulent processes. During convective conditions, pollutants in this layer quickly become uniformly mixed in the vertical. The resistance to pollutant transfer during these conditions is very small compared to the resistances in layers C, D, and E. However, during stable conditions, the mixed-layer resistance may be substantial (Wesely and Hicks, 1977). The treatment of the mixed-layer resistance is based on the overall boundary layer diffusivity parameterized in terms of micrometeorological scaling variables.

(C) Surface Layer. The surface layer is a shallow layer (~ 10 m) next to the ground that rapidly adjusts to changes in surface conditions. Because vertical fluxes are nearly constant, this layer is also called the constant-flux layer. The atmospheric resistance, r_a, is used to parameterize the rate of pollutant transfer in Layer C.

(D) Deposition Layer. Over very smooth surfaces, a thin non-turbulent layer (the deposition layer) develops just above the surface. For typically rough surfaces, this layer is constantly changing and is likely to be intermittently turbulent. For this reason, Hicks (1982) calls this layer the "quasi-laminar" layer. The primary transfer mechanisms across the laminar deposition layer are molecular diffusion for gases, and Brownian diffusion and inertial impaction for particles. However,

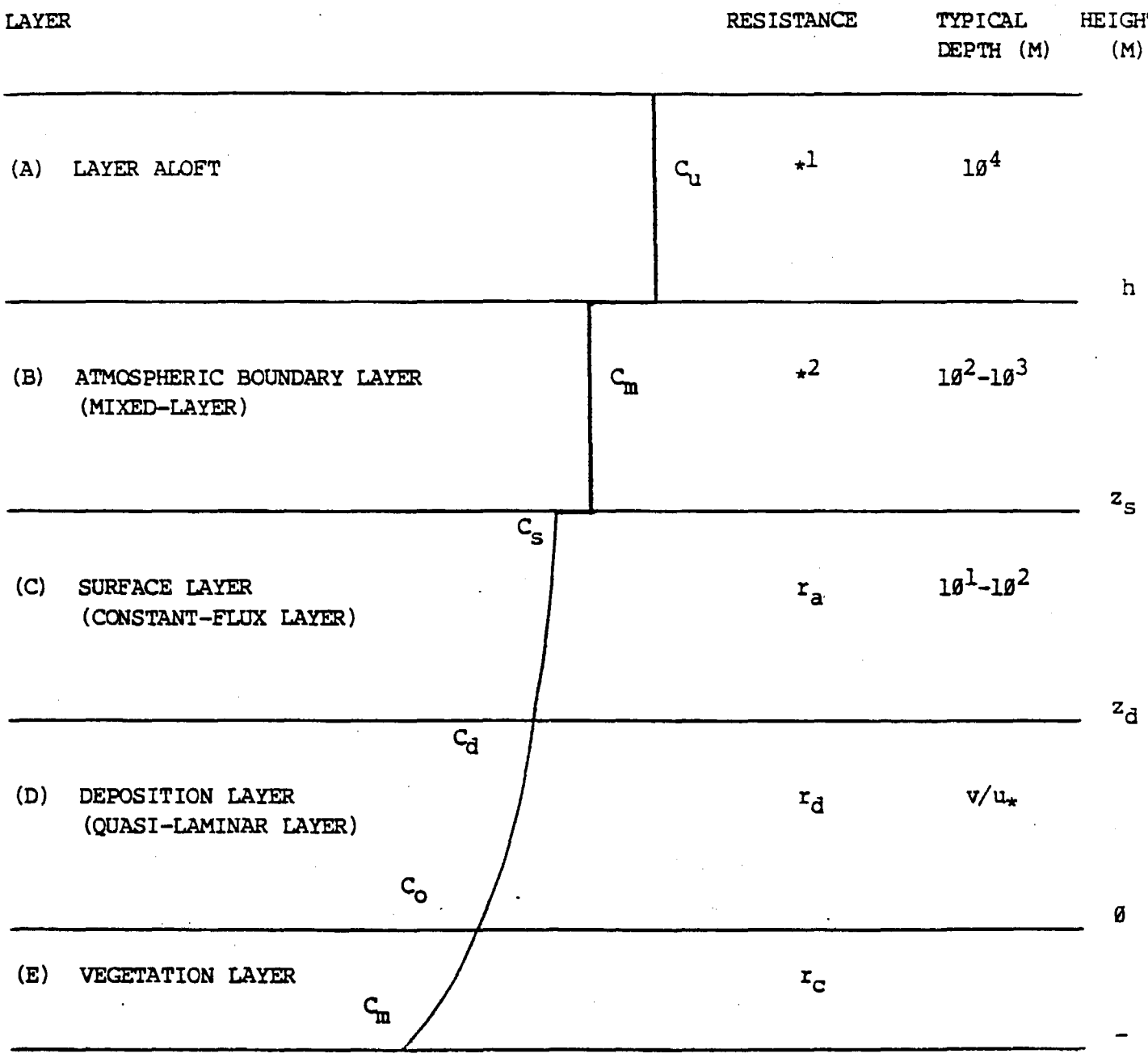

*1 Material in the top layer is not available for deposition at the surface until entrained into the mixed-layer.

*2 Overall mixed-layer resistance included in Eqn. (2.7-5)

Figure 2.7-3. Multilayer structure used in the dry deposition resistance model (adapted from Slinn et al., 1978).

surface roughness elements (e.g., leaf hairs) can sometimes penetrate the deposition layer, providing an alternate route for the pollutant transfer (Hicks, 1982). Under conditions of low atmospheric resistance, the deposition layer resistance, r_d, can be the dominant resistance controlling the rate of deposition for particles and some soluble, high molecular weight gases.

(E) Vegetation Layer. Vegetation is a major sink for many soluble or reactive gaseous pollutants. After passing through the stomata, soluble pollutants dissolve in the moist mesophyll cells in the interior of the leaves. Reactive pollutants may also interact with the exterior (cuticle) of the leaves. Due to the response of the stomata to external factors such as moisture stress, temperature, and solar radiation, the resistance in the vegetation layer (i.e., the canopy resistance, r_c) can show significant diurnal and seasonal variability. An alternate pathway that is potentially important in sparsely vegetated areas or overwater is deposition directly to the ground/water surface. Although not involving vegetation, it is convenient to include the ground/water surface resistance as a component of r_c because, like the vegetation resistances, it is a resistance in a layer below the laminar deposition layer.

In the CALPUFF model, the fraction of the pollutant mass above and below the current mixed layer is tracked. At any point in time, only pollutant material below the mixing height can be deposited at the surface. However, each time step as the mixing height changes, pollutant mass is transferred between Layers A and B. Typically, in the morning, as the boundary layer grows in response to solar heating of the land surface, material in the top layer is entrained into the mixed-layer and becomes available for dry deposition at the surface. In the evening, convective activity ceases, and material above the shallow nocturnal boundary layer height is isolated until the next diurnal cycle.

Once puffs have become uniformly mixed through the boundary layer, a surface depletion method (Scire et al., 1984) can be used to account for the mixed-layer (Layer B) resistance. The pollutant flux, F, at the reference height within the surface layer can be written as:

$$F = D_{b1} (\chi_m - \chi_s)/(h - z_s) = v_d \chi_s \qquad (2.7\text{-}2)$$

where χ_m is the pollutant concentration (g/m^3) within the mixed-layer,
χ_s is the pollutant concentration (g/m^3) at the top of the surface layer,
h is the mixed-layer height (m),
z_s is the surface layer height (m), and,
D_{b1} is an overall boundary layer eddy diffusivity (m^2/s).

The boundary layer eddy diffusivities during stable conditions (Brost and Wyngaard, 1978) can be expressed as:

$$D_{b1} = k_1 u_* h \qquad (2.7\text{-}3)$$

and during neutral or unstable conditions as:

$$D_{b1} = \text{Maximum } [k_1 u_* h \ , \ k_2 w_* h] \qquad (2.7\text{-}4)$$

where k_1 and k_2 are constants with default values of 0.01 and 0.1, respectively.

The term $v_d \chi_s$ can be written as $v_d' \chi_m$, where v_d' is an effective deposition velocity taking into account boundary layer mass transfer. From Eqn. (2.7-2), v_d' is:

$$v_d' = D_{b1} v_d / [D_{b1} + v_d (h - z_s)] \qquad (2.7\text{-}5)$$

When turbulent mixing within Layer B is rapid compared to the rate of deposition at the surface, the atmosphere quickly replaces material that is deposited. During these conditions, D_{b1} is large, and $v_d' \sim v_d$. However, the rate of deposition can be limited by the rate of pollutant transfer through Layer B to the vicinity of the surface. During stable conditions, D_{b1} may be small compared to $v_d(h-z_s)$, and v_d' may be substantially smaller than v_d. In the near-field of a source, before the plume has spread through the boundary layer, it is assumed that $v_d' \sim v_d$. This allows the near-field vertical Gaussian distribution to be maintained.

The resistances in the layers below the reference height in the surface constant-flux layer determine v_d. The parameterization of these resistances is discussed separately for gases and particles in Sections 2.7.2 and 2.7.3, respectively. Once v_d is determined, v_d' is computed from Eqn. (2.7-5). Each time step, the mass of the pollutant in the puff is adjusted to account for the dry removal:

$$Q_m(t+\Delta t) = Q_m(t)\ \exp\left[-(v_d'\,dt/\Delta s)\int_s^{s+\Delta s} g(s')ds'\right] \qquad (2.7\text{-}6)$$

where Q_m is the mass (g) of the pollutant in the puff below the mixing height (h) at time t and t+Δt,

Δt is the time step (s),

s, s+Δs are the positions of the puff at the beginning and end of the time step, and,

g(s) is the vertical term of the Gaussian puff equation. For a puff uniformly mixed in the vertical, g(s) = 1/h.

If user-specified deposition velocities are used for any of the pollutants, the effective deposition velocity, v_d', is set equal to the user specified value read from the VD.DAT file.

2.7.2 Resistance Deposition Model For Gases

At the reference height, z_s, the deposition velocity for gases is expressed (Wesely and Hicks, 1977; Hicks, 1982) as the inverse of a sum of three resistances.

$$v_d = (r_a + r_d + r_c)^{-1} \qquad (2.7\text{-}7)$$

where r_a is the atmospheric resistance (s/m) through the surface layer,

r_d is the deposition layer resistance (s/m), and,

r_c is the canopy (vegetation layer) resistance (s/m).

Atmospheric Resistance

The atmospheric resistance is obtained by integration of the micrometeorological flux-gradient relationships (Wesely and Hicks, 1977):

$$r_a = \frac{1}{k\, u_*}[\ln(z_s/z_o) - \phi_H] \qquad (2.7\text{-}8)$$

where z_s is the reference height (m),
z_o is the surface roughness length (m),
k is the von Karman constant (~ 0.4),
u_* is the friction velocity (m/s),
ϕ_H is a stability correction term, and,
L is the Monin-Obukhov length (m).

The stability correction term accounts for the effects of buoyancy on the eddy diffusivity of the pollutant. It is assumed that the pollutant transfer is similar to that for heat (Wesely and Hicks, 1977). A gridded field of surface roughness lengths is passed to the model in the output file of the meteorological model, CALMET. In CALMET, the surface roughness length is either estimated from the predominant land use of each grid cell, or, if available, based on actual values entered by the user. Over water, due to the effect of the wind on wave height, the surface roughness length varies as a function of wind speed, and is computed internally within CALGRID. Hosker (1974) parameterizes z_o over water as:

$$z_o = 2.0 \times 10^{-6}\, u^{2.5} \qquad (2.7\text{-}9)$$

where u is the wind speed (m/s) at 10 m.

Deposition Layer Resistance

Due to the importance of molecular diffusion to the transport through the laminar deposition layer, the deposition layer resistance for gaseous pollutants is parameterized in terms of the Schmidt number:

$$r_d = d_1 S_c^{\,d_2}/(k\, u_*) \qquad (2.7\text{-}10)$$

where S_c is the Schmidt number (υ/D),

υ is the kinematic viscosity of air (m^2/s),

D is the molecular diffusivity of the pollutant (m^2/s), and,

d_1, d_2 are empirical parameters.

Experimental studies summarized by Hicks (1982) suggest a range of values for the empirical variables of 1.6 to 16.7 for d_1 and 0.4 to 0.8 for d_2. Intermediate values of $d_1 = 5$, and $d_2 = 2/3$ are recommended based on Shepherd (1974), Slinn et al. (1978), and Hicks (1982).

Canopy Resistance

The canopy resistance is the resistance for gases in the vegetation layer. There are three main pathways for uptake/reaction of the pollutant within the vegetation or surface:

(1) Transfer through the stomatal pore and dissolution or reaction in the mesophyll cells.

(2) Reaction with or transfer through the leaf cuticle.

(3) Transfer into the ground/water surface.

In the resistance model, these pathways are treated as three resistances in parallel.

$$r_c = [LAI/r_f + LAI/r_{cut} + 1/r_g]^{-1} \qquad (2.7\text{-}11)$$

where r_f is the internal foliage resistance (s/m) (Pathway 1),

r_{cut} is the cuticle resistance (s/m), (Pathway 2),

r_g is the ground or water surface resistance (s/m), (Pathway 3), and,

LAI is the leaf area index (ratio of leaf surface area divided by ground surface area). The LAI is specified in the model as a function of land use type.

The first pathway is usually the most important for uptake of soluble pollutants in vegetated areas. The internal foliage resistance consists of two components:

$$r_f = r_s + r_m \qquad (2.7\text{-}12)$$

where r_s is the resistance (s/m) to transport through the stomatal pore, and,
r_m is the resistance (s/m) to dissolution or reaction of the pollutant in the mesophyll (spongy parenchyma) cells.

Stomatal action imposes a strong diurnal cycle on the stomatal resistance, and, due to its important role in determining deposition rates for gaseous soluble pollutants such as SO_2, on the deposition velocity, as well. Stomatal opening/closing is a response to the plant's competing needs for uptake of CO_2 and prevention of water loss from the leaves. The stomatal resistance can be written (O'Dell et al., 1977) as:

$$r_s = p/(bD) \qquad (2.7\text{-}13)$$

where p is a stomatal constant ($\simeq 2.3 \times 10^{-8}$ m^2),
b is the width of the stomatal opening (m), and,
D is the molecular diffusivity of the pollutant (m^2/s).

The width of the stomatal opening is a function of the radiation intensity, moisture availability, and temperature. The variation of b during periods when vegetation is active can be represented (Pleim et al., 1984) as:

$$b = b_{max}[S/S_{max}] + b_{min} \qquad (2.7\text{-}14)$$

where b_{max} is the maximum width (m) of the stomatal opening ($\sim 10 \times 10^{-6}$ m),
b_{min} is the minimum width (m) of the stomatal opening ($\sim 0.1 \times 10^{-6}$ m),
S is the solar radiation (W/m^2) received at the ground, and,
S_{max} is the solar radiation (W/m^2) at which full opening of the stomata occur.

However, during periods of moisture stress, the need to prevent moisture loss becomes critical, and the stomata close. It can be assumed that $b = b_{min}$ for unirrigated vegetation under moisture stress conditions. When vegetation is inactive (e.g., during the seasonal dry periods in much of California), the internal foliage resistance becomes very large, essentially cutting off Pathway 1. In CALGRID, the state of the unirrigated vegetation is specified as one of these states (A) active and unstressed, (B) active and stressed, or (C) inactive.

The effect of temperature on stomatal activity has been reviewed by Pleim et al. (1984). The most significant effects are due to temperature extremes. During cold periods ($T < 10^{\circ}$ C), metabolic activity slows, and b is set equal to b_{min}. During hot weather conditions ($T > \sim 35^{\circ}$ C), the stomata are fully open ($b = b_{max}$) to allow evaporative cooling of the plant (assuming the vegetation is in state A - active and unstressed). These temperature effects provide additional bounds on the value of r_s given by Eqn. (2.7-13).

Mesophyll Resistance

The mesophyll resistance depends on the solubility and reactivity of the pollutant. It is an input parameter supplied to the deposition model for each gaseous species. O'Dell et al. (1977) estimate the mesophyll resistance for several pollutants. For soluble pollutants such as HF, SO_2, Cl_2 and NH_3, $r_m \sim 0.0$. The mesophyll resistance can be large for less soluble pollutants such as NO_2 (~ 500 s/cm) and NO (9400 s/cm). For other pollutants, r_m can be estimated based on the solubility and reactivity characteristics of the pollutant.

Cuticle Resistance

The second pathway for deposition of gases in the vegetation layer is via the leaf cuticle. This includes potential direct passage through the cuticle or reaction of the pollutant on the cuticle surface. Hicks (1982) notes that measurements of SO_2 deposition to wheat (Fowler and Unsworth, 1979) show significant cuticle deposition. However, Hosker and Lindberg (1982) suggest that passage of gases through the cuticle is negligible. Therefore, the cuticle deposition is likely to be controlled by the pollutant

reactivity. Pleim et al. (1984) parameterize r_{cut} as a function of the pollutant reactivity of the depositing gas relative to the reference values for SO_2.

$$r_{cut} = (A_{ref}/A)r_{cut}(ref) \qquad (2.7\text{-}15)$$

where A is the reactivity parameter for the depositing gas,
A_{ref} is the reference reactivity of SO_2 (~ 8.0), and,
$r_{cut}(ref)$ is the empirically determined reference cuticle resistance (s/m) of SO_2.

Pleim et al. (1984) suggest $r_{cut}(ref)$ is about 17 s/cm. Reactivity values for other pollutants are estimated at 8.0 (NO_2), 15.0 (O_3), 18.0 (HNO_3), and 4.0 (PAN).

Ground/Water Resistance

The third pathway through the "vegetation layer" involves deposition directly to the ground or water surface. In moderately or heavily vegetated areas, the internal foliage and cuticle resistances usually control the total canopy resistance. However, in sparsely vegetated areas, deposition directly to the surface may be an important pathway. Over water, deposition of soluble pollutants can be quite rapid.

The ground resistance, r_g, over land surfaces can be expressed (Pleim et al., 1984) relative to a reference value for SO_2:

$$r_g = (A_{ref}/A)r_g(ref) \qquad (2.7\text{-}16)$$

where $r_g(ref)$ is the reference ground resistance of SO_2 (~ 5 s/cm).

Slinn et al. (1978) parameterize the liquid phase resistance of the depositing pollutant as a function of its solubility and reactivity characteristics. Their results can be expressed as:

$$r_g = H/(\alpha_* d_3 u_*) \qquad (2.7\text{-}17)$$

where H is the Henry's law constant, which is the ratio of gas to liquid phase concentration of the pollutant, ($H \sim 4 \times 10^{-2}$ (SO_2), 4×10^{-7} (H_2O_2), 8×10^{-8} (HNO_3), 2×10^{0} (O_3), 3.5×10^{0} (NO_2), 1×10^{-2} (PAN), and 4×10^{-6} (HCHO)),

α_* is a solubility enhancement factor due to the aqueous phase reactivity of the pollutant ($\alpha_* \sim 10^3$ for SO_2, ~ 1 for CO_2), and

d_3 is a constant ($\sim 4.8 \times 10^{-4}$).

2.7.3 Resistances for Particulate Matter

Because particulate matter does not interact with vegetation in the same way as gaseous pollutants, particle deposition velocities are commonly expressed only in terms of r_a, r_d and a gravitational settling term. The atmospheric resistance, r_a, for a particle is the same as for a gas (Eqn. 2.7-8) The resistance in the vegetation layer (r_c) is not a factor because once penetrating the deposition layer, particles are usually assumed to stick to the surface (e.g., Voldner et al., 1986). Therefore, their behavior is similar to highly soluble/reactive gases with $r_c \sim 0$. Based on an assumption of steady-state conditions, the deposition velocity for particles can be expressed (Slinn and Slinn, 1980; Pleim et al., 1984) as:

$$v = (r_a + r_d + r_a r_d v_g)^{-1} + v_g \qquad (2.7\text{-}18)$$

where v_g is the gravitational settling speed (m/s) of the particle.

There are three major mechanisms for transport of particles across the deposition layer. Small particles (< 0.1 μm diameter) are transported through the laminar deposition layer primarily by Brownian diffusion. This process becomes less efficient as the particle diameter increases. Particles in the 2-20 μm diameter range tend to penetrate the deposition layer by inertial impaction. The stopping time, t, defined as the settling velocity divided by the acceleration due to gravity, is a measure of tendency of a particle to impact. Inertial impaction is most effective in the 2-20 μm diameter range. Larger particles are dominated by gravitational settling effects. The effect

of the terms involving v_g in Eqn. (2.7-18) always is to increase the deposition velocity. Particles in the range of 0.1-2 μm diameter range, such as sulfate, have very small settling velocities and are not efficiently transported across the deposition layer by either the Brownian diffusion or the inertial impaction mechanism. As a result, these particles have the lowest deposition velocities.

The deposition layer resistance can be parameterized (e.g., Pleim et al., 1984) in terms of the Schmidt number (Sc = υ/D, where υ is the viscosity of air, and, for particles, D is the Brownian diffusivity of the pollutant in air) and the Stokes number (St = $(v_g/g)(u_*^2/\upsilon)$, where v_g is the gravitational settling velocity and g is the acceleration due to gravity).

$$r_d = (Sc^{-2/3} + 10^{-3/St})^{-1} u_*^{-1} \qquad (2.7\text{-}19)$$

The diffusivity of a particle in air, D, is a function of the particle size. Smaller particles tend to be more efficiently transported by Brownian motion, and therefore have higher diffusivities. The Stokes number is a measure of the likelihood of impaction of the particle. It increases with increasing particle size.

The gravitational settling velocity is a function of the particle size, shape, and density. For spheres, the settling velocity is given by the Stokes equation:

$$v_g = [(d_p)^2 g(\rho_p - \rho_g)C]/(18\ \upsilon) \qquad (2.7\text{-}20)$$

where d_p is the particle diameter (m)
ρ_p is the particle density (g/m^3),
ρ_g is the air density (g/m^3), and,
C is the Cunningham correction for small particles. This correction given by:

$$C = 1 + (2\ \lambda/d_p)[a_1 + a_2 \exp(-a_3 d_p/\lambda)] \qquad (2.7\text{-}21)$$

where λ is the mean free path of air molecules (6.53×10^{-6} cm), and
a_1, a_2, a_3 are constants (1.257, 0.40, 0.55, respectively).

Because of the sensitivity of the deposition velocity to particle size, the effective deposition velocity is computed for a number of individual size categories, and then weighted by the actual size distribution. The particle size distribution is specified in terms of the geometric mass mean diameter and geometric standard deviation of the distribution. For sulfate, the geometric mass mean diameter is approximately 0.5 μm with a geometric standard deviation of approximately 2 μm.

2.8 Chemical Transformation

One of the design criteria of the CALPUFF model required the capability of modeling linear chemical transformation effects in a manner consistent with the puff formulation of the model. The CALPUFF chemical module contains three options for dealing with chemical processes:

- A pseudo-first-order chemical reaction mechanism for the conversion of SO_2 to $SO_4^=$ and NO_x ($NO + NO_2$) to NO_3^-. This mechanism is based on the chemical transformation scheme used in the MESOPUFF II model (Scire et al., 1984) and incorporates the most significant dependencies of spatially and temporally varying environmental conditions on the transformation rates.

- User-specified 24-hour cycles of transformation rates. This option allows simulation of the diurnal, time-dependent behavior of the transformation rates. However, the transformation rates with this option are spatially uniform.

- No chemical transformation. An option is provided to completely by-pass the chemical transformation calculations. This will reduce computer requirements for situations or pollutants for which chemical transformation effects are not significant.

The user selects one of the above options by specifying a mechanism flag in the CALPUFF control flag (see Section 4.2.1). The MESOPUFF II mechanism (Option 1) uses ozone concentrations (along with radiation intensity) as surrogates for the OH concentration during the day when gas phase free radical chemistry is active. With Option 1, hourly observations of ozone concentrations at one or more monitoring stations can read from a data file (OZONE.DAT) to provide the necessary estimates of ozone concentrations (see Section 4.2.6).

If "user-specified" transformation rates are used (Option 2), the user must prepare a data file (CHEM.DAT) with a 24-hour diurnal cycle of typical transformation rates for each species (see Section 4.2.7).

2.8.1 Description of the MESOPUFF II Chemical Mechanism

The chemical processes included in the MESOPUFF II mechanism (Option 1) are the conversion of sulfur dioxide to sulfate and the conversion of nitrogen oxides to nitrate aerosol. Figures 2.8-1 and 2.8-2 illustrate the chemical pathways for SO_2 and NO_x oxidation and aerosol formation. Oxidation may occur by gas and aqueous phase reactions. The gas phase reactions for both SO_x and NO_x involve free radical photochemistry and, therefore, are coupled to the oxidation of reactive organic gases (ROG). Homogeneous gas phase reaction is the dominant SO_2 oxidation pathway during clear, dry conditions (Calvert et al., 1978). Ozone and hydrogen peroxide are believed to be the principal oxidants for aqueous-phase oxidation of SO_2.

The oxidation of NO_x is dependent on gas phase $ROG/NO_x/O_3$ photochemistry. It is generally more rapid than SO_2 oxidation. As shown in Figure 2.8-2, NO_x can be oxidized to nitric acid (HNO_3) and organic nitrates (RNO_3) such as peroxyacetylnitrate (PAN). Nitric acid combines with ammonia gas to form solid or aqueous ammonium nitrate (NH_4NO_3). Unlike sulfate formation, the nitrate process is reversible. Equilibrium is established between nitric acid, ammonia, and ammonium nitrate:

$$NH_4NO_3 \longleftrightarrow HNO_3(g) + NH_3(g) \qquad (2.8\text{-}1)$$

The equilibrium constant for this reaction ($K = [NH_3][HNO_3]/[NH_4NO_3]$) is a nonlinear function of temperature and relative humidity as shown in Figure 2.8-3 (Stelson and Seinfeld, 1982). The equilibrium constant can vary several orders of magnitude over a typical diurnal cycle. Given fixed amounts of total nitrate, ammonia, and water vapor, higher NH_4NO_3 concentrations are expected at night due to lower nighttime temperatures and higher relative humidities. Thus, the nitrate aerosol cannot be considered a stable product like sulfate. Also, unlike sulfate, the ambient concentration of nitrate is limited by the availability of ammonia which is preferentially scavenged by sulfate (Stelson et al., 1983).

The transformation pathways for the five active pollutants (SO_2, $SO_4^=$, NO_x, HNO_3, and NO_3^-) included in the MESOPUFF II scheme are shown in

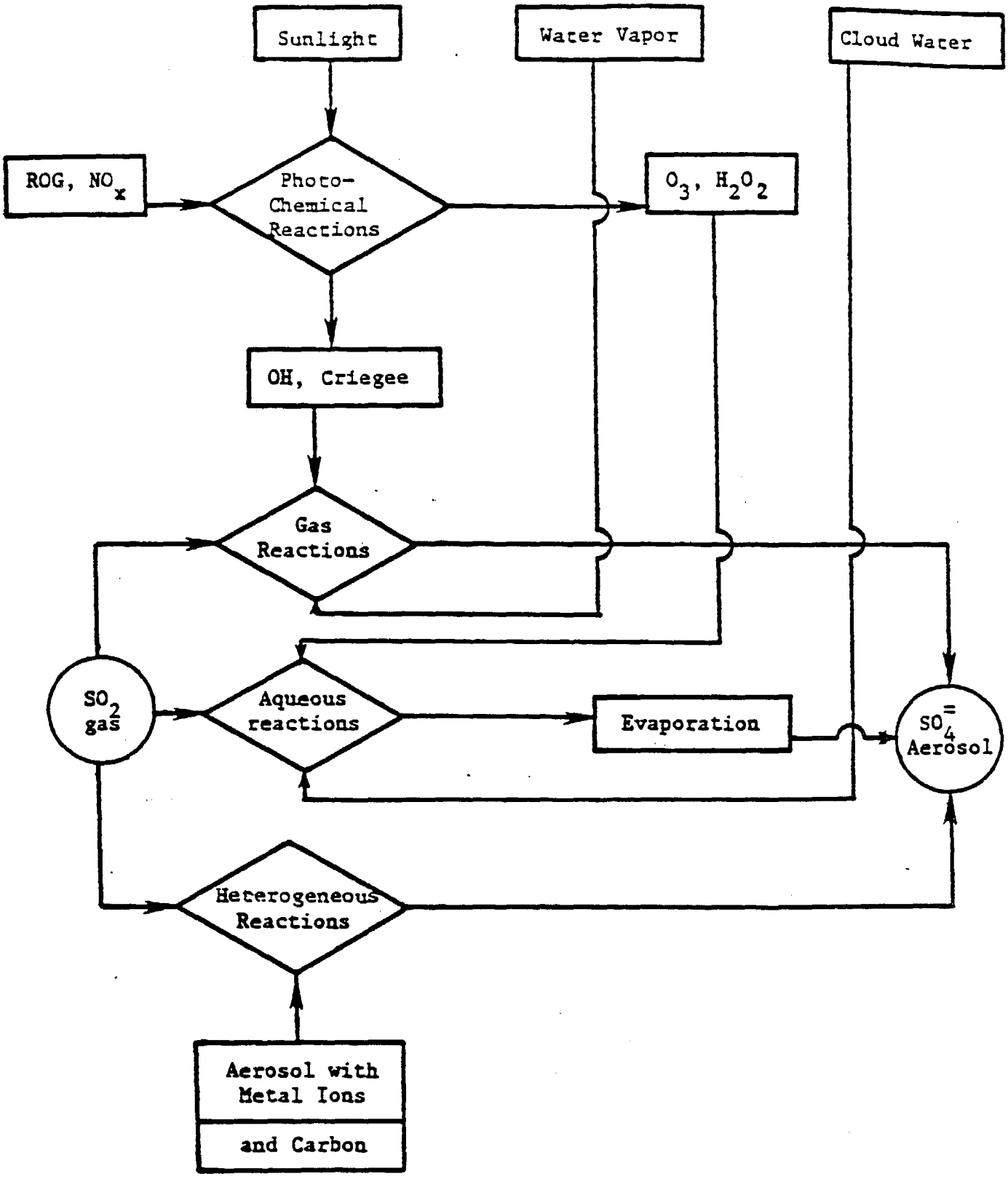

Figure 2.8-1. SO_2 oxidation pathways (from Scire et al., (1984)).

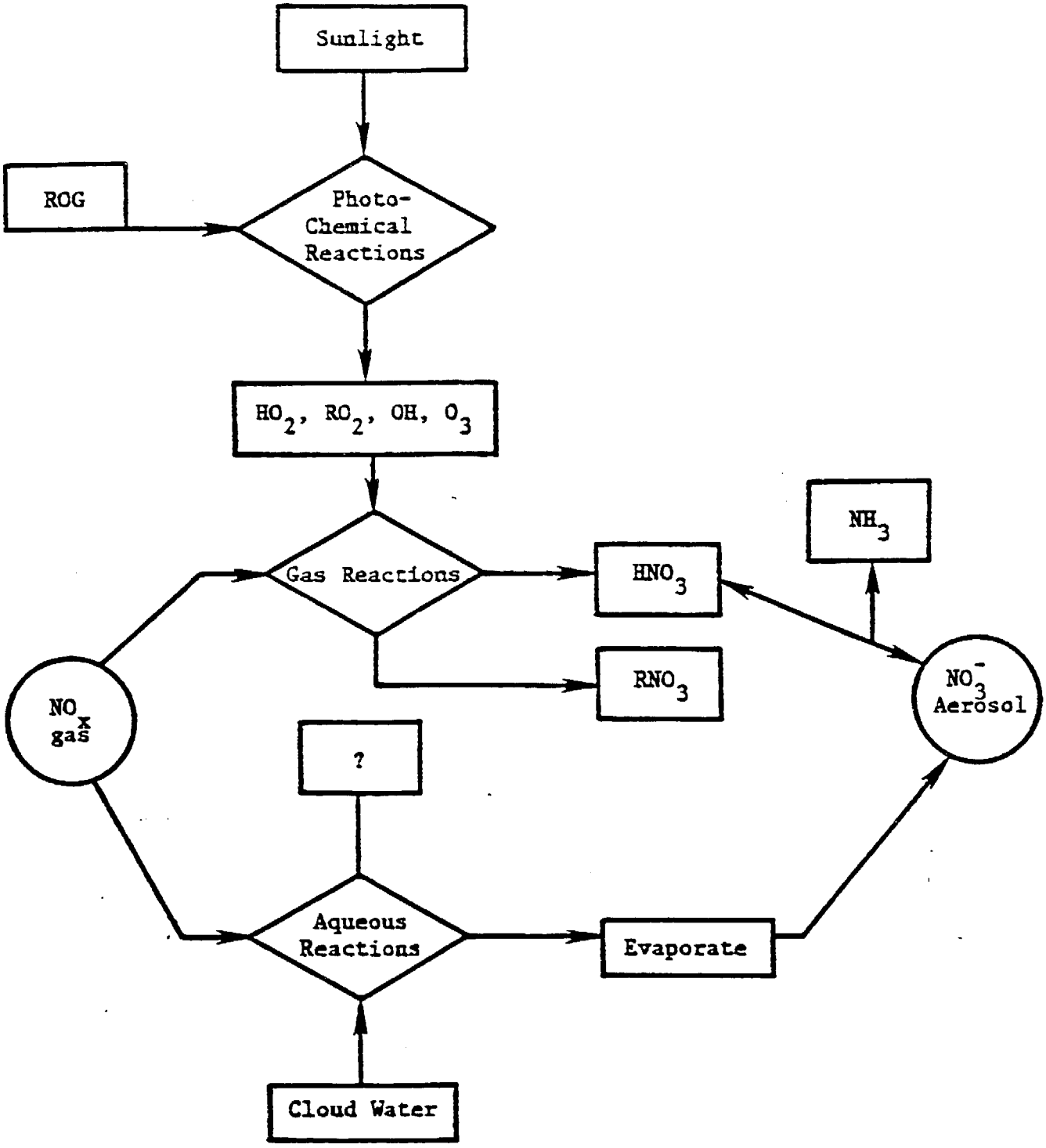

Figure 2.8-2. NO_x oxidation pathways (from Scire et al., 1984)).

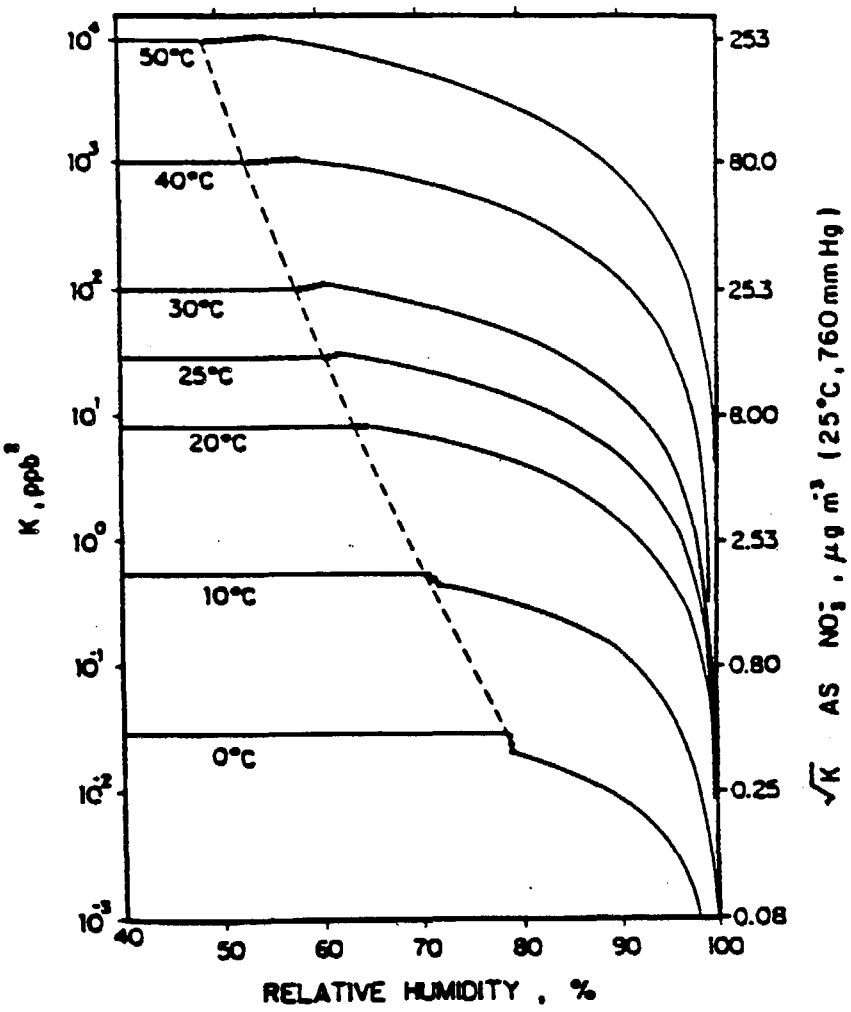

Figure 2.8-3. NH_4NO_3 dissociation constant as a function of temperature and relative humidity (from Stelson and Seinfeld, (1982)).

Figure 2.8-4. Transformation rate expressions were developed by statistically analyzing hourly transformation rates produced by a photochemical model. The photochemical model employed the RHC/NO_x/SO_x chemical mechanism of Atkinson et al. (1982). Plume SO_x/NO_x dispersing into background air containing ozone and reactive hydrocarbons was simulated over a wide range of conditions representing different solar radiation intensities, temperatures, dispersion conditions, background ozone and RHC concentrations, plume NO_x concentrations and emission times. The following transformation rate expressions, representing curve fits to the daytime hourly conversion rates predicted by the photochemical model, were determined:

$$k_1 = 36\ R^{0.55}\left[O_3\right]^{0.71} S^{-1.29} + k_{1(aq)} \qquad (2.8\text{-}2)$$

$$k_2 = 1206\ \left[O_3\right]^{1.5}\ S^{-1.41}\ \left[NO_x\right]^{-0.33} \qquad (2.8\text{-}3)$$

$$k_3 = 1261\ \left[O_3\right]^{1.45}\ S^{-1.34}\ \left[NO_x\right]^{-0.12} \qquad (2.8\text{-}4)$$

where k_1 is the SO_2 to SO_4 transformation rate (percent/hour),
k_2 is the NO_x to HNO_3 + RNO_3 transformation rate (percent/hour),
k_3 is the NO_x to HNO_3 (only) transformation rate (percent/hour),
R is the total solar radiation intensity (kw/m^2),
S is a stability index ranging from 2 to 6 (PGT class A and B=2, C=3, D=4, E=5, F=6),
RH is the relative humidity (percent),
$[O_3]$ is the background ozone concentration (ppm),
$[NO_x]$ is the plume NO_x concentration (ppm), and,
$k_{1(aq)}$ is the aqueous phase SO_2 oxidation term (percent/hour).

The aqueous phase component of the SO_2 conversion rate was parameterized as:

$$k_{1(aq)} = 3 \times 10^{-8}\ RH^4 \qquad (2.8\text{-}5)$$

Equations (2.8-2) to (2.8-4) apply only during daytime periods when gas phase free radical chemistry is active. The use of the ozone concentration

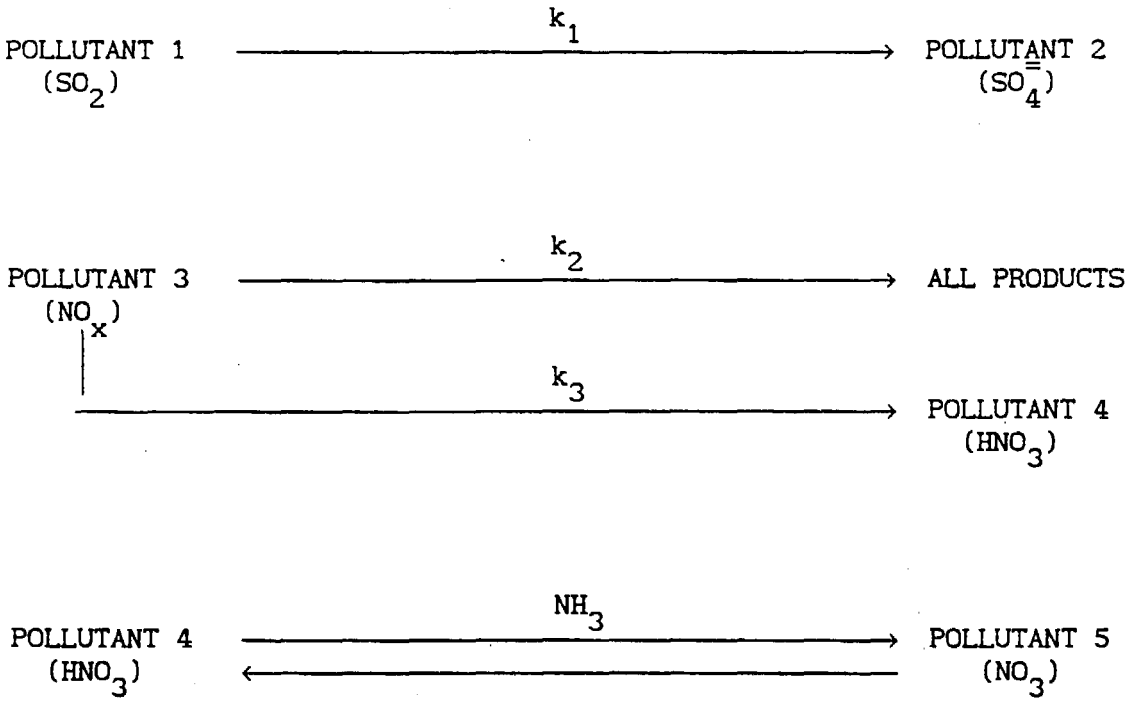

Figure 2.8-4. Schematic representation of chemical pathways in the five-pollutant system assumed with the MESOPUFF II chemical mechanism.

and the radiation intensity as surrogates for the OH concentration, as in the above equations, is appropriate only during the day. At night, SO_2 and NO_x oxidation rates resulting from heterogeneous reactions, are generally much lower than typical daytime rates (Wilson, 1981; Forrest et al., 1981). Nighttime oxidation rates of 0.2% and 2.0% for SO_2 and NO_x, respectively, are used as default values in the model.

Two options are provided for the specification of ozone concentrations: (1) hourly ozone data from a network of stations (OZONE.DAT, see Section 4.2.6), or, (2) a single, user-specified background ozone value may be used. The background ammonia concentration required for the HNO_3/NH_4NO_3 equilibrium calculation can be user-specified or a default value will be assumed.

The parameterized NO_x oxidation rate depends on the NO_x concentration. In situations where puffs overlap, it is necessary to estimate the total NO_x concentration at a particular point to properly determine k_2 and k_3. Similarly, the nitrate equilibrium relationship requires knowledge of the total (local average) SO_4, NO_x, and total nitrate (HNO_3 + NO_x) concentrations. Because of the preferential scavenging of ammonia by sulfate, the available ammonia is computed as total ammonia minus sulfate. The local average concentrations within a puff are estimated as the sum of contributions from the puff's own pollutants plus those of nearby puffs. Local average concentrations are separately computed for puffs within and above the mixed-layer.

2.9 Wet Removal

Many studies have shown that during rain events, wet scavenging of soluble or reactive pollutants can be of the order of tens of percent per hour (Barrie, 1981; Slinn et al., 1978; Levine and Schwartz, 1982; Scire and Venkatram, 1985). Gaseous pollutants are scavenged by dissolution into cloud droplets and precipitation. For SO_2, aqueous-phase oxidation can be an important removal pathway. Particulate pollutants are removed by both in-cloud scavenging (rainout) and below-cloud scavenging (washout). Over source-receptor distances of tens to hundreds of kilometers, wet scavenging can deplete a substantial fraction of the pollutant material from the puff.

A simple approach that has been shown (e.g., Maul, 1980) to yield realistic long-term estimates of wet removal is the empirically-based scavenging coefficient method. The depletion of a pollutant is represented as:

$$\chi_{t+dt} = \chi_t \exp[-\Lambda\Delta t] \qquad (2.9\text{-}1)$$

where χ is the concentration (g/m^3) at time t and t + Δt, and,
Λ is the scavenging ratio.

The scavenging ratio can be expressed as:

$$\Lambda = \lambda (R/R_1) \qquad (2.9\text{-}2)$$

where λ is the scavenging coefficient,
R is the precipitation rate (mm/hr), and,
R_1 is a reference precipitation rate of 1 mm/hr.

The scavenging coefficient depends on the characteristics of the pollutant (e.g., solubility and reactivity) as well as the nature of the precipitation. Table 2.9-1 contains the default values of the scavenging coefficient for SO_2, $SO_4^=$, NO_x, HNO_3, and NO_3^-. A precipitation code determined from the hourly surface meteorological observations of precipitation type (CD144 data) is used to determine if the value of λ for liquid or frozen

Table 2.9-1

Default Values of the Scavenging Coefficient, $\lambda(s^{-1})$

Pollutant	Liquid Precipitation	Frozen Precipitation
SO_2	3×10^{-5}	0.0
$SO_4^=$	1×10^{-4}	3×10^{-5}
NO_x	0.0	0.0
HNO_3	6×10^{-5}	0.0
NO_3^-	1×10^{-4}	3×10^{-5}

precipitation is most appropriate. The reported precipitation code is related to precipitation type as shown in Table 2.9-2. The liquid precipitation values of λ are used for precipitation codes 1-18. The frozen precipitation values are used for precipitation codes 19-45.

The user can override the default values of the scavenging coefficient by entering new values in the CALPUFF control file (see Section 4.2.1). An option is provided in the model to completely by-pass the wet removal calculation for pollutants or time periods for which it is not of importance.

Table 2.9-2

Conversion of Reported Precipitation
Type/Intensity To Precipitation Codes

Precipitation Code	Type	Intensity
Liquid Precipitation		
1	Rain	Light
2	Rain	Moderate
3	Rain	Heavy
4	Rain Showers	Light
5	Rain Showers	Moderate
6	Rain Showers	Heavy
7	Freezing Rain	Light
8	Freezing Rain	Moderate
9	Freezing Rain	Heavy
10	Not Used	-
11	Not Used	-
12	Not Used	-
13	Drizzle	Light
14	Drizzle	Moderate
15	Drizzle	Heavy
16	Freezing Drizzle	Light
17	Freezing Drizzle	Moderate
18	Freezing Drizzle	Heavy
Frozen Precipitation		
19	Snow	Light
20	Snow	Moderate
21	Snow	Heavy
22	Snow Pellets	Light
23	Snow Pellets	Moderate
24	Snow Pellets	Heavy
25	Not Used	-
26	Ice Crystals	*
27	Not Used	-
28	Snow Showers	Light
29	Snow Showers	Moderate
30	Snow Showers	Heavy
31	Not Used	-
32	Not Used	-
33	Not Used	-
34	Snow Grains	Light
35	Snow Grains	Moderate
36	Snow Grains	Heavy
37	Ice Pellets	Light
38	Ice Pellets	Moderate

Table 2.9-2 - Continued

Conversion of Reported Precipitation
Type/Intensity To Precipitation Codes

Precipitation Code	Type	Intensity
39	Ice Pellets	Heavy
40	Not Used	-
41	Hail	*
42	Not Used	-
43	Not Used	-
44	Small Hail	*
45	Not Used	-

* Intensity not currently reported for ice crystals, hail and small hail.

3. CALPUFF Model Structure

3.1 Memory Management

A flexible memory management system is used in CALPUFF which facilitates the user's ability to alter the dimension of the major arrays within the code. Arrays dealing with the number of horizontal or vertical grid cells, meteorological stations, chemical species, puffs, sources, and several other internal variables are dimensioned throughout the code with parameter statements. The declaration of the values of the parameters are stored in a file called 'PARAMS.PUF'. This file is automatically inserted into any CALPUFF subroutine or function requiring one of its parameters via FORTRAN 'include' statements. Thus, a global redimensioning of all of the model arrays dealing with the number of vertical layers, for example, can be accomplished simply by modifying the PARAMS.PUF file and recompiling the program.

The parameter file contains variables which set the array dimensions or the maximum allowed number of vertical layers, or horizontal grid cells, etc. The actual value of the variables for a particular run is set within the user input file (i.e., the control file), and can be less than the maximum value set by the parameter file.

A sample parameter file is shown in Table 3.1-1. In addition to the parameters specifying the maximum array dimensions of the major model arrays, the parameter file also contains variables determining the Fortran I/O unit numbers associated with each input and output file. For example, the input control file (IO5) and output list file (IO6) are normally associated with unit numbers 5 and 6. However, if these units are reserved on a particular computer system, these files can be redirected to other non-reserved units by setting IO5 and IO6 equal to 1 and 2, for example, as in the sample PARAMS.PUF file.

Table 3.1-1

Sample CALPUFF Parameter File

```
c------------------------------------------------------------------------
c --- PARAMETER statements                                        CALPUFF
c------------------------------------------------------------------------
c
c --- Specify parameters
      parameter(mxpuff=100)
      parameter(mxspec=5)
      parameter(mxnx=10,mxny=10,mxnz=20)
      parameter(mxnxg=10,mxnyg=10,mxrec=180)
      parameter(mxss=50,mxus=10,mxps=100)
      parameter(mxpt1=20,mxpt2=20,mxarea=20)
      parameter(mxpdep=1,mxint=9)
      parameter(mxoz=20)
      parameter(mxhill=50,mxtpts=25,mxrect=400)
      parameter(mxsg=12,mxvar=60,mxcol=132)
      parameter(io5=1,io6=2,io7=7,io8=8,io9=9,io10=10,io16=16,io18=18)
      parameter(io20=20,io22=22,io24=24,io26=26)
c
c --- Compute derived parameters
      parameter(mxnzp1=mxnz+1)
      parameter(mxnxy=mxnx*mxny)
      parameter(mxgsp=mxnxg*mxnyg*mxspec)
      parameter(mxrsp=mxrec*mxspec)
      parameter(mx2=2*mxspec,mx5=5*mxspec,mx6=6*mxspec)
      parameter(mxp7=7+mxspec)
c
c --- GENERAL PARAMETER definitions:
c        MXPUFF - Maximum number of active puffs allowed on the
c                 computational grid at one time
c        MXSLUG - Maximum number of active slugs allowed on the
c                 computational grid at one time (can be set to
c                 one if the slug option is not used)
c        MXSPEC - Maximum number of chemical species
c          MXNX - Maximum number of METEOROLOGICAL grid cells in
c                 the X direction
c          MXNY - Maximum number of METEOROLOGICAL grid cells in
c                 the Y direction
c          MXNZ - Maximum number of vertical layers in
c                 the METEOROLOGICAL grid
c         MXNXG - Maximum number of SAMPLING grid cells in
c                 the X direction
c         MXNYG - Maximum number of SAMPLING grid cells in
c                 the Y direction
c         MXREC - Maximum number of non-gridded receptors
c          MXSS - Maximum number of surface meteorological stations
c                 in the CALMET data
c          MXUS - Maximum number of upper air stations in the CALMET
c                 data
c          MXPS - Maximum number of precipitation stations in the
c                 CALMET data
```

Table 3.1-1 (Concluded)

Sample CALPUFF Parameter File

```
c         MXPT1 - Maximum number of point sources with constant
c                 emission parameters
c         MXPT2 - Maximum number of point sources with time-varying
c                 emission parameters
c        MXAREA - Maximum number of area sources with constant
c                 emission parameters (i.e., non-gridded area sources)
c        MXPDEP - Maximum number of particle species dry deposited
c         MXINT - Maximum number of particle size intervals used
c                 in defining mass-weighted deposition velocities
c          MXOZ - Maximum number of ozone data stations (for use in the
c                 chemistry module)
c        MXHILL - Maximum number of subgrid-scale (CTSG) terrain
c                 features
c        MXTPTS - Maximum number of points used to obtain flow
c                 factors along the trajectory of a puff over the hill
c        MXRECT - Maximum number of complex terrain (CTSG) receptors
c
c --- CONTROL FILE READER definitions:
c          MXSG - Maximum number of input groups in control file
c         MXVAR - Maximum number of variables in each input group
c         MXCOL - Maximum length (bytes) of a control file input record
c
c --- FORTRAN I/O unit numbers:
c           IO5 - Control file (CALPUFF.INP)     - input  - formatted
c           IO6 - List file (CALPUFF.LST)        - output - formatted
c
c           IO7 - Meteorological data file       - input  - unformatted
c                 (CALMET.DAT)
c
c           IO8 - Concentration output file      - output - unformatted
c                 (CONC.DAT)
c           IO9 - Dry flux output file           - output - unformatted
c                 (DFLX.DAT)
c          IO10 - Wet flux output file           - output - unformatted
c                 (WFLX.DAT)
c          IO16 - Pt. source emissions file      - input  - unformatted
c                 (PTEMARB.DAT) with arbitrarily
c                 varying point source emissions
c          IO18 - Gridded area source emissions - input  - unformatted
c                 file (AREM.DAT)
c          IO20 - User-specified deposition     - input  - formatted
c                 velocities (VD.DAT)
c          IO22 - Hourly ozone monitoring data  - input  - formatted
c                 (OZONE.DAT)
c          IO24 - User-specified chemical       - input  - formatted
c                 transformation rates
c                 (CHEM.DAT)
c          IO26 - Hourly turbulence measurements- input  - formatted
c                 sigma v, sigma w
c                 (SIGMA.DAT)
```

3.2 Structure of the CALPUFF Modules

Execution of the CALPUFF model is divided into three major phases: setup, computational, and termination (see Figure 3-1). In the setup phase of the model execution, a variety of initialization and one-time I/O and computational operations are performed, including the following:

- Opening of input and output files.
- Reading and processing the control file inputs which includes model option flags and run control variables.
- Reading and processing the time-invariant data records of the model's input data bases (i.e., meteorological data file, optional emissions files, ozone data files, and user-specified deposition velocities and transformation rate files).
- Performing consistency checks of the input data base information versus the control file inputs.
- Performing initialization and setup operations for the chemistry, dry deposition, dispersion coefficient, and sampling modules.
- Writing the header records to the model's output concentration and dry/wet deposition files.

The computational phase of the model includes the basic time loop within which the hourly concentrations and deposition fluxes are computed and, if appropriate, time averaged. The functions performed in the the computation phase include the following:

- Retrieving and processing time-averaging data from the meteorological, emissions, and ozone data files.

- Emitting, transporting, and removals puffs from the computation grid.

- Evaluating the effects of dispersion, chemical transformation, wet removal, dry deposition, and subgrid scale complex terrain.

- Sampling the puffs to determine concentrations and deposition fluxes at gridded and discrete receptors.

- Time-averaging and storing concentrations and deposition flux results to the appropriate output files.

The final phase of the model execution deals with run termination functions. The termination phase includes the closing of any active data files, computation of model run time, and printing of summary or normal termination messages.

A flow diagram for the setup module is provided in Figure 3.2-1. The flow diagram contains the name of each subroutine or function called by the setup module along with a brief description of the routine's purpose. Figure 3.2-2 is a flow diagram for the main computational routine, subroutine COMP, which contains the basic time loop and calls to all of the technical modules.

A complete listing of the subroutine/function call sequence, including high order subroutine/function calls, is provided in Appendix A. Also included in Appendix A is a cross referencing table, showing which routines call and are called by each subroutine/function in the model. A description of the purpose of each subroutine or function is contained in Appendix B.

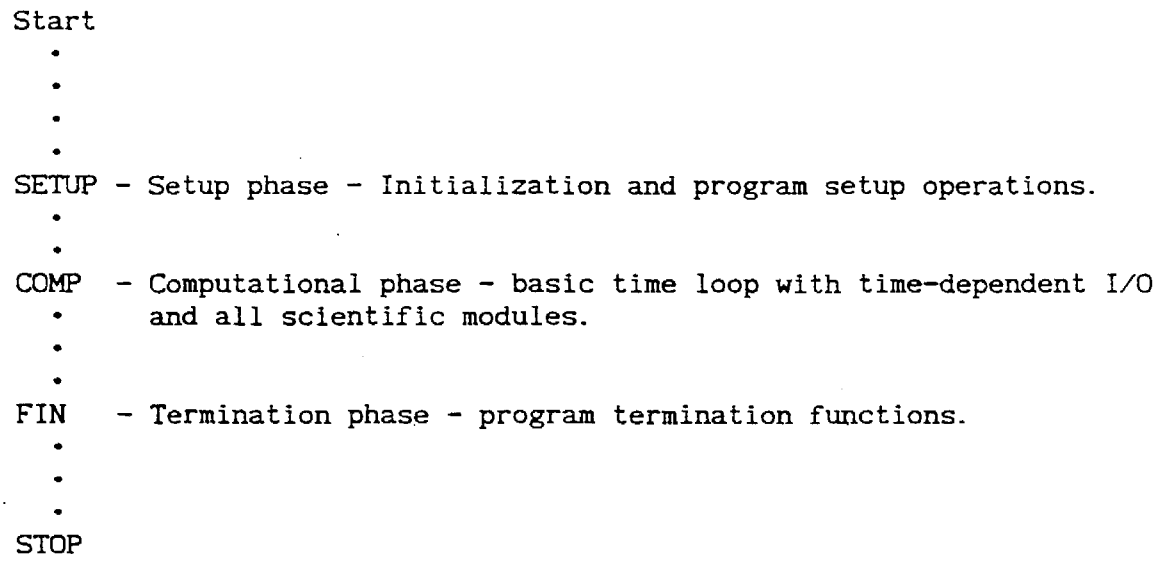

Figure 3.2-1. Flow diagram showing the subroutine calling sequence in the CALPUFF MAIN program.

```
Enter SETUP
  •
  •
DATETM  - Get date and time from the system clock.
  •
  •
OPENFL  - Open control file (input) and list file (output).
  •
  •
READCF  - Read the control file inputs.
  •
  •
SETCOM  - Set miscellaneous common block parameters (grid
  •         parameters, etc.)
  •
OPENOT  - Open all other input and output files.
  •
  •
RDHDEM2 - Read header records for the PTEMARB.DAT emission file
  •         (arbitrarily-varying point source emissions).
  •
RDHDEM4 - Read header records for the AREM.DAT emissions file (area
  •         source emissions).
  •
JULDAY  - Convert the beginning date to a Julian day.
  •
  •
CHEMI   - Perform setup operations for the chemistry module.
  •
  •
EMQA    - Perform QA checks on emission header record data, set up
  •         cross-referencing arrays.
  •
RDTIEM2 - Read the time-invariant data from the PTEMARB.DAT file
  •         (arbitrarily-varying emissions).
  •
MET1    - Read the header records for the CALMET.DAT file
  •         (meteorological data file).
  •
SIGSET  - Perform setup operations for the dispersion coefficient
  •         module.
  •
SLUGI   - Perform setup operations for the slug sampling function.
  •
  •
DRYI    - Perform setup operations for the dry deposition module.
  •
  •
WROUT1  - Write the header records to the CONC.DAT
  •         (concentrations), DFLX.DAT (dry deposition flux), and
  •         WFLX.DAT (wet deposition flux) output files.
  •
Return to MAIN PROGRAM
```

Figure 3.2-2. Flow diagram showing the subroutine/function calling sequence in the subroutine SETUP (Setup Phase).

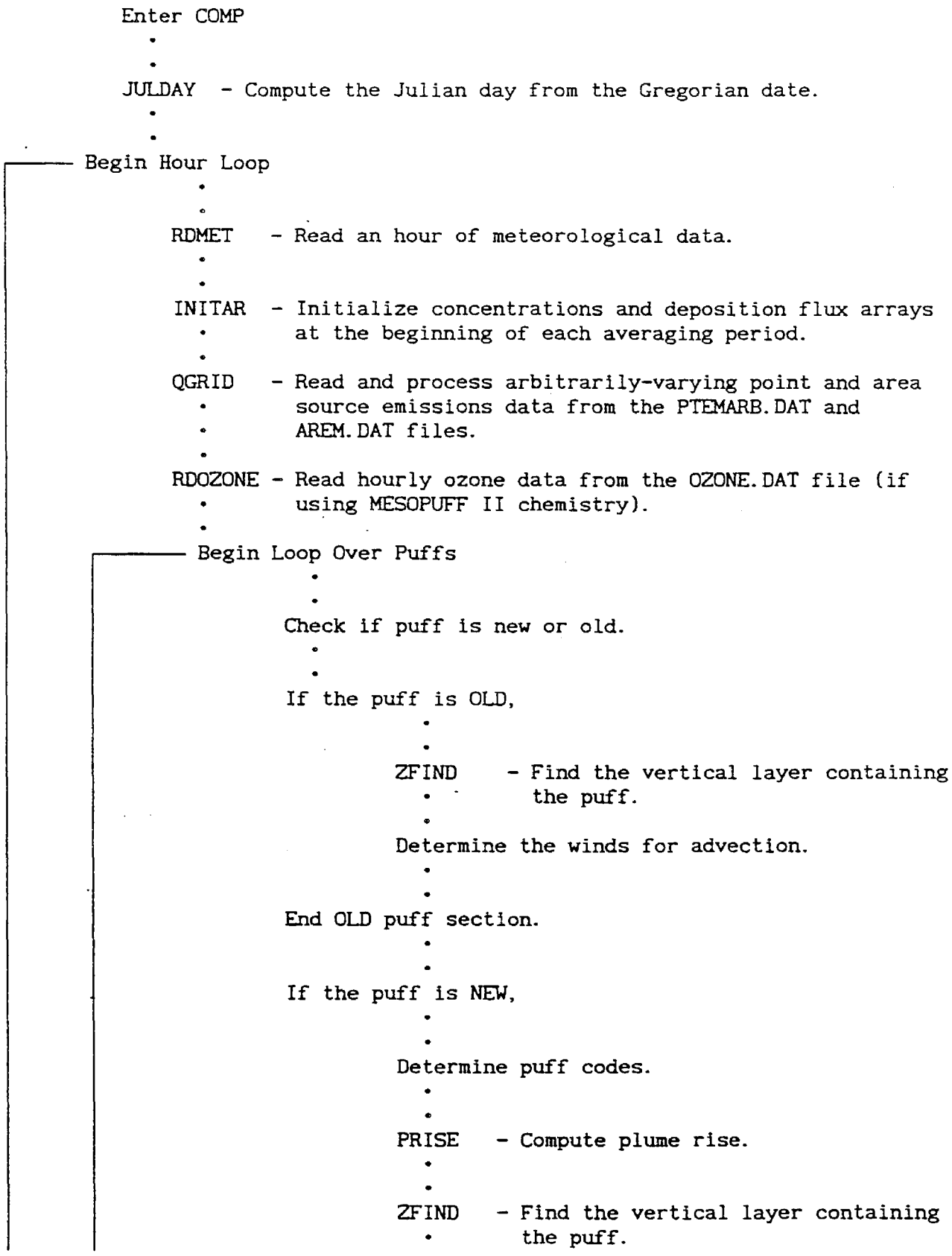

Figure 3.2-3. Flow diagram showing the subroutine calling sequence in Subroutine COMP (Computational Phase). - Continued

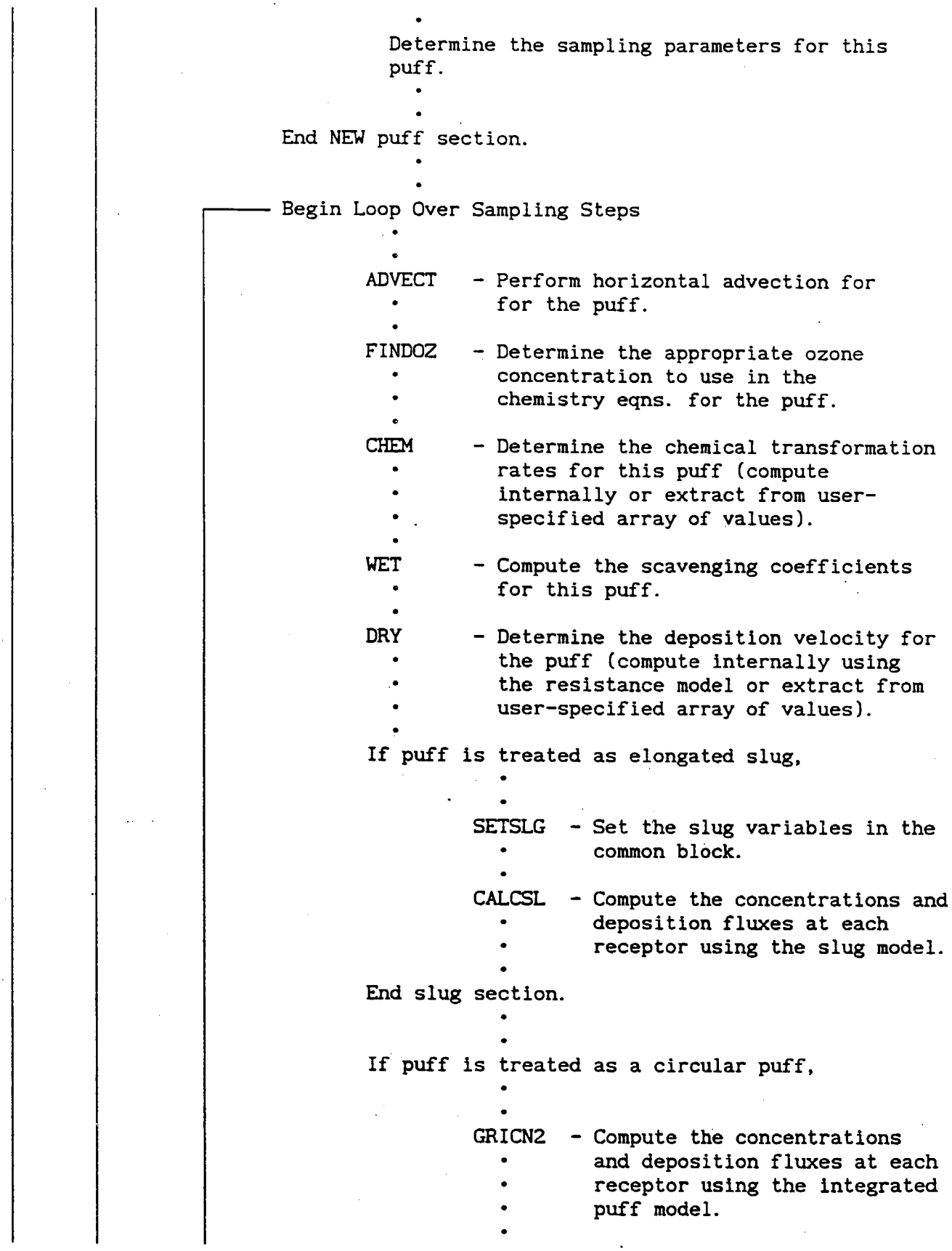

Figure 3.2-3. Flow diagram showing the subroutine calling sequence in Subroutine COMP (Computational Phase). - Continued

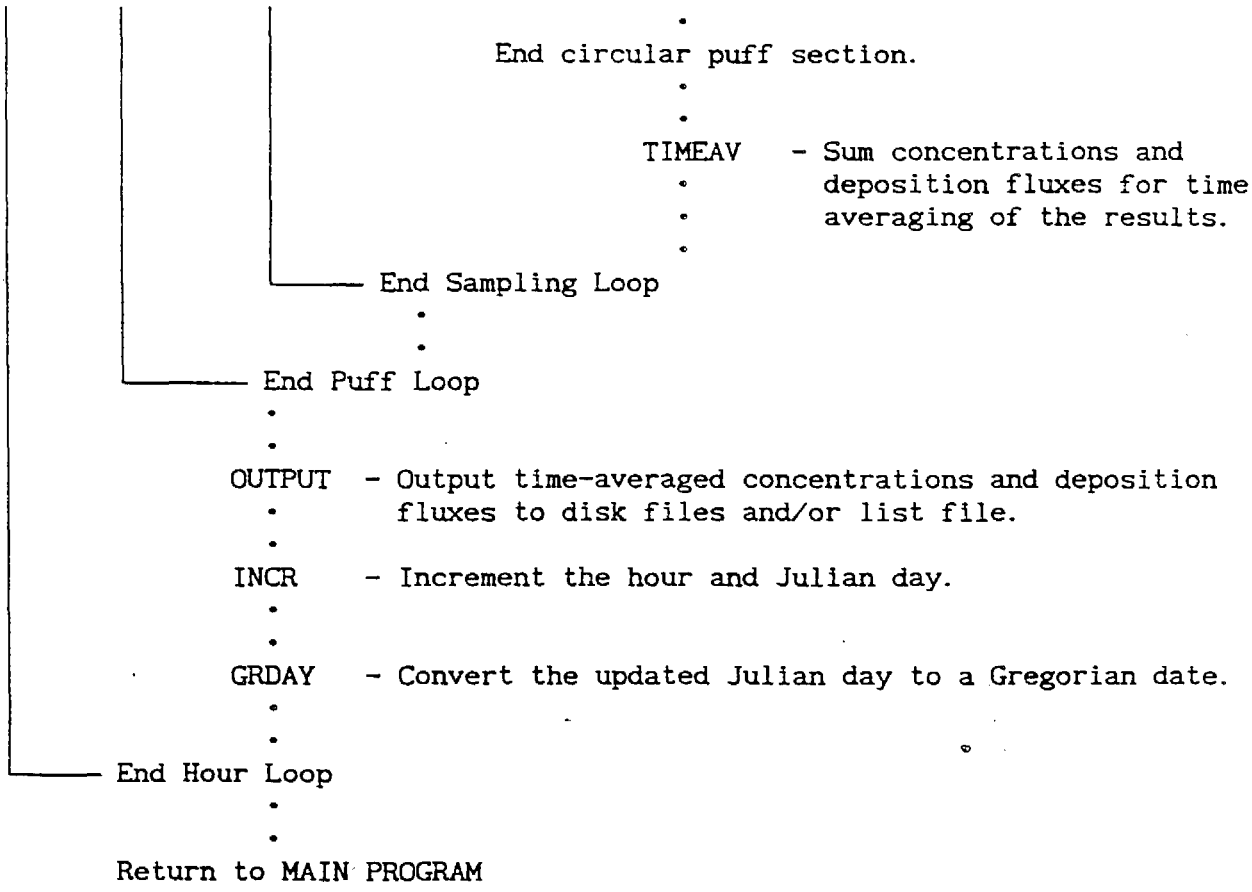

Figure 3.2-3. Flow diagram showing the subroutine calling sequence in Subroutine COMP (Computational Phase). - Concluded